SCUOLA DI DOTTORATO

UNIVERSITÀ DEGLI STUDI DI MILANO-BICOCCA

Department of

BIOTECHNOLOGY AND BIOSCIENCES

PhD program: TRANSLATIONAL AND MOLECULAR MEDICINE (DIMET)

Cycle: XXX

Heteromeric nicotinic receptors regulate developing and mature prefrontal circuits: interaction with other neuromodulators, and implications for sleep-related hypermotor epilepsy.

Surname: COATTI Name: AURORA

Registration number: 718138

Tutor: ANDREA BECCHETTI

Co-tutor: ALIDA AMADEO

Coordinator: ANDREA BIONDI

ACADEMIC YEAR: 2016-2017

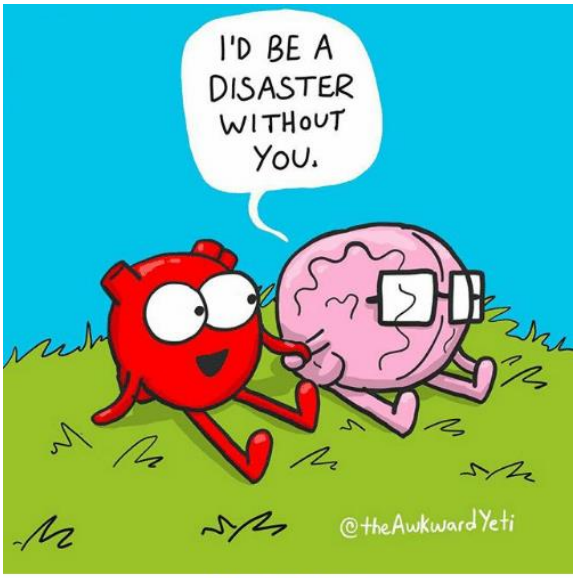

Modified from: theawkwardyeti.com

Table of Contents

Chapter 1

INTRODUCTION

PART I - THE PREFRONTAL CORTEX AND THE ASCENDING REGULATORY SYSTEMS

The human prefrontal cortex (PFC) fulfils several functions. It integrates motivational events, elaborates complex motor schemes, performs cognitive functions and processes, such as working memory, decision-making and planning of goal-oriented behaviours (Fuster and Bressler, 2015; Hoover and Vertes, 2007). The rodents' medial PFC (mPFC) consists of the frontal region 2 (Fr2), the anterior cingulate cortex (ACC), the prelimbic (PL) and the infralimbic (IL) area. Fr2, also known as secondary motor (M2) cortex (Franklin et al., 2011), is an associative cortex with premotor control functions and is considered homologous to the much larger human dorsolateral cortex (Uylings et al., 2003). It receives input from the primary motor and somatosensory cortices, and from subcortical structures as the thalamic and brain stem nuclei (Heidbreder and Groenewegen, 2003; Steriade and McCarley, 2005). This area projects to the primary motor cortex and to the dorsomedial striatum (Condè et al., 1995; Paxinos, 2015) and is especially involved in goal-oriented behaviour (Kargo et al., 2007).

In Fr2, the conspicuous layer V is notable for its large pyramidal cells with apical dendrites that terminate in superficial layers. These neurons constitute the main output channel to the subcortical regions, and they are tightly controlled by a dense network of GABAergic interneurons (Ozeki et al., 2009; Shu et al., 2003). A major GABAergic population is constituted by the parvalbumin-expressing fast-spiking (FS) interneurons, implicated in feed-back and feed-forward inhibition (e.g., Tremblay et al., 2016). Morphologically, these cells are basket and chandelier cells, which preferentially innervate respectively the soma and the axonal initial segment of pyramidal cells (Kawaguchi and Kubota, 1998; Kubota, 2014).

In general, the PFC local circuits are tightly controlled by the ascending regulatory systems, as PFC is anatomically connected with virtually all the neuromodulatory relays (Dembrow and Johnston, 2014).

THE ASCENDING REGULATORY SYSTEMS

The ascending regulatory system comprises interconnected nuclei in brainstem, basal forebrain and hypothalamus (**Fig 1**). Especially relevant is the balance between the cholinergic and noradrenergic activation, which exert their cortical effects by following two main pathways: 1) they directly project to the neocortex, where they extensively innervate the PFC; 2) they project to the thalamus, where they stimulate non-specific thalamocortical glutamatergic neurons (Jones, 2011).

The cholinergic pedunculopontine (PPT) and the laterodorsal pontine tegmentum (LDT) nuclei are highly active during wakefulness and rapid eye movement (REM) sleep, but not during slow wave sleep (SWS; Jones, 2005). The main noradrenergic nucleus, the *locus coeruleus* (LC), maximally discharges during active wakefulness and is almost silent during both REM and non-REM sleep (Aston-Jones and Bloom, 1981). The simultaneous presence of acetylcholine (ACh) and norepinephrine (NE) is necessary to sustain the waking state through cortical activation and muscle tone (Jones, 2005), while, during REM sleep, ACh release largely prevails. The serotonergic dorsal raphe nucleus (DR) seems to be implicated in less-aroused waking states (Jacobs and Fornal, 1991), while the dopaminergic median raphe nucleus (MR) stimulates arousal in relation with positive emotions during wakefulness and REM sleep (Maloney et al., 2002). Histaminergic cells, located in the posterior hypothalamus, also contribute to arousal and wakefulness (Saper et al., 2001).

Another system, implicated in global arousal, has been more recently discovered in the lateral hypothalamus, in which specific nuclei produce orexin neuropeptides. Orexins are mostly released during active wakefulness and exert a variety of physiological roles, ultimately sustaining exploratory and goal-oriented behaviours driven by physiological needs (Lee et al., 2005).

The above systems interact in a very complex way, through reciprocal connections and by cooperating in direct neuromodulation of the neocortex (Jones, 2005). Dysregulation of this subtle orchestration can alter the PFC function and cause several sleep-related disorders.

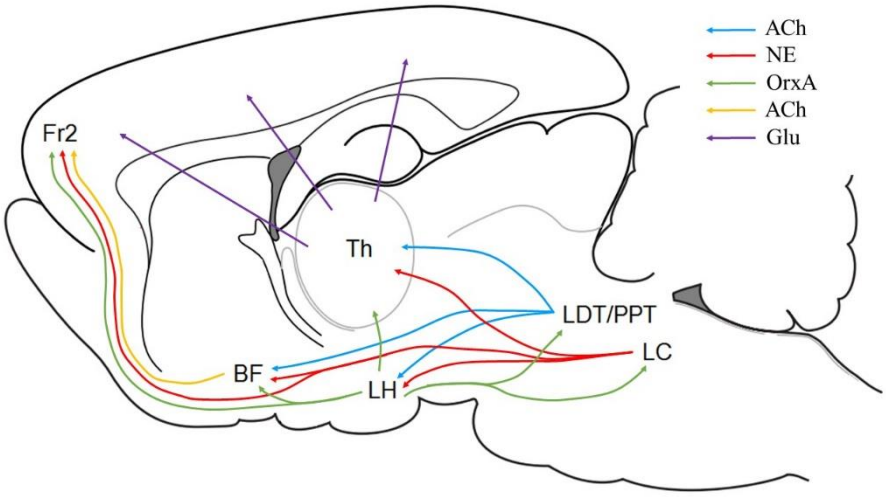

Fig 1 Projections of ascending regulatory systems. Many wake-promoting projections arise from neurons in basal forebrain (BF), lateral hypothalamus (LH), locus coeruleus (LC), laterodorsal tegmentum (LDT) and peduncolopontine tegmentum (PPT). Regulatory systems reciprocally interact, directly regulate Fr2 and project to the thalamus (Th), which in turn innervates the neocortex.

THE CHOLINERGIC SYSTEM

The cholinergic system is critical to sustain the cortical function and regulate the sleep/wake cycle. The basal forebrain nuclei innervate several paleo- and neo-cortical areas, the limbic system, amygdala and the hippocampus (Mesulam et al., 1983), whereas the PPT and the LDT mainly project to the thalamus and the neocortex (mainly to the PFC). Here, ACh enhances cortical arousal, and regulates executive and cognitive functions such as attentive tasks, working memory and decision-making (Wallace and Bertrand, 2013). The PPT/LDT nuclei

especially discharge during wakefulness and at the transition between slow-wave and REM sleep (Jones et al., 2008; Lee et al., 2005; Siegel, 2002), while they are silent during non-REM sleep. Therefore, ACh stimulates cortical arousal regardless of behavioural or motor activity. The cholinergic projections diffusely innervate large target areas and rarely terminate at synaptic contacts. Varicose axon arborisations contribute to diffuse volume transmission (Descarries et al., 1997), which modulates neurotransmitter release and somatic excitability of selected neuronal populations. ACh cooperates with the other neurotransmitters to finely control cortical activity (Couey et al., 2007; Jones et al., 2008) and the switch between different sleep states (Saper et al., 2010).

Nicotinic receptors

ACh can activate both nicotinic (nAChRs) and muscarinic (mAChRs) receptors, but the implication of nAChRs in regulating cortical excitability and function is increasingly recognized (Becchetti et al., 2015; Guillem et al., 2011). nAChRs are pentameric ligand-gated ion channels, belonging to the Cys-loop family. Five subunits surround a central pore, selective for cations (Albuquerque et al., 2009): implying that nAChR activation induces membrane depolarization. Each subunit presents four membrane spanning domains (M1-M4), and the channel gating depends on conformational changes in the M2 domain (Miyazawa et al., 2003; Morales-Perez et al., 2016). The neuronal nAChRs can be homopentamers or heteropentamers of $\alpha_{(2\text{-}10)}$ and $\beta_{(2\text{-}4)}$

subunits, which are encoded respectively by CHRNA(2-10) and CHRNB(2-4). The heteropentamer α4β2* and the homopentamer $(\alpha 7)_5$ are the main cortical nAChRs (Dani and Bertrand, 2007; Gotti et al., 2007). Homopentamers are more permeable to Ca^{2+} than α4β2* (Fucile, 2004), desensitize more quickly and have lower affinity for ACh and nicotine (EC_{50} > 100 μM, while EC_{50} of α4β2* is ~30 μM; Dani and Bertrand, 2007). Heteromeric nAChRs probably have a major role in the tonic control of neocortical arousal, as they can be activated by the relatively low ACh concentration diffusing by varicose cholinergic fibres. The affinity for ACh and the desensitization kinetics is also influenced by the stoichiometry of receptor's subunits (Nelson et al., 2003). The specific effects of nAChRs may depend on the receptors' localization in different neuronal compartments. They can mediate post-synaptic effects if they are expressed on somata or dendrites (Hogg et al., 2003), otherwise, if expressed on pre-synaptic boutons, nAChRs stimulate neurotransmitter release (Paterson and Nordberg, 2000) by regulating calcium influx. Moreover, nAChRs are observed extra-synaptically (Gotti and Clementi, 2004). Nicotinic receptors in PFC support attentional performance and sensory processing (Sarter et al., 2009). Studies in the mouse, show that decreasing the expression of nicotinic subunits leads to reduced attention performances in challenging conditions (Bailey et al., 2010) and impairs working memory (Castner et al., 2011; Croxson et al., 2011). Alterations in nAChRs expression are also widespread in a variety of neurological and psychiatric diseases, such as the Alzheimer's disease, dementias, autism, anxiety, depression, schizophrenia and epilepsy (Dani and Bertrand, 2007; Picciotto et al., 2002). However, until now, the only

clear aetiologic role of nAChRs in neurological disorders is established for sleep-related hypermotor epilepsy.

nAChRs modulate both glutamatergic and GABAergic transmission in the deep layers of Fr2

The cholinergic fibres densely innervate Fr2, and ACh excites layer V cells through β2* nAChRs (Aracri et al, 2010; Aracri et al., 2013), thus regulating the local circuit activity. As previously mentioned, heteromeric nAChRs give a major contribution to the tonic control of cortical excitability. In general, the global nAChR effect on deep layers of PFC is excitatory. However, the mechanistic details are very complex. β2* nAChRs are known to modulate glutamate release from both thalamocortical fibres (Lambe et al., 2003) and intrinsic glutamatergic terminals (Aracri et al., 2013). This effect can be exerted at the pre-synaptic level, by a depolarization-dependent activation of voltage-gated channels, accompanied by Ca^{2+} influx through the nAChRs itself (Dani and Bertrand, 2007). On the other hand, the direct excitation of pyramidal cell somata by nAChRs is more controversial, and is probably limited to specific neuronal populations (e. g. Couey et al., 2007; Kassam et al., 2008; Zolles et al., 2009). Because however the pyramidal neuron activity is strictly controlled by GABAergic neurons, the nicotinic regulation of GABAergic transmission becomes also pivotal in determining the local circuit output. In fact, heteromeric nAChRs also control GABA release onto pyramidal cells at the pre-synaptic level (Aracri et al., 2010; Klaassen et al., 2006). Finally, the

cholinergic modulation of the cell somata of distinct interneuron classes and of reciprocal inhibition between interneuron populations are still poorly understood (Aracri et al., 2017 and references therein).

ACH COOPERATES WITH OTHER NEUROTRANSMITTERS TO CONTROL CORTICAL AROUSAL

Orexin regulates glutamatergic transmission in PFC

The hypotalamic orexin neurons release orexin A and B (OrxA and OrxB; Sakurai et al., 1998), also known as Hypocretin 1 and 2 (de Lecea et al., 1998). These neurons receive afferents from other ascending regulatory systems as well as PFC and amygdala. They discharge during active wakefulness, and are thought to sustain arousal during physiologically motivated behaviours (Jones, 2008; Kukkonen, 2013; Lee et al., 2005). A deficit in orexinergic system leads to narcolepsy with cataplexy (a sudden loss of muscle tone accompanied by full conscious awareness, typically triggered by positive emotions) in both humans and animal models (Chemelli et al., 1999; Peyron et al., 2000). Orexins excite all the subcortical arousal nuclei (Sutcliffe and de Lecea, 2002), thereby increasing the release of cortical neuromodulators, including ACh (Fadel et al., 2005). They modulate attention and executive function by exciting the nonspecific thalamocortical neurons (Bayer et al., 2002; Peyron et al., 1998) that target the apical dendrites of pyramidal neurons in PFC layer V (Lambe et al., 2007). In addition, orexin fibres also directly and densely innervate the PFC (Fadel and

Deutch, 2002; Peyron et al 1998), where they set the proper level of arousal (Boutrel et al., 2010). In fact, direct infusion of orexin into the PFC increases the attentive tasks in rats (Lambe et al., 2005). Moreover, in orexin KO mice, the mPFC was found to mediate the cataplexy-sustaining mechanisms, in association with positive emotional stimuli (Oishi et al., 2013). Orexins act through G protein coupled receptors (OrxR1 and R2), leading to intracellular events, such as protein kinase C activation (Kukkonen and Leonard, 2014), which regulate neuronal activity e. g. by inhibiting K^+ voltage-gated channels (Xia et al., 2005) and hyperpolarization-activated HCN channels (Li et al., 2010). OrxR1 preferentially binds OrxA (with a EC_{50} of 30 nM, compared to OrxB with 2.5 µM EC_{50} value), while OrxR2 indistinctly binds both OrxA and B (with, respectively, 34 nM and 60 nM EC_{50} values; Ammoun et al., 2003; Sakurai et al 1998). The overall OrxRs distribution is complex and depends on cortical area. In fact, information about the expression and function of orexin peptides and receptors in different neocortex regions and layers is fragmentary. OrxR1 mRNA is generally detected in layer V of motor areas in rat (Marcus et al., 2001), and is also highly expressed in layer V of murine prelimbic PFC, where OrxR1 mediates the excitation of pyramidal neurons (Li et al., 2010). In layer V of the murine Fr2, conspicuous OrxR1 labelling was observed in pyramidal neuron somata and in intracortical glutamatergic terminals (but not in GABAergic structures). Here, OrxA stimulates pre-synaptic glutamate release onto FS interneurons, which in turn stimulates GABA release onto pyramidal neurons (Aracri et al., 2015). Therefore, OrxA also indirectly regulates layer V interneurons, by regulating the glutamatergic drive onto FS. Moreover, OrxRs are observed in layer I,

where the apical dendrite tufts of layer V pyramidal cells extend (Liu and Aghajanian, 2008). Little is known about the direct regulation exertex by Orx onto pyramidal neurons in Fr2.

Functional interaction between the cholinergic and orexinergic systems

Many aspects of the interplay between cholinergic and orexinergic transmission remain to be determined. Orexinergic neurons stimulate the cholinergic nuclei in basal forebrain and LDT/PPT (Eggermann et al., 2001; Fadel and Burk, 2010), which is thought to be crucial to regulate awakening (Li et al., 2016), and the cortical executive functions. In particular, several studies suggest that intrabasalis OrxA stimulates a prolonged ACh release in the PFC (Fadel et al., 2005; Piantadosi et al., 2015). Moreover, a direct interaction between ACh and Orx has been described in the PFC thalamocortical terminals. Thalamic projections to PFC funnel the ascending arousal pathways and are crucial for executive aspects of attention. Nicotine and OrxB pre-synaptically stimulate the same thalamocortical fibres in PFC, without a post-synaptic effect (Lambe and Aghajanian 2003; Lambe et al., 2003; Lambe et al., 2005). Physiologically, ACh and Orx are present together only during wakefulness, but an alteration of orexinergic system also alters REM sleep, when the cholinergic tone is high (Vassalli et al., 2013). This further suggests a possible correlation between the orexinergic and cholinergic systems. As for Fr2, both nAChRs and OrxRs are widely expressed in the intracortical

glutamatergic fibres (Aracri et al., 2015): ACh and Orx may thus cooperate in modulating overall glutamate release in Fr2 deep layers.

Norepinephrine modulation is synapse-specific

The LC widely innervates cortical and subcortical regions. NE exerts a widespread modulation of neuronal circuits that is crucial for alert waking and state-dependent cognitive processes, as decision-making, fight-or-flight response, attention and memory (Berridge and Waterhouse, 2003). During waking, in response to sensory stimuli, LC neurons increase their firing rate to sustain enhanced forebrain arousal, preventing sleep (Berridge and Abercrombie, 1999), whereas they are silent during the REM sleep-associated forebrain activation. The noradrenergic system is controlled by orexinergic input, as orexinergic neurons directly project to LC, mediating cortical arousal (Peyron et al., 1998). NE also cooperates with ACh to sustain both behavioural and forebrain arousal states. In neocortex, NE release has a diffuse nature, and is not closely matched to synaptic junctions (Bach-y-Rita, 1996). The relative cellular mechanisms are incompletely understood. NE acts through three main receptor classes: α1, α2 and β1 (Iversen et al., 2008). Their distribution and second messenger coupling are highly variable. While βRs are preferentially post-synaptic and coupled to Gs/cAMP cascade, α1Rs and α2Rs are pre-synaptic and mainly coupled to the phosphoinositol and Gi/cAMP systems, respectively (Dolhman et al., 1991). Many studies investigated the NE actions on neuronal physiology, indicating a complex cell-specific pattern. (Foehring et al.,

1989; Roychowdhury et al., 2014; Salgado et al., 2010). For example, NE produces either membrane depolarization or hyperpolarization depending on receptor distribution and single cell membrane properties (Berridge and Waterhouse, 2003). In layer V of rat mPFC, NE depresses glutamate release and enhances GABA release, suggesting the existence of NE-controlled GABAergic network in the PFC, where layer V constitutes a "bottleneck for behavioural inhibition" (Roychowdhury et al., 2014). Several studies described a depressive effect on both NMDA and non-NMDA glutamate receptors (Law-Tho et al., 1993, in prefrontal cortex; Lehmenkuhler et al., 1991, in motor cortex) while others showed an increase of glutamate-evoked excitatory cortical responses in somatosensory cortex (Mouradian et al., 1991). Wang et al. (2013) analysed the NE action on layer V pyramidal neurons and FS in juvenile rat prefrontal local circuitry. NE depressed glutamatergic transmission onto FS, but not onto pyramidal cells, and did not alter GABAergic transmission. Kawaguchi and Shindou (1998) observed an excitation of GABAergic cells by NE administration. Moreover, Salgado and colleagues showed the ability of NE of shifting the inhibition from distal to somatic. (Salgado et al., 2010). The issue is quite complex, we can conclude that the effects of NE in PFC are synapse-specific, which underlines the importance of carrying out further studies in the different prefrontal regions.

PART II - NICOTINIC RECEPTORS AND SLEEP-RELATED HYPERMOTOR EPILEPSY

A clear aetiologic role of nAChRs is established for nocturnal frontal lobe epilepsy (NFLE), which was recently renamed sleep-related hypermotor epilepsy (SHE), to better highlight the relation with sleep and the motor aspects of the attacks (Tinuper et al., 2016). This syndrome is a focal epilepsy, characterized by motor seizures, often arising in the frontal regions during stage II of sleep. This phase is characterized by biphasic slow waves (k-complexes) and high frequency sleep spindles (Luthi, 2014). Sudden arousals and fragmentation of sleep are also described in patients (Picard and Brodtkorb, 2008). The autosomal dominant form (ADNFLE) of the disease is often linked to mutant subunits of the heteromeric nAChRs (Ferini-Strambi et al., 2012; Picard and Brodtkorb, 2008). To date, four mutations in CHRNA4, two in CHRNA2 and six in CHRNB2 are known to be linked to ADNFLE, in line with the major role of heteromeric nAChRs in the control of cortical excitability (Wallace and Bertrand, 2013). When expressed in heterologous systems, most of these mutations lead to a gain of nAChR function, e. g. because of increased sensitivity to the agonist or other kinetic alterations (Becchetti et al., 2015). Because nAChRs regulate both synaptic maturation during development and the excitability in adult networks, a general problem in the field is understanding whether and how hyperfunctional nAChRs can lead to the pathology by affecting both of these processes.

Murine models of ADNFLE

During the last ten years, several mouse models of ADNFLE were generated, which mimic several features of this syndrome, such as alterations in arousal/sleep physiology and the occurrence of seizures. Knock-in strains were produced in C57BL/6J background, expressing α4-S252F or α4-+L264 mutations, homologous to the human α4-S248F and α4-(776ins3) mutations (Klaassen et al., 2006). These mice show a severe profile, with recurrent seizures not related to sleep. Teper generated a mixed CD1-129/Sv strain expressing α4-S248F, with a milder phenotype, including motor features but not spontaneous epileptiform EEG waves (Teper et al., 2007). β2-V287L is another widely studied mutant subunit (De Fusco et al., 2000). A knock-in strain expressing this mutation in C57BL/6 mice displays a disturbed sleep pattern, hypersensitivity to nicotine, but no spontaneous seizures (Xu et al., 2011). The same mutation expressed in rats produces seizures similar to "paroxysmal arousals" that are observed in human ADNFLE (Shiba et al., 2015). All of these knock-in models rarely show morphological changes in the brain. To better understand the pathogenic mechanism, Manfredi and colleagues developed conditional strains expressing, in FVB background, the β2-V287L subunit, under control of the tetracycline promoter (TET-off system; Manfredi et al., 2009). Expression of β2-V287L produces spontaneous seizures, generally occurring during periods of increased delta wave activity. Silencing the transgene expression by administering doxycycline in adult mice does not revert the epileptic phenotype. On the other hand, no seizures are observed when the transgene is silenced until the

postnatal day 15, even if the transgene is expressed at later stages. This suggests that β2-V287L exerts the epileptogenic action during sensitive phase of network development. Thus, critical stages of synaptic stabilization may be implicated in ADNFLE, in line with recent evidence indicating that nAChRs are involved in neuronal development (Bruel-Jungerman et al., 2011; Molas and Dierssen, 2014).

The mature neocortical circuit in an ADNFLE model expressing β2-V287L

Understanding the modulation exerted by nicotine on PFC synaptic transmission is crucial to investigate the implication of mutant nAChRs in the ADNFLE phenotype (Picard and Brodkorb, 2008). A typical feature of ADNFLE is the presence of stereotyped motor events accompanying the seizures, suggesting an activation of motor patterns. Fr2 (also known as M2; Aracri et al., 2015) is a premotor area and could be particularly relevant for ADNFLE. Moreover, this area is very sensitive to nicotinic stimulation in layer V (Aracri et al., 2010, 2013). In the last few years, we have investigated the mature ADNFLE network rearrangement and sensitivity to the modulation exerted by nicotine, by using Manfredi's murine model (Manfredi et al., 2009). We observed that persistent β2-V287L expression can alter the excitatory/inhibitory balance both in basal conditions and in response to nicotinic exposure. Exclusively in transgenic mice, we observed anomalous inhibitory events when the network was disinhibited by 4-Aminopyridine (4AP) and 0 $[Mg^{2+}]_o$ (Avoli et al., 2005; Trevelyan et

al., 2007), and rebound paroxysmal excitatory events and oscillatory epileptiform activity, after Mg^{2+} reintroduction. Therefore, β2-V287L induces a hyperexcitabilty in the transgenic mature network, which does not depend on nAChRs activation, but is due to stable synaptic alterations. We hypothesize these latter result from nAChR dysfunction during the synaptogenesis. In addition, in mice expressing the transgene, the nicotinic effects are amplified because of the presence of mutant hyperfunctional nAChRs, which further promotes hyperexcitability in layer V of Fr2 (Meneghini et al., 2017).

PART III - NICOTINIC RECEPTORS REGULATE THE DEVELOPING CORTICAL CIRCUITS

Cortical development is very complex: around birth, neurite outgrowth, synaptogenesis, myelinisation and circuit maturation constitute the so-called “brain growth spurt” (Eriksson et al., 2000), which leads to the highly interconnected structure of the mature brain. In rodents, at birth, pyramidal neurons and interneurons present scarce functional synapses. Subsequently, small apical dendrites show GABAergic post-synaptic currents. Finally, glutamatergic transmission appears (Ben-Ari et al., 2012).

The developmental expression of nAChRs and their role in cortical network maturation

Nicotinic receptors are among the first membrane proteins to appear during embryogenesis: both nAChR subunits and mRNAs are detectable in pre-migratory neural crest cells *in vitro* (Howard et al., 1995), which will give rise to most peripheral neurons. From embryonic day 2 they are detectable in the murine central nervous system (Zoli et al. 1995) and in autonomic and sensory neurons (Role and Berg, 1996). nAChRs expression anticipates cholinergic innervation and is responsible for neuronal differentiation. Cholinergic neurons are generated between E11 and E16 (Lauder and Schambra, 1999), but cholinergic innervation in the forebrain is detectable during the first postnatal weeks (Mansvelder and Role, 2006) and is involved in

synaptic refinement. Between P7 and P14, different nAChR subtypes reach the highest expression levels in the rodent hippocampus and neocortex (Molas and Dierssen, 2014), which is thought to be required for brain circuit maturation and excitatory glutamatergic synaptogenesis. In particular, β2 mRNA is low on P7 and increases by P14, while α7 is maximum at P7; α4 peaks on P14 and remains high on P28 (Abreu-Villaça et al., 2011). After the second postnatal week the nAChRs mRNA expression tends to decrease. In adult brains, the expression of most nAChR genes reaches the steady state.

The nAChRs roles depend on regional and temporal expression of the different subunits. After knocking-out β2 or α7, widespread changes in synapse distribution and dendritic structure are observed (Molas and Dierssen, 2014). Moreover, cortical cholinergic de-afferentiation results in smaller somata, dendritic abnormalities and altered connectivity (Hohmann, 2003). Consistently, the cholinergic system maturation is crucial for proper cognitive development, and impairment of nAChRs is linked to developmental disorders (Bruel-Jungerman et al., 2011). ACh may act as a trophic factor, promoting a favourable environment for neuronal maturation and contributing to enhance synaptic signalling. In particular, heteromeric nAChRs deeply affect the formation of dendritic spines and the localization of glutamatergic synapses (Lozada et al., 2012), which is likely to have long-term effects on signal integration and transmission (Yuste and Bonhoeffer, 2001). A possible mechanism is the regulation of cytoskeletal dynamics, through nAChR-regulated Ca^{2+} influx, stimulating CaMKII-dependent signalling and other Ca^{2+}-sensitive events. Moreover, nAChRs can directly interact with cell adhesion molecules like neurexin-1 or

ephrinB2, to induce synapse formation (Cheng et al., 2009; Liu et al., 2008). Finally, because nicotinic receptors modulate the release of other neurotransmitters, they are believed to be relevant for a proper maturation of several neurotransmitter systems (Abreu-Villaça et al., 2011).

Importantly, the peak of postnatal expression of nAChRs coincides with the excitatory to inhibitory GABAergic switch, which is also implicated in neuronal circuit maturation.

The excitatory to inhibitory GABAergic switch

The γ-aminobutyric acid (GABA) is the main inhibitory neurotransmitter in the mature central nervous system. The rapid GABAergic effect is mediated by the ionotropic receptors ($GABA_ARs$), which are permeable to Cl^- and HCO_3^- (with HCO_3^-/Cl^- permeability ratio of 0.2 – 0.4; Kaila, 1994; Farrant and Kaila, 2007). Because of the prevalence of Cl^- permeability, the $GABA_AR$ reversal potential is largely dependent on the equilibrium potential for Cl^- (E_{Cl}).

According to the Nernst equation, $E_{Cl} = \frac{RT}{zF} * \ln \frac{[Cl-]o}{[Cl-]i}$, where R is the gas constant, F the Faraday constant, T the temperature, z the valence of the ion. $[Cl^-]_o$ is quite stable at ~120 mM. Therefore, $[Cl^-]_i$ is the crucial parameter. In adult neurons, $[Cl^-]_i$ is about 6-7 mM and E_{Cl} is ~ -80 mV. Therefore, E_{GABA} is approximately -70 mV, close to the resting membrane potential (V_{rest}). In this case, opening $GABA_ARs$ tends to maintain V_{rest} far from the spike threshold. In immature neurons, $[Cl^-]_i$ is about 25-30 mM, so that E_{Cl} is considerably depolarized (-30 to -50

mV). Hence, $GABA_A$ activation induces an efflux of Cl^-, which depolarizes the target cell (Ben-Ari et al., 2012; Kaila et al., 2014). Hence, during development, GABA exerts an excitatory role, which is necessary for neuronal maturation and circuits integration (Ge et al., 2006), probably through mechanisms depending on the regulation of voltage-dependent calcium channels. One such mechanism is the generation of synchronized "giant depolarizing potentials", which are implicated in neuronal differentiation and maturation of the synaptic connections (Ben-Ari, 2002).

$[Cl^-]_i$ is mainly set by the balance of two cation-chloride cotransporters: the Na^+-K^+-Cl^- Cotransporter type 1 (NKCC1) and the K-Cl^- Cotransporter type 2 (KCC2). NKCC1 is ubiquitously and highly expressed during embryogenesis and early postnatal life (Blaesse and Schmidt, 2015; Hubner et al., 2001). By exploiting the sodium and potassium gradients, NKCC1 pumps Cl^- inwardly, at the nominal thermodynamic equilibrium of -8 mV (Kaila et al., 2014). This guarantees the early depolarizing effect of GABA. After the first postnatal week, KCC2 expression in neurons gradually increases, and reaches its peak by the end of the second postnatal week (Rivera et al., 1999). KCC2 takes advantage of transmembrane K^+ gradient to extrude Cl^- (Kaila et al., 2014). This produces a negative shift of E_{Cl}, which allows the inhibitory action of GABA. Moreover, KCC2 is thought to also exert more direct effects on glutamatergic synaptogenesis by physically interacting with several membrane and cytoscheletral proteins of the dendritic spine (Kovàcs et al., 2014). The expression ratio of NKCC1 and KCC2 and their serine-threonine phosphorylation state are crucial to finely modulate E_{Cl}, and thus the GABA function,

during development. Overall, the precise timing of the GABAergic switch is fundamental for proper network maturation (Ge et al., 2006). An unbalanced cotransporters' activity is implicated in epileptogenesis (Kahle et al., 2014).

nAChRs role in the GABAergic switch

Recent evidence suggests that the above-mentioned role of nAChRs in synaptogenesis may also involve the Cl^- transporters. In fact, the expression of the ADNFLE-linked mutant α4-S284L subunit in mice is accompanied by an altered KCC2/NKCC1 ratio (Yamanada et al., 2013; Zhu et al., 2008), and nicotine modulates KCC2 during early postnatal life in rat hippocampus (Damborsky and Winzer-Serhan, 2012). Moreover, the spontaneous nAChRs activity regulates the timing of GABAergic switch in neuronal cultures (Liu et al., 2006). In particular, the excitatory GABAergic response is sustained in the presence of different nAChR blockers. Moreover, in α7 nAChR knock-out mice, the GABAergic switch results delayed, as NKCC1 is abnormally high and KCC2 remains lower than in wild type. The underlying cellular and molecular mechanisms are poorly understood; one possibility is that nicotine modulates expression of the chloride cotransporter genes by regulating calcium influx (Liu et al., 2006).

SCOPE OF THE THESIS

The aim of this thesis is to characterize some aspects of the fine adjustment of prefrontal cortex (PFC) function exerted by the cholinergic and other neuromodulatory systems, as the noradrenergic and orexinergic, in developing and mature networks. In particular, I focus on the activity of pyramidal cells in layer V, which are a central component of the cortical circuit excitability. In this way, I intend to comprehend how dysregulation of regulatory systems alters cortical excitability and the possible implications in several sleep-related pathologies, such as ADNFLE and narcolepsy with cataplexy.

In chapter 2, I investigated how β2-V287L, a mutant subunit of the nicotinic receptor (nAChR) linked to ADNFLE, affects the development of thalamic and cortical networks, in a murine model of ADNFLE. β2-V287L turned out to alter the timing of expression of KCC2 in PFC, and thus the GABAergic switch, which may explain the widespread alterations of synaptic balance and excitability observed in the mature circuits of mice expressing β2-V287L.

Chapter 3 explores some aspects of the complex interplay between the main neurotransmitters involved in cortical arousal, i. e. acetylcholine (ACh), norepinephrine (NE) and orexin A (OrxA), onto layer V excitability. ACh, NE and OrxA turned out to cooperate to enhance the excitatory input onto pyramidal neurons.

These investigations may yield new insights into the complex regulation of the PFC microcircuit and the pathogenic mechanisms responsible of altered cortical activity in some sleep-related disorders.

REFERENCES

Abreu-Villaça, Y., Filgueiras, C. C., & Manhães, A. C. (2011). Developmental aspects of the cholinergic system. *Behavioural Brain Research*, *221*(2), 367-378.

Albuquerque, E. X., Pereira, E. F., Alkondon, M., & Rogers, S. W. (2009). Mammalian nicotinic acetylcholine receptors: from structure to function. *Physiological Reviews*, *89*(1), 73-120.

Ammoun, S., Holmqvist, T., Shariatmadari, R., Oonk, H. B., Detheux, M., Parmentier, M., ... & Kukkonen, J. P. (2003). Distinct recognition of OX1 and OX2Receptors by orexin peptides. *Journal of Pharmacology and Experimental Therapeutics*, *305*(2), 507-514.

Aracri, P., Amadeo, A., Pasini, M. E., Fascio, U., & Becchetti, A. (2013). Regulation of glutamate release by heteromeric nicotinic receptors in layer V of the secondary motor region (Fr2) in the dorsomedial shoulder of prefrontal cortex in mouse. *Synapse*, *67*(6), 338-357.

Aracri, P., Banfi, D., Pasini, M. E., Amadeo, A., & Becchetti, A. (2015). Hypocretin (orexin) regulates glutamate input to fast-spiking interneurons in layer V of the Fr2 region of the murine prefrontal cortex. *Cerebral Cortex*, *25*(5), 1330-1347.

Aracri, P., Consonni, S., Morini, R., Perrella, M., Rodighiero, S., Amadeo, A., & Becchetti, A. (2010). Tonic modulation of GABA release by nicotinic acetylcholine receptors in layer V of the murine prefrontal cortex. *Cerebral Cortex*, *20*(7), 1539-1555.

Aracri, P., Meneghini, S., Coatti, A., Amadeo, A., & Becchetti, A. (2017). α4β2∗ nicotinic receptors stimulate GABA release onto fast-spiking cells in layer V of mouse prefrontal (Fr2) cortex. *Neuroscience*, *340*, 48-61.

Aston-Jones, G., & Bloom, F. E. (1981). Activity of norepinephrine-containing locus coeruleus neurons in behaving rats anticipates

fluctuations in the sleep-waking cycle. *Journal of Neuroscience*, *1*(8), 876-886.

Avoli, M., Louvel, J., Pumain, R., & Köhling, R. (2005). Cellular and molecular mechanisms of epilepsy in the human brain. *Progress in Neurobiology*, *77*(3), 166-200.

Bach-y-Rita, P. (1996). Nonsynaptic diffusion neurotransmission and brain plasticity. *The Neuroscientist*, *2*(5), 260-261.

Bailey, C. D., De Biasi, M., Fletcher, P. J., & Lambe, E. K. (2010). The nicotinic acetylcholine receptor α5 subunit plays a key role in attention circuitry and accuracy. *Journal of Neuroscience*, *30*(27), 9241-9252.

Bayer, L., Eggermann, E., Saint-Mleux, B., Machard, D., Jones, B. E., Mühlethaler, M., & Serafin, M. (2002). Selective action of orexin (hypocretin) on nonspecific thalamocortical projection neurons. *Journal of Neuroscience*, *22*(18), 7835-7839.

Becchetti, A., Aracri, P., Meneghini, S., Brusco, S., & Amadeo, A. (2015). The role of nicotinic acetylcholine receptors in autosomal dominant nocturnal frontal lobe epilepsy. *Frontiers in Physiology*, *6*.

Ben-Ari, Y. (2002). Excitatory actions of gaba during development: the nature of the nurture. *Nature Reviews Neuroscience*, *3*(9), 728-739.

Ben-Ari, Y., Khalilov, I., Kahle, K. T., & Cherubini, E. (2012). The GABA excitatory/inhibitory shift in brain maturation and neurological disorders. *The Neuroscientist*, *18*(5), 467-486.

Berridge, C. W., & Abercrombie, E. D. (1999). Relationship between locus coeruleus discharge rates and rates of norepinephrine release within neocortex as assessed by in vivo microdialysis. *Neuroscience*, *93*(4), 1263-1270.

Berridge, C. W., & Waterhouse, B. D. (2003). The locus coeruleus–noradrenergic system: modulation of behavioral state and state-dependent cognitive processes. *Brain Research Reviews*, *42*(1), 33-84.

Blaesse, P., & Schmidt, T. (2015). K-Cl cotransporter KCC2—a moonlighting protein in excitatory and inhibitory synapse development and function. *Pflügers Archiv-European Journal of Physiology*, *467*(4), 615-624.

Boutrel, B., Cannella, N., & de Lecea, L. (2010). The role of hypocretin in driving arousal and goal-oriented behaviors. *Brain Research*, *1314*, 103-111.

Bruel-Jungerman, E., Lucassen, P. J., & Francis, F. (2011). Cholinergic influences on cortical development and adult neurogenesis. *Behavioural Brain Research*, *221*(2), 379-388.

Castner, S. A., Smagin, G. N., Piser, T. M., Wang, Y., Smith, J. S., Christian, E. P., ... & Williams, G. V. (2011). Immediate and sustained improvements in working memory after selective stimulation of α7 nicotinic acetylcholine receptors. *Biological Psychiatry*, *69*(1), 12-18.

Chemelli, R. M., Willie, J. T., Sinton, C. M., Elmquist, J. K., Scammell, T., Lee, C., ... & Fitch, T. E. (1999). Narcolepsy in orexin knockout mice: molecular genetics of sleep regulation. *Cell*, *98*(4), 437-451.

Cheng, S. B., Amici, S. A., Ren, X. Q., McKay, S. B., Treuil, M. W., Lindstrom, J. M., ... & Anand, R. (2009). Presynaptic targeting of α4β2 nicotinic acetylcholine receptors is regulated by neurexin-1β. *Journal of Biological Chemistry*, *284*(35), 23251-23259.

Condé, F., Maire-lepoivre, E., Audinat, E., & Crepel, F. (1995). Afferent connections of the medial frontal cortex of the rat. II. Cortical and subcortical afferents. *Journal of Comparative Neurology*, *352*(4), 567-593.

Couey, J. J., Meredith, R. M., Spijker, S., Poorthuis, R. B., Smit, A. B., Brussaard, A. B., & Mansvelder, H. D. (2007). Distributed network actions by nicotine increase the threshold for spike-timing-dependent plasticity in prefrontal cortex. *Neuron*, *54*(1), 73-87.

Croxson, P. L., Kyriazis, D. A., & Baxter, M. G. (2011). Cholinergic modulation of a specific memory function of prefrontal cortex. *Nature Neuroscience*, *14*(12), 1510-1512.

Damborsky, J. C., & Winzer-Serhan, U. H. (2012). Effects of sex and chronic neonatal nicotine treatment on Na 2+/K+/Cl− co-transporter 1, K+/Cl− co-transporter 2, brain-derived neurotrophic factor, NMDA receptor subunit 2A and NMDA receptor subunit 2B mRNA expression in the postnatal rat hippocampus. *Neuroscience*, *225*, 105-117.

Dani, J. A., & Bertrand, D. (2007). Nicotinic acetylcholine receptors and nicotinic cholinergic mechanisms of the central nervous system. *Annual Review of Pharmacology and Toxicology*, *47*, 699-729.

De Fusco, M., Becchetti, A., Patrignani, A., Annesi, G., Gambardella, A., Quattrone, A., ... & Casari, G. (2000). The nicotinic receptor β2 subunit is mutant in nocturnal frontal lobe epilepsy. *Nature Genetics*, *26*(3), 275-276.

De Lecea, L., Kilduff, T. S., Peyron, C., Gao, X. B., Foye, P. E., Danielson, P. E., ... & Frankel, W. N. (1998). The hypocretins: hypothalamus-specific peptides with neuroexcitatory activity. *Proceedings of the National Academy of Sciences*, *95*(1), 322-327.

Dembrow, N., & Johnston, D. (2014). Subcircuit-specific neuromodulation in the prefrontal cortex. *Frontiers in Neural Circuits*, *8*.

Descarries, L., Gisiger, V., & Steriade, M. (1997). Diffuse transmission by acetylcholine in the CNS. *Progress in Neurobiology*, *53*(5), 603-625.

Dohlman, H. G., Thorner, J., Caron, M. G., & Lefkowitz, R. J. (1991). Model systems for the study of seven-transmembrane-segment receptors. *Annual Review of Biochemistry*, *60*(1), 653-688.

Eggermann, E., Serafin, M., Bayer, L., Machard, D., Saint-Mleux, B., Jones, B. E., & Mühlethaler, M. (2001). Orexins/hypocretins excite basal forebrain cholinergic neurones. *Neuroscience*, *108*(2), 177-181.

Eriksson, P., Ankarberg, E., & Fredriksson, A. (2000). Exposure to nicotine during a defined period in neonatal life induces permanent changes in brain nicotinic receptors and in behaviour of adult mice. *Brain Research*, *853*(1), 41-48.

Fadel, J., & Burk, J. A. (2010). Orexin/hypocretin modulation of the basal forebrain cholinergic system: role in attention. *Brain Research*, *1314*, 112-12.

Fadel, J., & Deutch, A. Y. (2002). Anatomical substrates of orexin–dopamine interactions: lateral hypothalamic projections to the ventral tegmental area. *Neuroscience*, *111*(2), 379-387.

Fadel, J., Pasumarthi, R., & Reznikov, L. R. (2005). Stimulation of cortical acetylcholine release by orexin A. *Neuroscience*, *130*(2), 541-547.

Farrant, M., & Kaila, K. (2007). The cellular, molecular and ionic basis of GABA A receptor signalling. *Progress in Brain Research*, *160*, 59-87.

Ferini-Strambi, L., Sansoni, V., & Combi, R. (2012). Nocturnal frontal lobe epilepsy and the acetylcholine receptor. *The Neurologist*, *18*(6), 343-349.

Foehring, R. C., Schwindt, P. C., & Crill, W. E. (1989). Norepinephrine selectively reduces slow Ca2+-and Na+-mediated K+ currents in cat neocortical neurons. *Journal of Neurophysiology*, *61*(2), 245-256.

Franklin, K. J. B., Chudasama, Y., Watson, C., Paxinos, G., & Puelles, L. (2011). The prefrontal cortex. *The Mouse Nervous System*, 727-735.

Fucile, S. (2004). Ca 2+ permeability of nicotinic acetylcholine receptors. *Cell Calcium*, *35*(1), 1-8.

Fuster, J. M., & Bressler, S. L. (2015). Past makes future: Role of pFC in prediction. *Journal of Cognitive Neuroscience*.

Ge, S., Goh, E. L., Sailor, K. A., Kitabatake, Y., Ming, G. L., & Song, H. (2006). GABA regulates synaptic integration of newly generated neurons in the adult brain. *Nature*, *439*(7076), 589-593.

Gotti, C., & Clementi, F. (2004). Neuronal nicotinic receptors: from structure to pathology. *Progress in Neurobiology*, *74*(6), 363-396.

Gotti, C., Moretti, M., Gaimarri, A., Zanardi, A., Clementi, F., & Zoli, M. (2007). Heterogeneity and complexity of native brain nicotinic receptors. *Biochemical Pharmacology*, *74*(8), 1102-1111.

Guillem, K., Bloem, B., Poorthuis, R. B., Loos, M., Smit, A. B., Maskos, U., ... & Mansvelder, H. D. (2011). Nicotinic acetylcholine receptor β2 subunits in the medial prefrontal cortex control attention. *Science*, *333*(6044), 888-891.

Heidbreder, C. A., & Groenewegen, H. J. (2003). The medial prefrontal cortex in the rat: evidence for a dorso-ventral distinction based upon functional and anatomical characteristics. *Neuroscience & Biobehavioral Reviews*, *27*(6), 555-579.

Hogg, R. C., Raggenbass, M., & Bertrand, D. (2003). Nicotinic acetylcholine receptors: from structure to brain function. *Reviews of Physiology, Biochemistry and Pharmacology* (pp. 1-46). Springer Berlin Heidelberg.

Hohmann, C. F. (2003). A morphogenetic role for acetylcholine in mouse cerebral neocortex. *Neuroscience & Biobehavioral Reviews*, *27*(4), 351-363.

Hoover, W. B., & Vertes, R. P. (2007). Anatomical analysis of afferent projections to the medial prefrontal cortex in the rat. *Brain Structure and Function*, *212*(2), 149-179.

Howard, M. J., Gershon, M. D., & Margiotta, J. F. (1995). Expression of nicotinic acetylcholine receptors and subunit mRNA transcripts in cultures of neural crest cells. *Developmental Biology*, *170*(2), 479-495.

Hübner, C. A., Lorke, D. E., & Hermans-Borgmeyer, I. (2001). Expression of the Na-K-2Cl-cotransporter NKCC1 during mouse development. *Mechanisms of Development*, *102*(1), 267-269.

Iversen, L., Iversen, S., Bloom, F. E., & Roth, R. H. (2008). *Introduction to Neuropsychopharmacology*. Oxford University Press.

Jacobs, B. L., & Fornal, C. A. (1991). Activity of brain serotonergic neurons in the behaving animal. *Pharmacological Reviews*, *43*(4), 563-578.

Jones, B. E. (2005). From waking to sleeping: neuronal and chemical substrates. *Trends in Pharmacological Sciences*, *26*(11), 578-586.

Jones, B. E. (2008). Modulation of cortical activation and behavioral arousal by cholinergic and orexinergic systems. *Annals of the New York Academy of Sciences*, *1129*(1), 26-34.

Jones, B. E. (2011). Neurobiology of waking and sleeping. *Handbook of Clinical Neurology*, *98*, 131.

Kahle, K. T., Merner, N. D., Friedel, P., Silayeva, L., Liang, B., Khanna, A., ... & Dion, P. A. (2014). Genetically encoded impairment of neuronal KCC2 cotransporter function in human idiopathic generalized epilepsy. *EMBO Reports*, e201438840.

Kaila, K. (1994). Ionic basis of GABA A receptor channel function in the nervous system. *Progress in Neurobiology*, *42*(4), 489-537.

Kaila, K., Price, T. J., Payne, J. A., Puskarjov, M., & Voipio, J. (2014). Cation-chloride cotransporters in neuronal development, plasticity and disease. *Nature Reviews Neuroscience*, *15*(10), 637-654.

Kargo, W. J., Szatmary, B., & Nitz, D. A. (2007). Adaptation of prefrontal cortical firing patterns and their fidelity to changes in action–reward contingencies. *Journal of Neuroscience*, *27*(13), 3548-3559.

Kassam, S. M., Herman, P. M., Goodfellow, N. M., Alves, N. C., & Lambe, E. K. (2008). Developmental excitation of corticothalamic

neurons by nicotinic acetylcholine receptors. *Journal of Neuroscience*, *28*(35), 8756-8764.

Kawaguchi, Y., & Kubota, Y. (1998). Neurochemical features and synaptic connections of large physiologically-identified GABAergic cells in the rat frontal cortex. *Neuroscience*, *85*(3), 677-701.

Kawaguchi, Y., & Shindou, T. (1998). Noradrenergic excitation and inhibition of GABAergic cell types in rat frontal cortex. *Journal of Neuroscience*, *18*(17), 6963-6976.

Klaassen, A., Glykys, J., Maguire, J., Labarca, C., Mody, I., & Boulter, J. (2006). Seizures and enhanced cortical GABAergic inhibition in two mouse models of human autosomal dominant nocturnal frontal lobe epilepsy. *Proceedings of the National Academy of Sciences*, *103*(50), 19152-19157.

Kovács, K., Basu, K., Rouiller, I., & Sík, A. (2014). Regional differences in the expression of K+–Cl− 2 cotransporter in the developing rat cortex. *Brain Structure and Function*, *219*(2), 527-538.

Kubota, Y. (2014). Untangling GABAergic wiring in the cortical microcircuit. *Current opinion in Neurobiology*, *26*, 7-14.

Kukkonen, J. P. (2013). Physiology of the orexinergic/hypocretinergic system: a revisit in 2012. *American Journal of Physiology-Cell Physiology*, *304*(1), C2-C32.

Kukkonen, J. P., & Leonard, C. S. (2014). Orexin/hypocretin receptor signalling cascades. *British Journal of Pharmacology*, *171*(2), 314-331.

Lambe, E. K., & Aghajanian, G. K. (2003). Hypocretin (orexin) induces calcium transients in single spines postsynaptic to identified thalamocortical boutons in prefrontal slice. *Neuron*, *40*(1), 139-150.

Lambe, E. K., Liu, R. J., & Aghajanian, G. K. (2007). Schizophrenia, hypocretin (orexin), and the thalamocortical activating system. *Schizophrenia Bulletin*, *33*(6), 1284-1290.

Lambe, E. K., Olausson, P., Horst, N. K., Taylor, J. R., & Aghajanian, G. K. (2005). Hypocretin and nicotine excite the same thalamocortical synapses in prefrontal cortex: correlation with improved attention in rat. *Journal of Neuroscience*, *25*(21), 5225-5229.

Lambe, E. K., Picciotto, M. R., & Aghajanian, G. K. (2003). Nicotine induces glutamate release from thalamocortical terminals in prefrontal cortex. *Neuropsychopharmacology*, *28*(2), 216-225.

Lauder, J. M., & Schambra, U. B. (1999). Morphogenetic roles of acetylcholine. *Environmental Health Perspectives*, *107*(Suppl 1), 65.

Law-Tho, D., Crepel, F., & Hirsch, J. C. (1993). Noradrenaline Decreases Transmission of NMDA-and Non-NMDA-receptor Mediated Monosynaptic EPSPs in Rat Prefrontal Neurons In Vitro. *European Journal of Neuroscience*, *5*(11), 1494-1500.

Lee, M. G., Hassani, O. K., & Jones, B. E. (2005). Discharge of identified orexin/hypocretin neurons across the sleep-waking cycle. *Journal of Neuroscience*, *25*(28), 6716-6720.

Lehmenkühler, C., Walden, J., & Speckmann, E. J. (1991). Decrease of N-Methyl-D-aspartate responses by noradrenaline in the rat motorcortex in vivo. *Neuroscience Letters*, *121*(1), 5-8.

Li, B., Chen, F., Ye, J., Chen, X., Yan, J., Li, Y., ... & Hu, Z. (2010). The modulation of orexin A on HCN currents of pyramidal neurons in mouse prelimbic cortex. *Cerebral Cortex*, *20*(7), 1756-1767.

Li, S. B., Jones, J. R., & de Lecea, L. (2016). Hypocretins, neural systems, physiology, and psychiatric disorders. *Current Psychiatry Reports*, *18*(1), 7.

Liu, R. J., & Aghajanian, G. K. (2008). Stress blunts serotonin-and hypocretin-evoked EPSCs in prefrontal cortex: role of corticosterone-mediated apical dendritic atrophy. *Proceedings of the National Academy of Sciences*, *105*(1), 359-364.

Liu, Z., Conroy, W. G., Stawicki, T. M., Nai, Q., Neff, R. A., & Berg, D. K. (2008). EphB receptors co-distribute with a nicotinic receptor

subtype and regulate nicotinic downstream signaling in neurons. *Molecular and Cellular Neuroscience*, *38*(2), 236-244.

Liu, Z., Neff, R. A., & Berg, D. K. (2006). Sequential interplay of nicotinic and GABAergic signaling guides neuronal development. S*cience*, *314*(5805), 1610-1613.

Lozada, A. F., Wang, X., Gounko, N. V., Massey, K. A., Duan, J., Liu, Z., & Berg, D. K. (2012). Induction of dendritic spines by β2-containing nicotinic receptors. *Journal of Neuroscience*, *32*(24), 8391-8400.

Lüthi, A. (2014). Sleep spindles: where they come from, what they do. *The Neuroscientist*, *20*(3), 243-256.

Maloney, K. J., Mainville, L., & Jones, B. E. (2002). c-Fos expression in dopaminergic and GABAergic neurons of the ventral mesencephalic tegmentum after paradoxical sleep deprivation and recovery. *European Journal of Neuroscience*, *15*(4), 774-778.

Manfredi, I., Zani, A. D., Rampoldi, L., Pegorini, S., Bernascone, I., Moretti, M., ... & Sala, M. (2009). Expression of mutant β2 nicotinic receptors during development is crucial for epileptogenesis. *Human Molecular Genetics*, *18*(6), 1075-1088.

Mansvelder, H. D., & Role, L. W. (2006). Neuronal receptors for nicotine: functional diversity and developmental changes. *Brain Development: Normal Processes and the Effects of Alcohol and Nicotine*, 341-362.

Marcus, J. N., Aschkenasi, C. J., Lee, C. E., Chemelli, R. M., Saper, C. B., Yanagisawa, M., & Elmquist, J. K. (2001). Differential expression of orexin receptors 1 and 2 in the rat brain. *Journal of Comparative Neurology*, *435*(1), 6-25.

Meneghini, S., Brusco, S., Coatti, A., Aracri. P., Modena. D., Carraresi. L., Arcangeli. A., Amadeo. A., & Becchetti, A. (2017). The role of neuronal nicotinic receptors in the pathogenesis of autosomal dominant nocturnal frontal lobe epilepsy: a study on wild-type and conditional

transgenic mice expressing the β2-V287L subunit. *Fondazione Telethon XIX Scientific Convention.*

Mesulam, M., Mufson, E. J., Levey, A. I., & Wainer, B. H. (1983). Cholinergic innervation of cortex by the basal forebrain: cytochemistry and cortical connections of the septal area, diagonal band nuclei, nucleus basalis (substantia innominata), and hypothalamus in the rhesus monkey. *Journal of Comparative Neurology*, *214*(2), 170-197.

Miyazawa, A., Fujiyoshi, Y., & Unwin, N. (2003). Structure and gating mechanism of the acetylcholine receptor pore. *Nature*, *423*(6943), 949-955.

Molas, S., & Dierssen, M. (2014). The role of nicotinic receptors in shaping and functioning of the glutamatergic system: A window into cognitive pathology. *Neuroscience & Biobehavioral Reviews*, *46*, 315-325.

Morales-Perez, C. L., Noviello, C. M., & Hibbs, R. E. (2016). X-ray structure of the human α4β2 nicotinic receptor. *Nature*, *538*(7625), 411-415.

Mouradian, R. D., Sessler, F. M., & Waterhouse, B. D. (1991). Noradrenergic potentiation of excitatory transmitter action in cerebrocortical slices: evidence for mediation by an α 1 receptor-linked second messenger pathway. *Brain Research*, *546*(1), 83-95.

Nelson, M. E., Kuryatov, A., Choi, C. H., Zhou, Y., & Lindstrom, J. (2003). Alternate stoichiometries of α4β2 nicotinic acetylcholine receptors. *Molecular Pharmacology*, *63*(2), 332-341.

Oishi, Y., Williams, R. H., Agostinelli, L., Arrigoni, E., Fuller, P. M., Mochizuki, T., ... & Scammell, T. E. (2013). Role of the medial prefrontal cortex in cataplexy. *Journal of Neuroscience*, *33*(23), 9743-9751.

Ozeki, H., Finn, I. M., Schaffer, E. S., Miller, K. D., & Ferster, D. (2009). Inhibitory stabilization of the cortical network underlies visual surround suppression. *Neuron*, *62*(4), 578-592.

Paterson, D., & Nordberg, A. (2000). Neuronal nicotinic receptors in the human brain. *Progress in Neurobiology*, *61*(1), 75-111.

Paxinos, G. (2015). Brain, Behaviour and Evolution. In *GeNeDis 2014* (pp. 1-1). Springer, Cham.

Peyron, C., Faraco, J., Rogers, W., Ripley, B., Overeem, S., Charnay, Y., ... & Li, R. (2000). A mutation in a case of early onset narcolepsy and a generalized absence of hypocretin peptides in human narcoleptic brains. *Nature Medicine*, *6*(9), 991-997.

Peyron, C., Tighe, D. K., Van Den Pol, A. N., De Lecea, L., Heller, H. C., Sutcliffe, J. G., & Kilduff, T. S. (1998). Neurons containing hypocretin (orexin) project to multiple neuronal systems. *Journal of Neuroscience*, *18*(23), 9996-10015.

Piantadosi, P. T., Holmes, A., Roberts, B. M., & Bailey, A. M. (2015). Orexin receptor activity in the basal forebrain alters performance on an olfactory discrimination task. *Brain Research*, *1594*, 215-222.

Picard, F., & Brodtkorb, E. (2008). Familial frontal lobe epilepsy. *Epilepsy. A Comprehensive Textbook*, 2495-2502.

Picciotto, M. R., Brunzell, D. H., & Caldarone, B. J. (2002). Effect of nicotine and nicotinic receptors on anxiety and depression. *Neuroreport*, *13*(9), 1097-1106.

Rivera, C., Voipio, J., Payne, J. A., Ruusuvuori, E., Lahtinen, H., Lamsa, K., ... & Kaila, K. (1999). The K+/Cl− co-transporter KCC2 renders GABA hyperpolarizing during neuronal maturation. *Nature*, *397*(6716), 251-255.

Role, L. W., & Berg, D. K. (1996). Nicotinic receptors in the development and modulation of CNS synapses. *Neuron*, *16*(6), 1077-1085.

Roychowdhury, S., Zwierzchowski, A. N., Garcia-Oscos, F., Olguin, R. C., Delgado, R. S., & Atzori, M. (2014). Layer-and area-specificity of the adrenergic modulation of synaptic transmission in the rat neocortex. *Neurochemical Research*, *39*(12), 2377-2384.

Sakurai, T., Amemiya, A., Ishii, M., Matsuzaki, I., Chemelli, R. M., Tanaka, H., ... & Arch, J. R. (1998). Orexins and orexin receptors: a family of hypothalamic neuropeptides and G protein-coupled receptors that regulate feeding behavior. *Cell*, *92*(4), 573-585.

Salgado, H., Garcia-Oscos, F., Patel, A., Martinolich, L., Nichols, J. A., Dinh, L., ... & Atzori, M. (2010). Layer-specific noradrenergic modulation of inhibition in cortical layer II/III. *Cerebral Cortex*, *21*(1), 212-221.

Saper, C. B., Chou, T. C., & Scammell, T. E. (2001). The sleep switch: hypothalamic control of sleep and wakefulness. *Trends in Neurosciences*, *24*(12), 726-731.

Saper, C. B., Fuller, P. M., Pedersen, N. P., Lu, J., & Scammell, T. E. (2010). Sleep state switching. *Neuron*, *68*(6), 1023-1042.

Sarter, M., Parikh, V., & Howe, W. M. (2009). nAChR agonist-induced cognition enhancement: integration of cognitive and neuronal mechanisms. *Biochemical Pharmacology*, *78*(7), 658-667.

Shiba, Y., Mori, F., Yamada, J., Migita, K., Nikaido, Y., Wakabayashi, K., ... & Ueno, S. (2015). Spontaneous epileptic seizures in transgenic rats harboring a human ADNFLE missense mutation in the β2-subunit of the nicotinic acetylcholine receptor. *Neuroscience research*, *100*, 46-54.

Shu, Y., Hasenstaub, A., & McCormick, D. A. (2003). Turning on and off recurrent balanced cortical activity. *Nature*, *423*(6937), 288-293.

Siegel, J. (2002). The neural pathways that produce arousal. *The Neural Control of Sleep and Waking*, 47-52.

Steriade, M., & McCarley, R. W. (2005). Brain control of sleep and wakefulness.

Sutcliffe, J. G., & de Lecea, L. (2002). The hypocretins: setting the arousal threshold. *Nature Reviews Neuroscience*, *3*(5), 339-349.

Teper, Y., Whyte, D., Cahir, E., Lester, H. A., Grady, S. R., Marks, M. J., ... & Labarca, C. (2007). Nicotine-induced dystonic arousal complex in a mouse line harboring a human autosomal-dominant nocturnal frontal lobe epilepsy mutation. *Journal of Neuroscience*, *27*(38), 10128-10142.

Tinuper, P., Bisulli, F., Cross, J. H., Hesdorffer, D., Kahane, P., Nobili, L., ... & Bassetti, C. (2016). Definition and diagnostic criteria of sleep-related hypermotor epilepsy. *Neurology*, *86*(19), 1834-1842.

Tremblay, R., Lee, S., & Rudy, B. (2016). GABAergic interneurons in the neocortex: from cellular properties to circuits. *Neuron*, *91*(2), 260-292.

Trevelyan, A. J., Sussillo, D., & Yuste, R. (2007). Feedforward inhibition contributes to the control of epileptiform propagation speed. *Journal of Neuroscience*, *27*(13), 3383-3387.

Uylings, H. B., Groenewegen, H. J., & Kolb, B. (2003). Do rats have a prefrontal cortex? *Behavioural Brain Research*, *146*(1), 3-17.

Vassalli, A., Dellepiane, J. M., Emmenegger, Y., Jimenez, S., Vandi, S., Plazzi, G., ... & Tafti, M. (2013). Electroencephalogram paroxysmal theta characterizes cataplexy in mice and children. *Brain*, *136*(5), 1592-1608.

Wallace, T. L., & Bertrand, D. (2013). Importance of the nicotinic acetylcholine receptor system in the prefrontal cortex. *Biochemical Pharmacology*, *85*(12), 1713-1720.

Wang, S., Kurada, L., Cilz, N. I., Chen, X., Xiao, Z., Dong, H., & Lei, S. (2013). Adenosinergic depression of glutamatergic transmission in the entorhinal cortex of juvenile rats via reduction of glutamate release probability and the number of releasable vesicles. *PloS One*, *8*(4), e62185.

Xia, J., Chen, X., Song, C., Ye, J., Yu, Z., & Hu, Z. (2005). Postsynaptic excitation of prefrontal cortical pyramidal neurons by hypocretin-

1/orexin a through the inhibition of potassium currents. *Journal of Neuroscience Research*, *82*(5), 729-736.

Xu, J., Cohen, B. N., Zhu, Y., Dziewczapolski, G., Panda, S., Lester, H. A., ... & Contractor, A. (2011). Altered activity–rest patterns in mice with a human autosomal-dominant nocturnal frontal lobe epilepsy mutation in the β2 nicotinic receptor. *Molecular Psychiatry*, *16*(10), 1048-1061.

Yamada, J., Zhu, G., Okada, M., Hirose, S., Yoshida, S., Shiba, Y., ... & Liu, F. (2013). A novel prophylactic effect of furosemide treatment on autosomal dominant nocturnal frontal lobe epilepsy (ADNFLE). *Epilepsy Research*, *107*(1), 127-137.

Yuste, R., & Bonhoeffer, T. (2001). Morphological changes in dendritic spines associated with long-term synaptic plasticity. *Annual Review of Neuroscience*, *24*(1), 1071-1089.

Zhu, G., Okada, M., Yoshida, S., Ueno, S., Mori, F., Takahara, T., ... & Sato, A. (2008). Rats harboring S284L Chrna4 mutation show attenuation of synaptic and extrasynaptic GABAergic transmission and exhibit the nocturnal frontal lobe epilepsy phenotype. *Journal of Neuroscience*, *28*(47), 12465-12476.

Zoli, M., Le Novere, N., Hill, J. A., & Changeux, J. P. (1995). Developmental regulation of nicotinic ACh receptor subunit mRNAs in the rat central and peripheral nervous systems. *Journal of Neuroscience*, *15*(3), 1912-1939.

Zolles, G., Wagner, E., Lampert, A., & Sutor, B. (2008). Functional expression of nicotinic acetylcholine receptors in rat neocortical layer 5 pyramidal cells. *Cerebral Cortex*, *19*(5), 1079-1091.

Chapter 2

POSTNATAL CHANGES IN K^+/Cl^- COTRANSPORTER-2 EXPRESSION IN THE FOREBRAIN OF MICE BEARING A MUTANT NICOTINIC SUBUNIT LINKED TO SLEEP-RELATED EPILEPSY

Alida Amadeo[a], Aurora Coatti[b*], Patrizia Aracri[b*], Miriam Ascagni[a], Davide Iannantuoni[a], Debora Modena[a], Laura Carraresi[d], Simone Brusco[b], Simone Meneghini[b], Annarosa Arcangeli[c], Maria Enrica Pasini[a], Andrea Becchetti[b]

Submitted: Neuroscience

[a]Department of Biosciences, University of Milano

[b]Department of Biotechnology and Biosciences, and NeuroMI-Milan Center of Neuroscience, University of Milano-Bicocca.

[c]Department of Experimental and Clinical Medicine, University of Florence.

[d]Dival Toscana Srl, Sesto Fiorentino, Firenze.

*These authors equally contributed to the paper.

Abbreviations

ADNFLE: autosomal dominant nocturnal frontal lobe epilepsy; AP: action potential; CTRL: transgenic mice not expressing β2-V287L; DLG: dorsal lateral geniculate thalamic nucleus; KCC2: K^+/Cl^- cotransporter-2; MAP: microtubule-associated protein; nAChR: nicotinic acetylcholine receptor; NKCC1: $Na^+/K^+/Cl^-$ cotransporter-1; PFC: prefrontal cortex; PV: paraventricular thalamic nucleus; RT: reticular thalamic nucleus; SS: somatosensory cortex; TH: thalamus; VB: ventrobasal thalamic complex; VLG: ventral lateral thalamic geniculate nucleus.

ABSTRACT

The $Na^+/K^+/Cl^-$ cotransporter-1 (NKCC1) and the K^+/Cl^- cotransporter-2 (KCC2) set the transmembrane Cl^- gradient in developing and mature brains, and are implicated in epileptogenesis. How these transporters are regulated in prefrontal cortex (PFC) and thalamus is largely unknown. We first studied the distribution of NKCC1 and KCC2 in developing wild-type (WT) mice. The amount of NKCC1 and KCC2 in PFC and somatosensory cortex progressively increased during the first two postnatal weeks. NKCC1 was found in neurons as well as astrocytes. KCC2 was mainly localized in neuronal somata at birth, and subsequently migrated to the somatodendritic membranes. Next, we investigated a mouse model of Autosomal Dominant Nocturnal Frontal Lobe Epilepsy (ADNFLE), bearing the mutant β2-V287L subunit of the nicotinic acetylcholine receptor (nAChR). In mice expressing the transgene, the KCC2 amount in PFC layer V was lower than in the control littermates at postnatal day 8 (P8), but reached higher amounts by P60. Consistently, the time course of the GABAergic excitatory to inhibitory switch was delayed in PFC layer V of mice carrying β2-V287L. Irrespective of genotype, NKCC1 and KCC2 were highly expressed in the neuropil of thalamic nuclei at birth. Their amount remained high in the adult sensory nuclei, whereas a significant decrease of KCC2 was observed in the reticular nucleus by P40. Such a decrease was more pronounced in mice expressing β2-V287L. Our results indicate that β2-containing nAChRs affect KCC2 expression levels during synaptogenesis as well as in mature circuits, which may contribute to the pathogenesis of sleep-related frontal epilepsy.

INTRODUCTION

The $Na^+/K^+/Cl^-$ cotransporter-1 (NKCC1) and the K^+/Cl^- cotransporter-2 (KCC2) are major regulators of the intracellular Cl^- concentration ($[Cl^-]_i$; Kaila et al., 2014a). In developing brains, the comparatively large amount of NKCC1 in neurons and astrocytes causes a high $[Cl^-]_i$. This maintains the reversal potential of the $GABA_A$ receptor currents (E_{GABA}) at depolarized values (Ben Ari et al., 2007). Under these conditions, GABA release produces depolarizing effects that modulate neuronal maturation and synaptogenesis (Ben Ari et al., 2007; Cancedda et al., 2007). Around birth, KCC2 expression progressively increases. By lowering $[Cl^-]_i$, KCC2 leads E_{GABA} to the typical hyperpolarized values observed in the adult brain (Rivera et al., 1999; Kaila et al., 2014a). In the murine neocortex, such 'GABAergic switch' occurs during the two first postnatal weeks, and is concomitant with the formation of GABAergic synapses (Takayama and Inoue, 2010). Therefore, it is thought to regulate the postnatal maturation of neuronal circuits (Ben-Ari et al., 2007; Ge et al., 2006).

The delicate balance of abundance and activity of NKCC1 and KCC2 is implicated in epileptogenesis as well as in the compensatory responses observed in hyperexcitable networks (Kaila et al., 2014b; Khirug et al., 2010). In fact, genetic variants of these cotransporters are linked to human idiopathic epilepsy (Kahle et al., 2014; Puskarjov et al., 2014). Epilepsy, however, comprises a heterogeneous spectrum of disorders (Jensen, 2011). The role of NKCC1 and KCC2 was extensively studied in parietal and temporal lobe epilepsy (Aronica et al., 2007; Awad et al., 2016; Dzhala et al., 2005; Karlócai et al., 2016;

Li et al., 2008; Pathak et al., 2007; Talos et al., 2012; Zhu et al., 2008), but not in frontal epilepsy. The latter presents different pathophysiological features, particularly in relation to the sleep-waking cycle. In the frontal lobe, sleep favors focal seizures, but not the occurrence of secondary generalization, whereas the opposite applies to the other cortical regions (Shouse and Quigg, 2008).

To address these issues, we focused on Autosomal Dominant Nocturnal Frontal Lobe Epilepsy (ADNFLE), the mendelian form of hypermotor sleep-related epilepsy, which is characterized by focal hyperkinetic seizures mainly occurring during stage II of sleep (Tinuper et al., 2016). ADNFLE is frequently caused by point mutations on genes coding for α or β subunits of the neuronal nicotinic acetylcholine receptor (nAChR; Tinuper et al., 2016). In the mammalian neocortex, the most widespread heteromeric nAChR is α4β2, and the first ADNFLE mutations identified on these subunits were α4-S248F (Steinlein et al., 1995) and β2-V287L (De Fusco et al., 2000). In heterologous expression systems, ADNFLE mutations often increase the nAChR function by augmenting its sensitivity to the agonists, or causing other kinetic alterations, at least in the heterozygous state (Becchetti et al., 2015). The first conditional murine model of ADNFLE, expressing β2-V287L in the brain under control of a tetracycline promoter, suggested that the transgene could exert its effects during synaptogenesis (Manfredi et al., 2009). Mice carrying β2-V287L develop spontaneous epileptiform seizures, mostly occurring during periods of increased delta electroencephalographic activity, which is typical of slow-wave sleep. For the epileptic phenotype to manifest, β2-V287L must be expressed throughout brain development, until the end of the second

postnatal week (Manfredi et al., 2009). These results agree with recent lines of evidence suggesting that nAChRs regulate synaptogenesis, even though the underlying cellular mechanisms are largely unknown (Molas and Dierssen, 2014). Because the spontaneous nAChR activity affects the developmental GABAergic switch in neuronal cultures (Liu et al., 2006), we hypothesized that nAChRs could also interact with the Cl^- cotransporters during neocortex maturation. In fact, both β2-containing nAChRs (Lozada et al., 2012) and KCC2 (Fiumelli et al., 2013; Li et al., 2007; Puskarjov et al., 2014) are involved in maturation and remodeling of dendritic spines. Moreover, rats expressing another nAChR mutation linked to ADNFLE (i.e. α4-S284L) display an altered KCC2/NKCC1 messenger ratio (Yamada et al., 2013).

The timing of NKCC1 and KCC2 appearance in neocortex and thalamus (TH) was previously studied in rats (Barthó et al., 2004; Clayton et al., 1998; Kovács et al., 2014; Wang et al., 2002; Yan et al., 2001), mice (Hübner et al., 2001; Markkanen et al., 2014; Stein et al., 2004; Takayama and Inoue, 2010), and humans (Hyde et al., 2011; Sedmak et al., 2016). However, no detailed analysis is available in mouse for associative cortices and TH nuclei, the most relevant regions for a sleep-related frontal epilepsy. To investigate the possible interplay between α4β2 nAChRs and our cotransporters, we first determined the NKCC1 and KCC2 expression in neocortex and TH of wild-type (WT) mice. Next, we studied if the cotransporters' expression was altered when β2-V287L was present throughout brain development. The morphological analysis was coupled with a patch-clamp study of E_{GABA} time course in prefrontal layer V, which is the most susceptible to develop epileptiform activity (Telfeian and Connors, 1998). Our results

suggest that β2-containing nAChRs interact with KCC2 during postnatal development, and that this mechanism may contribute to epileptogenesis.

MATERIALS AND METHODS

Animals

Mice were kept in pathogen-free conditions, with a 12 h light-dark cycle, and free access to water and food. All procedures followed the Italian law (2014/26, implementing the 2010/63/UE) and were approved by the local Ethical Committees and the Italian Ministry of Health. For the biochemical and morphological analyses of WT mice, we used 52 FVB mice (Harlan) of either sex, at the following postnatal (P) days: P0 (n = 5); P1 (n = 7); P2 (n = 4); P5 (n = 5); P7 (n = 7); P12 (n = 2); P14 (n = 5); P19 (n = 2); P21-22 (n = 4); P40-60 (n = 11). Moreover, six embryos of embryonic days 14-15 (E14-E15) were extracted from a P40 pregnant animal. The transgenic strain we used was the S3 line of double transgenic FVB (tTA:Chrnb2V287L) mice, which express β2-V287L under a tetracycline-controlled transcriptional activator (tTA). These mice were compared with their littermates not expressing β2-V287L (controls, CTRL), which were either WT or bearing TRE-Chrnb2V287L or PrnP-tTA genotypes (Manfredi et al., 2009). By using 14 animals of either sex for each experimental group (CTRL and β2-V287L), we studied P8 (n = 6), P21 (n = 6), and P60 (n = 16). To determine E_{GABA} in brain slices, we used a total of 15 CTRL (all PrnP-tTA) and 9 β2-V287L mice, whose age and sex distribution is detailed in the Results.

Brain regions.

For Western blot, we used frontal (FrCtx) and parietal (ParCtx) cortical regions, and TH. For immunohistochemistry and densitometric

analyses, by PFC we refer to the entire secondary motor region (also known as M2, or Fr2) in the dorsomedial shoulder of prefrontal cortex. According to Franklin and Paxinos (2008), coronal prefrontal sections were cut between +2.58 and +1.14 mm from bregma. For SS, we sampled the extended SS region between +1.98 and +0.02 mm from bregma. Thalamic sections for reticular (RT), dorsal lateral geniculate (DLG), paraventricular (PV) and ventrobasal nuclei (VB) were prepared between -0,58 and -1,82 mm from bregma. For patch-clamp experiments, coronal PFC (Fr2) slices were cut between +2.68 mm and +2.10 mm from bregma.

Chemicals and drugs

Chemicals and drugs were purchased from Sigma-Aldrich, except for D(-)-2-amino-5-phosphono-pentanoic acid (AP5), 6-cyano-7-nitroquinoxaline-2,3-dione (CNQX), and tetrodotoxin (TTX), which were purchased from Tocris Bioscience (UK). Stock solutions of gramicidin D (100 mg/ml) and CNQX (20 mM) were prepared in dimethylsulfoxide. Stock solutions of GABA, AP5, and TTX were prepared in distilled water and stored at -20°C.

Western blot analysis

Blots were prepared from mice brains as previously described (Aracri et al. 2013), and incubated for 2 h in 5% non-fat dry milk in 50 mM Tris-buffered saline (TBS), supplemented with 0.1% (v/v) Tween 20 (TBST), at room T°. After overnight incubation at 4 °C with the primary antibody, membranes were thoroughly washed with TBST buffer, and further incubated for 1 h with horseradish peroxidase-conjugated

secondary IgG. After five washes, the bound antibody was visualized with the enhanced chemiluminescence assay (Amersham). The same membranes were reblotted with anti-□-tubulin monoclonal antibody (1:1000), as a loading control. To this purpose, primary and secondary antibodies were removed from the membrane by incubation for 15 min at 37 °C in Restore Western Blotting stripping buffer (Pierce Biotechnology). Next, membranes were washed twice with TBST, and processed with primary and secondary (horse anti-mouse biotin conjugated, Vector; 1:10000) antibodies. The band intensities were quantified by densitometric analysis (NIH ImageJ software) on scanned films. The immunoreactivity detected with anti-cotransporter antibodies was normalized to the one obtained with anti-β-tubulin.

Tissue preparation for immunohistochemistry

Postnatal mice were anesthetized with isoflurane and intraperitoneal 4% chloral hydrate (4 ml/100 g, for mice younger than P14; 2 ml/100 g, for older mice), and sacrificed by intracardiac perfusion as described (Aracri et al., 2013). Embryos at E14-E15 were quickly removed from the perfused pregnant mouse, and their heads immersed in 4% paraformaldehyde in PB, for 24 h at 4°C. Next, brains were removed and stored for 5 to 10 days in the same fresh fixative. Both embryonic and postnatal (until P14) brains were embedded in 5% agarose. Serial coronal brain sections (50 □m thick) were cut with a VT1000S vibratome (Leica Microsystems).

Primary antibodies

Anti-NKCC1: T4 monoclonal antibody, originated from human colonic crypt (T84 cell) NKCC1, against the carboxy-terminus M902 to S1212 (Developmental Studies Hybridoma Bank; 1:100). Anti-KCC2: polyclonal, made in rabbit, against the N-terminal His-tag fusion protein, corresponding to residues 932-1043 of rat KCC2 (Millipore; diluted 1:600). Anti-VGAT (vesicular GABA transporter): polyclonal, made in rabbit against the synthetic peptide corresponding to the N-terminal 75-87 amino acids of the rat protein (Synaptic Systems; 1:800). Anti-VGLUT1 (vesicular glutamate transporter type 1): polyclonal, made in rabbit against Strep-TagR-fusion proteins containing the amino acid residues 456–560 of the rat VGLUT1/BNPI (brain-specific Na1-dependent inorganic phosphate transporter; Synaptic Systems; 1:500). Anti-MAP2 (microtubule-associated protein 2): monoclonal, made in mouse against the rat brain MAP2 (1:1000). Anti-neurofilament H, non-phosphorylated: monoclonal, made in mouse, (SMI32; Sternberger Monoclonals; 1:1000). Anti-GAD67 (glutamic acid decarboxylase type 1/67kDa): polyclonal, made in goat against the human recombinant glutamate-decarboxylase type 1, rhGAD1 (aa 2-97) derived from *E. coli* (R&D Systems; 1:300).

Immunoperoxydase histochemistry for light and electron microscopy

The immunoreaction was carried out as reported (Aracri et al., 2010), except that a mild pretreatment with ethanol (10%, 25%, 10% in PBS) was applied to increase the immunoreagent penetration. The reaction specificity was assessed by negative controls, e.g. omission of primary antiserum. In these cases, no specific staining was observed. Briefly,

sections were examined on a Leica DMRB microscope, and images were acquired using a Leica DCF 480 camera coupled to a personal computer. To generate **Table 1**, two independent observers assessed the cotransporters' distribution in different brain regions. At least 3 mice were examined for each developmental stage. We analyzed at least 3-4 sections for each cortical region (PFC, SS), and 5-6 sections representative of the whole rostro-caudal thalamic extension. Several images were acquired per section. For ultrastructural analysis, sections were osmicated and epoxy-embedded after completion of the immunoenzymatic procedure. After polymerization, small areas from cerebral cortex and TH were cut with a razor blade and glued to blank resin blocks for sectioning with a Reichert ultramicrotome. Ultrathin sections (50–70 nm) collected on Cu/Rh grids were counterstained with lead citrate, or left unstained, and examined with a Zeiss LEO912AB electron microscope.

Immunofluorescence histochemistry

Sections were permeabilized and blocked as described for immunoperoxydase histochemistry. They were next incubated for two nights in a mixture of one/two primary antibodies, after staining with NeuroTrace™ (1:50, Molecular Probes) and/or before staining with Hoechst (Molecular Probes), as necessary for cytoarchitecture analysis and cell counting. For NeuroTrace™ staining, sections were treated as previously described (Aracri et al., 2010). After washing the primary antibodies with PBS, sections were incubated in the following mixture of secondary fluorescent antibodies: indocarbocyanine (Cy)2 (Jackson; 1:200), or CF™488A-conjugated donkey anti-rabbit IgG (Biotium;

1:200), Cy3-conjugated donkey anti-mouse (1:200) or RedX-conjugated donkey anti-goat (Jackson; 1:200), for 75 min at room temperature. After rinsing, samples were mounted on coverslips (sometimes after nuclear staining with Hoechst) with PBS/glycerol (1:1 v/v) and inspected with a Leica TCS-NT laser scanning confocal microscope, to visualize double or triple fluorescent labeling.

Colocalization analysis

Confocal micrographs were collected with a Leica SP2 laser scanning confocal microscope. Identical parameters were used to acquire images from cortical and TH areas for the colocalization analysis of NKCC1 with VGAT or VGLUT1, which was carried out as previously described (Aracri et al., 2013). The degree of colocalization of KCC2 with GAD67 was calculated by comparing the Manders' coefficients, computed with the JACoP plug-in of ImageJ software (Bolte and Cordeliéres, 2006).

Densitometric analysis

For all regions and ages, confocal microscope images were acquired at 40X, by using identical parameters, and analyzed with ImageJ. Cortical layers and TH nuclei were identified with NeuroTrace™ and/or nuclear counterstaining; at least three/four distinct images at 40X magnification were acquired to sample the different areas. For each animal, the mean fluorescence intensity of each image was divided by the number of cells therein (counted with ImageJ). The values thus obtained were averaged among animals before plotting. For the densitometric analysis of

NKCC1, we selected fluorescent images with low background (comparable to those shown in **Fig. 5**).

Patch-clamp in brain slices

Mice were sacrificed after deep isoflurane anesthesia, and brains extracted as reported (Aracri et al., 2013). Coronal sections (300 μm thick) were cut from Fr2 PFC. Experiments were performed at 33-34°. E_{GABA} was measured with the perforated patch method. The extracellular solution contained (mM): 135 NaCl, 21 $NaHCO_3$, 0.6 $CaCl_2$, 3 KCl, 1.25 NaH_2PO_4, 1.8 $MgSO_4$, 10 D-glucose, aerated with 95% O_2 and 5% CO_2 (pH 7.4). Pipette contained (mM): 140 K-Gluconate, 5 KCl, 1 $MgCl_2$, 2.5 BAPTA, 10 HEPES, pH 7.25 (adjusted with KOH). Gramicidin (up to 20 μg/mL) was only added to the solution filling the pipette shank. Borosilicate (Science Products) micropipettes (2-3 MΩ) were prepared with a P-97 Micropipette Puller (Sutter). GABA was applied onto the cell soma, by pressure ejection through a micropipette connected to a Narishige IM-3 microinjector. The recording apparatus was as described (Aracri et al., 2017). The comparison of the action potential (AP) firing of pyramidal neurons in mice expressing or not β2-V287L was carried out in a separate set of experiments. The resting membrane potential (V_{rest}) was measured in open circuit mode soon after patch rupture. Spike-width was measured at half-amplitude between AP threshold and peak. After-hyperpolarization was calculated as the difference between the most negative potential reached after repolarization and the AP threshold. Capacitance and series resistance (up to ~75%) were always compensated. E_{GABA} was determined by applying five consecutive 0.5

s voltage ramps from -80 mV to -20 mV (or -85 mV to -40 mV), in either presence or absence of GABA (100 µM). The background currents were subtracted from the currents obtained in the presence of GABA. Holding potential was -68 mV. Measurements were carried out in the presence of extracellular TTX (0.5 µM), to block voltage-gated Na^+ currents, AP5 (50 µM) and CNQX (10 µM), to block ionotropic glutamate receptors. No leak subtraction procedure was ever applied. No correction for junction potentials was applied to the reported values of membrane potential. Data were analysed with Clampfit 10.6 (Molecular Devices), and OriginPro 9.1 (OriginLab).

Statistical analysis

Data are given as mean values ± SEM. Unless otherwise indicated, the number of experiments (n) is the number of tested mice. Statistical comparisons between two populations were carried out with unpaired Student's t-test, after testing for data normality (with a Kolmogorov-Smirnov test), and variance homogeneity (with F-test). In case of unequal variances, the Welch's correction was applied. The E_{GABA} determinations carried out in cells from the same animal were averaged, to avoid bias from nested data (Aracri et al., 2017). Multiple comparisons were analyzed with one-way ANOVA followed by Bonferroni's post-hoc test, after checking for normality (Kolmogorov-Smirnov test) and variance homogeneity (Brown-Forsythe test). Unless otherwise indicated, detailed statistics for the densitometry results are given in the figure legends. In the figures, p values are indicated by * ($0.01 < p \leq 0.05$) or ** ($p \leq 0.01$).

RESULTS

Western blot analysis of NKCC1 and KCC2 in postnatal developing cortex and TH of WT mice

We first compared the cotransporters' expression in FrCtx, ParCtx and TH of mouse brains at P1, P5, P7, P14, P22 and P40. Expression was detected with either anti-NKCC1 or anti-KCC2, and quantified in each band by densitometry. As a reference for protein expression, we used β-tubulin. Representative blots are shown in **Fig. 1A**. The average values of relative protein content from at least 3 experiments are reported in **Fig. 1B** for NKCC1 (left panel) and KCC2 (right panel). In FrCtx and ParCtx, the NKCC1 amount progressively increased until P14, and remained essentially stable thereafter. The amount of KCC2 was quasi-stationary for FrCtx and ParCtx, although in FrCtx maximal expression was reached by P7. In TH, both NKCC1 and KCC2 gave stable bands, respectively at 145 kDa and 140 kDa, throughout postnatal development (**Fig. 1B**). These data show that the amount of NKCC1 and KCC2 in the neocortex tends to increase during the two first postnatal weeks, whereas TH reaches the steady state expression around birth.

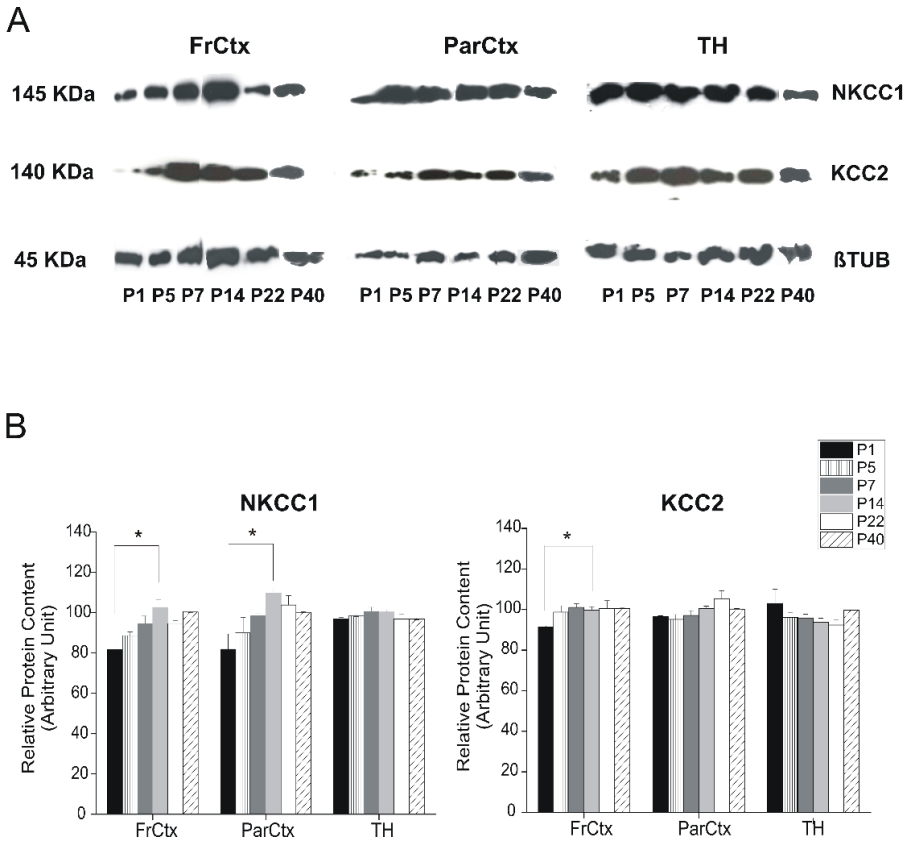

Fig. 1 Western blot analysis of the postnatal expression of NKCC1 and KCC2 in WT neocortex (FrCtx and ParCtx) and TH. Protein samples were prepared mouse brains, at the indicated postnatal ages, and probed with either anti-NKCC1 monoclonal, or anti-KCC2 polyclonal, or anti-β tubulin monoclonal antibody. (A) Representative blots for the different experimental conditions. (B) Densitometric analysis of the cotransporters' bands. Bars give the mean relative protein content at the indicated ages. A progressive postnatal increase in NKCC1 expression (left panel) was observed both in FrCtx (P1, 81.6 ± 3.7 vs P14, 102.5 ± 3.9; $p < 0.01$ with ANOVA; n = 3) and ParCtx (P1, 81.8 ± 7.6 vs P14, 109.6 ± 2.7; $p < 0.01$ with ANOVA; n = 3). For KCC2 expression (right panel) a significant increase was only observed in FrCtx (P1, 91.7 ± 0.65 vs P14, 101.1 ± 1.7; $p < 0.01$ with ANOVA; n = 3).

Topographic distribution of NKCC1 and KCC2 in developing cortex and TH of WT mice

The immunoperoxidase localization at P0-P1 (**Fig. 2A-C**) and P19-P21 (**Fig. 2D-F**) showed wide expression of NKCC1 in neocortex since birth, with no clear differences among layers or nuclei. NKCC1 was mainly found in the apical dendrites of PFC and SS neurons almost irrespective of age, although the overall signal tended to peak at P19-P21 (**Fig. 2D-E**). As for TH, the NKCC1 immunoreactivity was stronger and more stable in the anterior and posterior TH nuclei (i.e. the specific nuclei). Examples at P0-P1 and P19-P21 are shown, respectively, in **Fig. 2C** and **2F**. By contrast, NKCC1 tended to decrease in the medial and intralaminar TH nuclei, as well as in the rostral pole of RT (i.e. the non-specific nuclei; data not shown).

The KCC2 distribution is illustrated in **Fig. 3**. Clusters of a few KCC2 positive (+) neurons were observed at P0-P1 in layer V of PFC, and more abundantly in SS, along with an intense immunoreactivity in the marginal zone (**Fig. 3A-B**). In TH, conspicuous labeling at birth was detected throughout the neuropil, except for RT (**Fig. 3C**). The anterior TH group displayed the highest labeling, followed by the posterior group and by the medial/intralaminar group. In agreement with the Western blot results, immunoreactivity for KCC2 progressively increased in the postnatal neocortex (**Fig. 3A-B, D-E**). At P19-P21, KCC2 was mainly found in the neuropil of PFC and SS (**Fig. 3D-E**). At this stage, a slight overall KCC2 decrease was observed in TH (**Fig. 3C, F**). RT was almost devoid of KCC2 in its central region, whereas the lateral and medial borders displayed a fair labeling (**Fig. 3F**), which

increased and became homogeneous in adulthood only in the rostral pole (not shown).

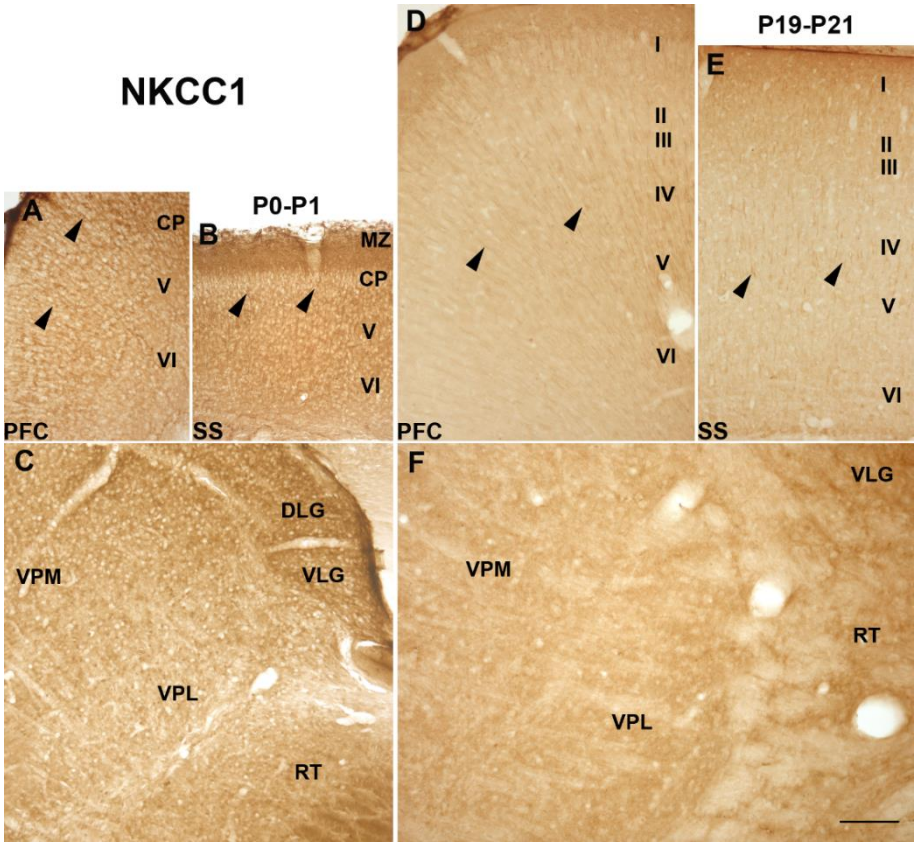

Fig. 2 Topographical distribution of NKCC1 in developing WT forebrain. Immunohistochemical localization of NKCC1 in PFC (A, D), SS (B, E) and TH (C, F) of P0-P1 (A-C), and P19-P21 (D-F) mice. At both stages, NKCC1 was widely expressed in neocortex and TH, and mainly localized in the apical dendrites of PFC and SS pyramidal cells (arrowheads in A-B, D-E). At P19-P21 (D-E), the overall immunoreactivity slightly decreased in TH (F), although NKCC1 expression remained cospicuous in the ventroposterior thalamic nuclei (C, F). *CP*, cortical plate; *MZ*, marginal zone; *I-VI*, cortical layers; *VPM*, ventral posteromedial thalamic nucleus; *VPL*, ventral posterolateral thalamic nucleus. Scale bar: 150 µm.

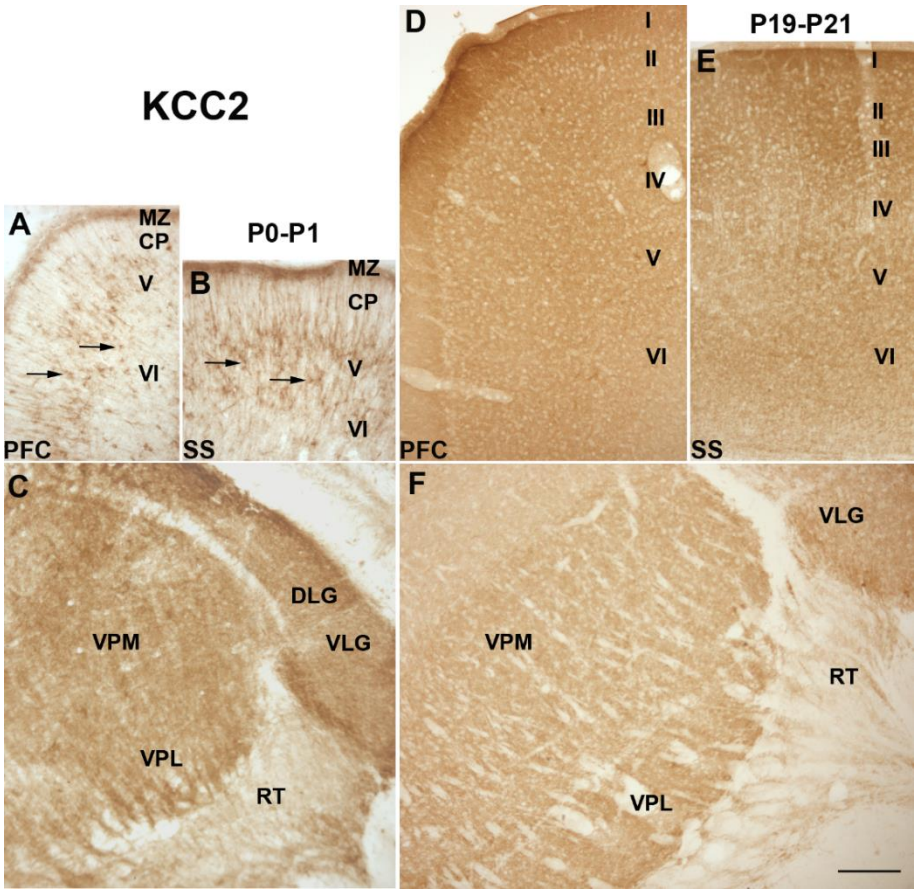

Fig. 3 Topographical distribution of KCC2 in developing WT forebrain. Immunohistochemical localization of KCC2 in P0-P1 (A-C) and P19-P21 (D-F) mice. At birth, KCC2 was mainly confined to the neuronal cell bodies in PFC (A) and SS (B), and clusters of KCC2+ neurons were mainly found in layer V (arrows in A-B). At P19-P21, KCC2 was distributed throughout the neuropil in PFC (D) and SS (E). In TH nuclei, KCC2 was already present at P0-P1 in the neuropil of all regions, except RT (C). At P21, KCC2 expression in TH slightly decreased (F), and only a weak immunoreactivity was observed in the lateral and medial borders of RT (F). CP, cortical plate; MZ, marginal zone; I-VI, cortical layers; VPL, ventral posterolateral thalamic nucleus; VPM, ventral posteromedial thalamic nucleus. Scale bar: 150 µm.

These results suggest that KCC2 is expressed in TH earlier than in the neocortex. Consistently, in E14-E15 mice, KCC2 immunoreactivity was weak in frontal and parietal preplate isocortices (**Fig. 6F-G**), but more conspicuous in the ventral (especially the ventral lateral geniculate nucleus, VLG, **Fig. 6H**) and dorsal TH (**Fig. 6I**).

Table 1 provides a summary of the age-dependent distribution of NKCC1 and KCC2, as obtained by immunohistochemical data.

Table 1 - Developmental distribution of NKCC1 and KCC2 in the forebrain of WT mouse.

	E14-E15	P0-P2		P7	P14	P19-P21		P40	
	KCC2	**NKCC1**	**KCC2**	**KCC2**	**KCC2**	**NKCC1**	**KCC2**	**NKCC1**	**KCC2**
PFC	+/-	+++	+	++	++	++	+++	++	+++
SS	+/-	+++	++	++	++	++	++	++	++
TH ant	+	+++	+++	++	++	+++	++	+++	++
TH me	+/-	++	+++	++	++	+/++	+	++	+
TH VB	+	+++	+++	+++	+++	+++	++	+++	++
TH RT	++	+++	++	+	+	++	+/++	++	+/++
TH LG	+++	+++	+++	+++	+++	+++	+++	+++	+++

Semi-quantitative analysis of the distribution of Cl^- transporters in different brain regions, at different ages, based on immunohistochemical localization, using anti-NKCC1 or anti-KCC2 antibodies, as indicated. PFC: prefrontal cortex; SS: somatosensory cortex; TH ant: anterior thalamic area; TH me: medial thalamus, i.e. intralaminar and midline nuclei; TH VB: thalamic ventrobasal complex; TH RT: reticular thalamic nucleus; TH LG: lateral geniculate thalamic nuclei (comprising both DLG and VLG). -: negative; +/-: scarce; +: moderately positive; ++: positive; +++: markedly positive

Cellular distribution of NKCC1 and KCC2, in developing WT mice

NKCC1 was generally found in both glial cells and neurons (**Fig. 4A-D, 5A**). In cortical pyramidal cells, NKCC1 labeling was faint in cell bodies (**Fig. 4A**), but intense in the apical dendrites (**Fig. 2D-E; 4A; 5B**). In TH, strong immunoreactivity was also observed in thin (**Fig. 4C**) and thick fiber bundles (such as those of internal capsule; **Fig. 4B**). The axonal and glial expression of NKCC1 was confirmed by ultrastructural analysis, and pre-embedding immunolocalization also revealed NKCC1+ synaptic boutons (**Fig. 4D**). By double immunofluorescence confocal microscopy, these synaptic terminals were identified as being mainly GABAergic (i.e. VGAT+) in the developing TH nuclei (e.g. VB; **Fig. 5C**), but mostly glutamatergic (i.e. VGLUT1+) in the mature PFC (**Fig. 5D**). Transient expression of NKCC1 in VGLUT1+ terminals was also observed in RT at birth (data not shown).

By contrast, KCC2 was only expressed in neurons (**Fig. 4E**), and its distribution became increasingly polarized during development. In the neonatal neocortex, KCC2 was mainly confined to the neuronal cell bodies (**Fig. 3A-B; 4F; 5A; 6A, C**). After P5, the transporter was also found in dendrites, and outlined the cell membranes (**Fig. 3D-E; 4E, G; 5B; 6B, D**). In TH, such developmental shift occurred before birth (**Fig. 6H-I**), and postnatal neurons showed maximal KCC2 expression in the neuropil (i.e. dendrites), even in the scarcely labeled RT (**Fig. 3C, F; 4H; 6E**). As for the neurochemical nature of KCC2+ neurons, in neonatal neocortex both MAP2+ pyramidal neurons and GABAergic GAD67+ neurons showed cytoplasmic immunoreactive puncta,

probably vesicles, which also spread to proximal dendrites (**Fig. 6A, C**). After P7, KCC2 mainly outlined the pyramidal neuron membranes (i.e. SMI32+; **Fig. 6B, D**), whereas in GAD67+ structures (i.e. comprising neuronal cell bodies, processes and puncta), KCC2 was confined to the dendritic shafts (**Fig. 6D**).

A different pattern was observed in TH. The GABAergic neurons, which were mainly concentrated in RT, showed a weak KCC2 expression. An exception was constituted by the dendrites of the GAD67+ cells located on the medial border of RT **(Fig. 6E**), which were also identified as MAP2+ dendritic compartments (not shown). KCC2 was however intensely expressed by the dendritic neuropil of all TH neurons (**Fig. 4H; 6E**).

Fig. 4 Cellular distribution of NKCC1 and KCC2 during WT development. Immunoperoxidase localization of NKCC1 at P60 in SS (A), and in TH at P7 (B) and P14 (C). NKCC1 was found in glial cells and neurons of both neocortex (arrows in A) and TH (arrows in B). NKCC1 staining was particularly intense in cortical apical dendrites (arrowheads in A), and in TH thin and thick axonal fibers (arrowheads in C), such as those of internal capsule (arrowhead in B). Electron microscopy for TH at P60 is shown in (D) for NKCC1, which was found in the axons of myelinated fibers (f), glial processes (g) and small synaptic terminals (t) contacting distal dendrites (d). Electron microscopy for PFC at P60 is shown in (E) for KCC2, which was exclusively

localized in cell bodies (CB) and proximal dendrites (D). The immunoperoxidase localization of KCC2 in PFC is shown at P2 (F), and P19 (G). At birth, KCC2 was localized in multipolar neurons (arrows in F). Subsequently, KCC2 became distributed in the neuropil and outlined cell membranes (arrows in G). In TH (H) KCC2 was mainly expressed by the dendritic neuropil, even in the scarcely labeled RT. *IC*, internal capsule; *N*, nucleus. Scale bars: 50 µm (A); 40 µm (B-C, F-G); 0.5 µm (D); 2 µm (E); 80 µm (H).

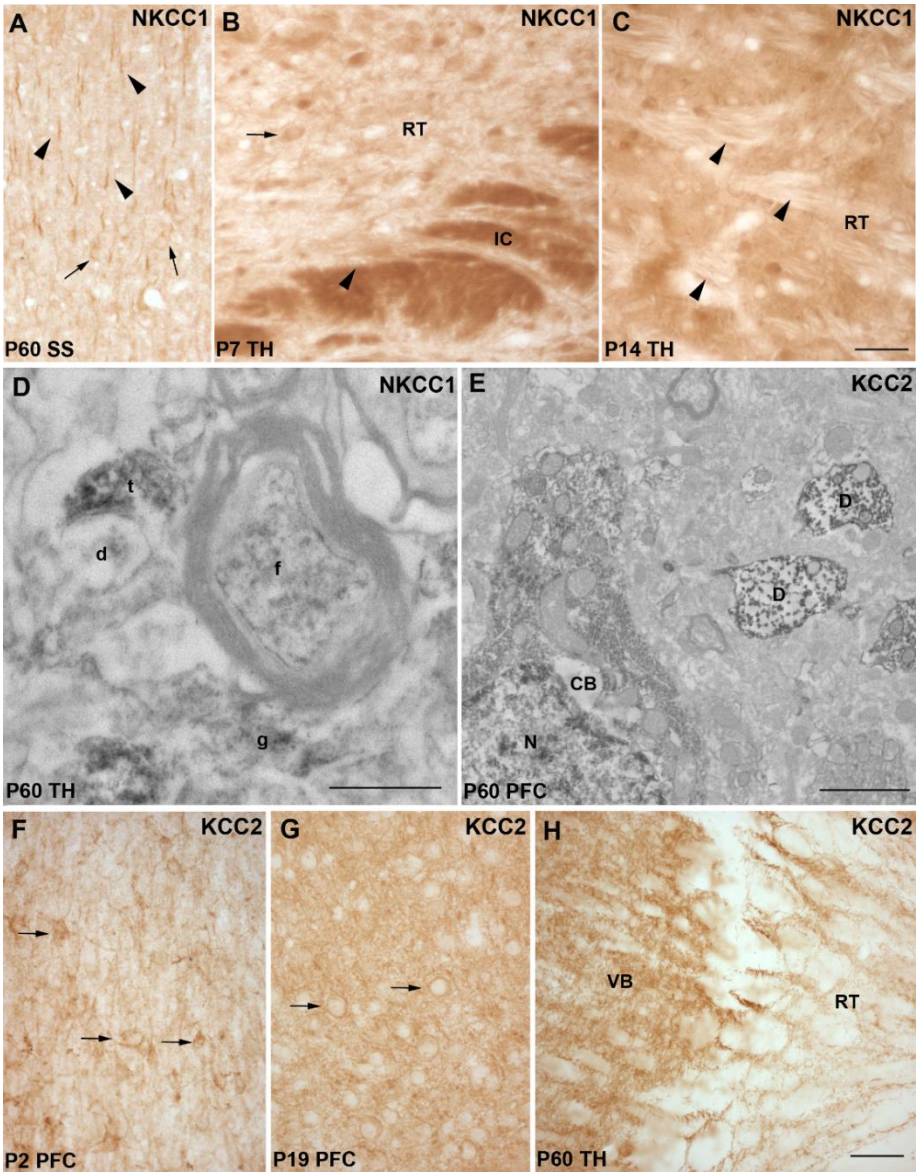

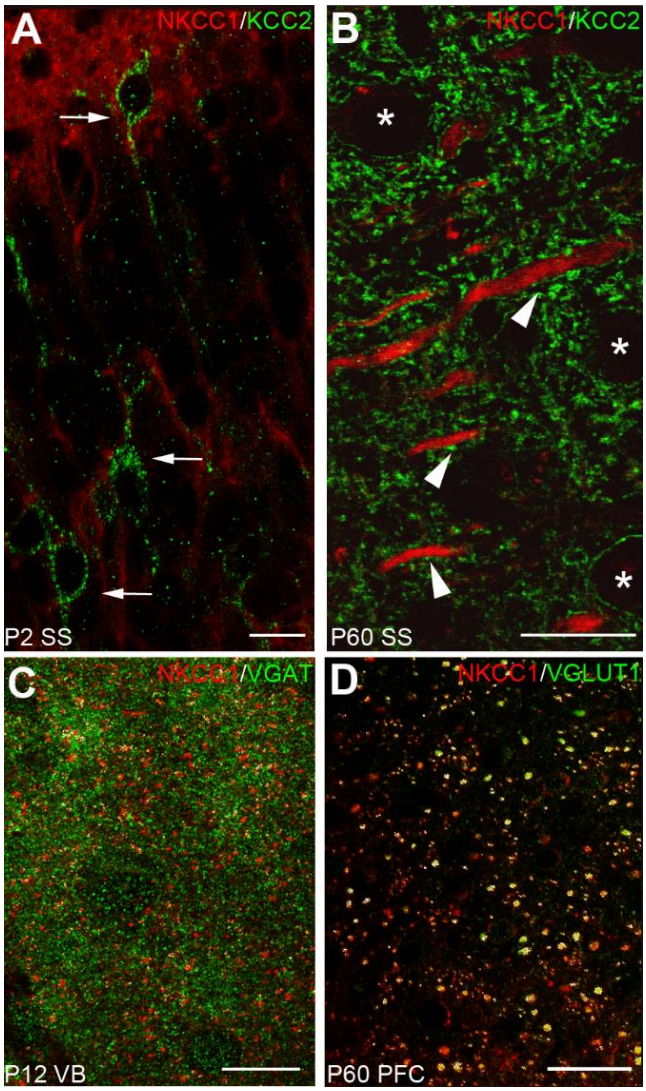

Fig. 5 Colocalization of NKCC1 with KCC2 and synaptic markers during WT development. (A-B) Double immunofluorescence combining the NKCC1 (red) and KCC2 (green) signals, in SS. At P2 (A), the expression of NKCC1 was ubiquitous, especially in the neuropil; KCC2 displayed punctate labeling in the somatodendritic compartment of a fraction of neurons (arrows in A). At P60 (B), KCC2 and NKCC1 were present in the same apical dendrites, but appeared to be segregated (arrowheads in B); moreover, KCC2 displayed a cell-surface localization (asterisks in B). (C) Colocalization of NKCC1 (red) and VGAT (green; labeling GABAergic synapses), in VB at P12. (D) Colocalization of NKCC1 (red) and VGLUT1 (green; labeling glutamatergic synapses), in PFC at P60. White spots mark colocalization sites. Scale bars: 20 µm.

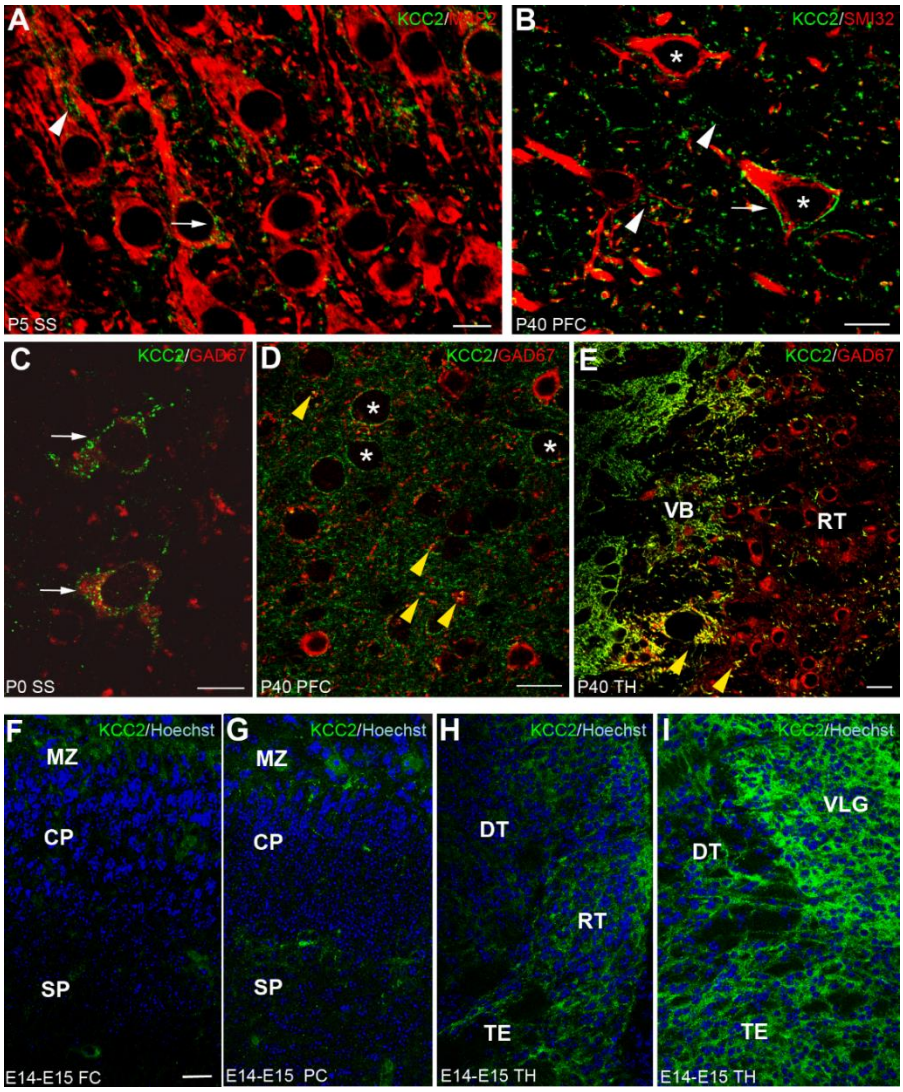

Fig. 6 Localization of KCC2 during WT development. Double immunofluorescence in SS (A, C), PFC (B, D) and TH (E). Representative images are shown for KCC2 (green) and MAP2 (red) at P5 (A), KCC2 (green) and SMI32 (red) at P40 (B), KCC2 (green) and GAD67 (red) at P0 and P40 (C-E). Around birth, KCC2 was mainly expressed in neuronal cell bodies in the neocortex (arrows in A, C). The MAP2+ pyramidal neurons and the GAD67+ interneurons showed cytoplasmic stained puncta, probably vesicles, spreading to proximal dendrites (A, C). In P40 neocortex, KCC2 was also found in dendrites (white arrowheads in B) and outlined pyramidal cell membranes (asterisks in B, D), whereas only a small fraction of the GAD67+ dendritic shafts (yellow arrowheads in D) also displayed KCC2 labeling. In TH (E), KCC2 was found in the dendritic neuropil of all TH neurons, and in the medial

border of RT, where it displayed colocalization with GAD67 (yellow arrowheads in E). (F-I) Immunofluorescence staining for KCC2 (green) in embryonic (E14-E15) cortical and TH tissues. Nuclei were stained with Hoechst (blue). KCC2 immunoreactivity was faint in frontal (FC) and parietal (PC) pre-plate isocortex (F-G), but strong in the rostral (H) and caudal (I) TH. *MZ*, marginal zone; *CP*, cortical plate; *SP*, subplate; *DT*, dorsal TH; *TE* thalamic eminence. Scale bars: 10 µm (A, C); 50 µm (B); 20 µm (D-I).

Quantitative analysis of KCC2 distribution in postnatal forebrain of WT mice

To define more rigorously the spatiotemporal distribution of KCC2, we carried out a densitometric analysis on SS, the associative PFC, and the TH nuclei representative of functional groups (RT; VB, DLG, relay nuclei, and PV midline non-specific nucleus), at P2 and P40. Typical sections are shown in **Fig. 7A-B**. Sections were labeled for KCC2 and NeuroTrace™ (examples are shown in **Fig. 7E-G**). The intensity values for KCC2 fluorescence were divided by the number of cells identified with NeuroTrace™. The mean values obtained from 4 mice per age were plotted in **Fig. 7C** (neocortex) and **Fig. 7D** (TH). In the neocortex, KCC2 strongly increased between P2 and P40, especially in PFC layers II/III, where the mean fluorescence intensity per cell quadrupled. The effect was less marked in SS (**Fig. 7C**). In contrast, the postnatal expression of KCC2 in the selected TH nuclei was heterogeneous, revealing that the global pattern determined by Western blot (**Fig. 1**). poorly represented the expression trends of specific nuclei. In particular, KCC2 significantly decreased in RT from P2 to P40 (in spite of the selective increase observed in its rostral pole), whereas it tended

to increase in VB. The other relay nucleus, DLG, and PV showed negligible postnatal changes in KCC2 expression (**Fig. 7D**).

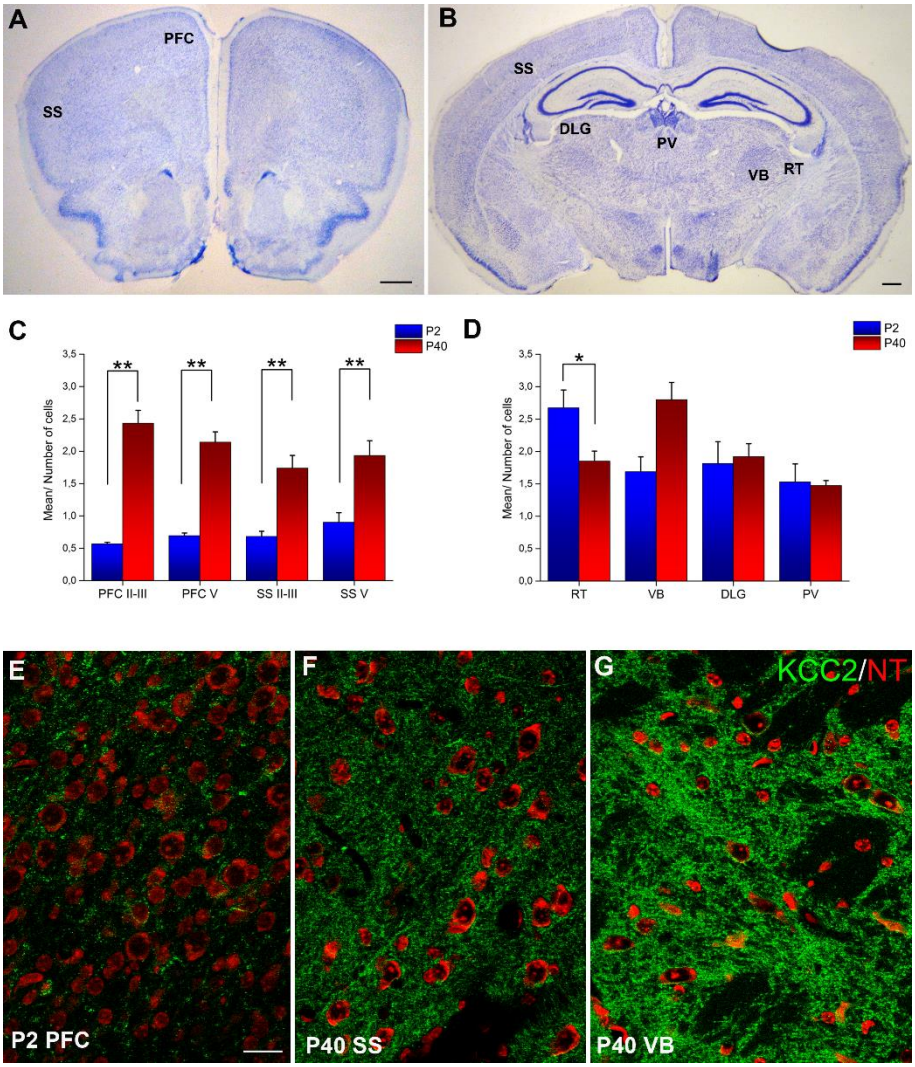

Fig. 7 Densitometric analysis of KCC2 amounts in developing WT forebrain. (A-B) Thionine-stained coronal sections of adult murine brain indicating our target areas. (C-D) Densitometric analysis of KCC2 immunofluorescence in the neocortex (C) and TH (D) of P2 and P40 WT male mice. Bars are mean fluorescence intensity values divided by the number of neurons. KCC2 increased in PFC during development, especially in layers II-III, where the mean fluorescence intensity per cell was 0.57 ±

0.022 at P2, and 2.4 ± 0.57 at P40 ($p < 0.01$, with t-test; n = 4). The average percentage increase between P2 and P40 was ~321% in layers II/III, and ~207% in layer V. Similar results were obtained in SS, where the mean fluorescence intensity per cell in layers II/III was 0.68 ± 0.08 at P2, and 1.74 ± 0.2 at P40 ($p < 0.01$, with t-test; n = 4). The corresponding values in layer V were 0.93 ± 0.14 at P2, and 1.92 ± 0.21 at P40 ($p < 0.01$, with t-test; n = 4**).** In TH, the time course of KCC2 expression was more heterogeneous. The mean fluorescence per cell decreased by ~30% in RT (2.73 ± 0.098 at P2, and 1.77 ± 0.20 at P40; $p < 0.05$ with t-test; n = 4). The differences observed in VB, DLG and PV were not statistically significant (D). (E-G) Representative immunofluorescence staining for KCC2 (green) and NeuroTrace™ (red; NT) are shown for PFC at P2 (E), for SS at P40 (F), and for VB at P40 (G). Scale bars: 600 µm (A); 450 µm (B); 20 µm (E-G).

The KCC2 amounts were altered in mice expressing the β2-V287L nAChR subunit

We next studied the cotransporters' amounts in mice expressing the transgene (β2-V287L) and the control littermates (CTRL). Considering the nature of ADNFLE, we focused on PFC and TH, and used SS as the classical reference cortex. Between the first and the second postnatal week, the maturation of synaptic circuits is accompanied by an increase in nAChR subunit expression (Molas and Dierssen, 2014). Therefore, we compared P8, P21 and adult (P60) tissue. The densitometric analysis was as described for WT mice (**Fig. 7C-D**), except that Hoechst 33258 was sometimes added to, or replaced, NeuroTrace™. **Fig. 8** shows the results obtained in the neocortex at P8 (**Fig. 8A-D**), P21 (**Fig. 8E-H**) and P60 (**Fig. 8I-L**). The time course of KCC2 expression in the transgenic strain was similar to the one observed in WT mice. The main differences between β2-V287L and CTRL mice were observed in PFC layer V, where smaller amounts of KCC2 were observed at P8 in β2-

V287L mice (**Fig. 8C**). Such difference disappeared by P21 (**Fig. 8G**), and the effect was reversed at P60, when KCC2 expression was significantly higher in β2-V287L mice (**Fig. 8K**). In particular, in layer V, the ratio between the mean KCC2 fluorescence per cell in CTRL and β2-V287L decreased from ~1.32 (P8) to ~0.83 (P60). At the same ages, no differences were found in the KCC2 amounts in SS (**Fig. 8D, H, L**).

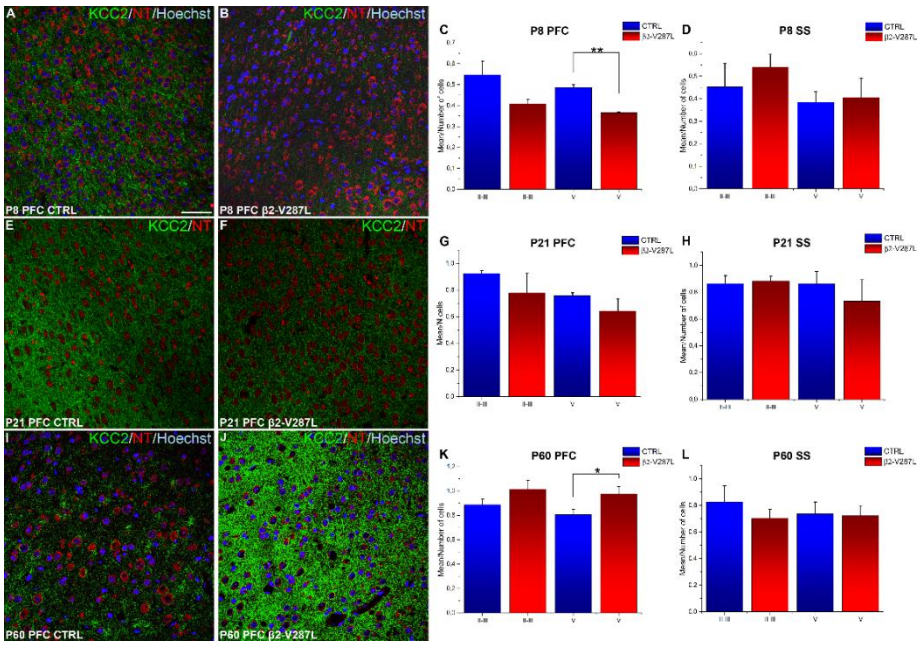

Fig. 8 Effect of β2-V287L on KCC2 expression in neocortex during postnatal development. Immunofluorescence for KCC2 (green) counterstained with NeuroTrace™ (red; NT) and Hoechst (blue), in PFC layer V of CTRL (A, E, I) and β2-V287L (B, F, J) mice, at the indicated ages. The corresponding densitometric analyses are summarized in the bar graphs for layers II/III and V from P8 (n = 3), P21 (n = 3) and P60 (n = 8) mice in PFC (respectively C, G, K), and SS (respectively D, H, L). Bars give average fluorescence intensity values divided by the number of neurons. At P8, KCC2 expression in PFC layer V (C) was significantly lower in β2-V287L (0.49 ± 0.014, vs. 0.37 ± 0.004 in CTRL; $p < 0.01$, with t-test; n = 3) (C). The opposite was observed at P60, when KCC2 significantly increased in layer V of β2-V287L (0.98 ± 0.06, vs. 0.81 ± 0.05 in CTRL; $p < 0.05$, with t-test; n = 8) (K). No peculiar trend was observed in SS. Scale bar: 20 µm.

In rats, sexual dimorphism in cotransporters' expression is observed in the substantia nigra (Galanopoulou et al., 2003), hypothalamus (Perrot-Sinal et al., 2007), and hippocampus/entorhinal cortex (Damborsky and Winzer-Serhan, 2012; Galanopoulou, 2008; Murguía-Castillo et al., 2013). Hence, we also show the distribution among sexes of our P60 mice. The densitometric results for PFC (**Fig. 9A**) and SS (**Fig. 9B**) are plotted for individual male (black) and female (white) mice. No sex-dependent difference was apparent between the indicated experimental groups.

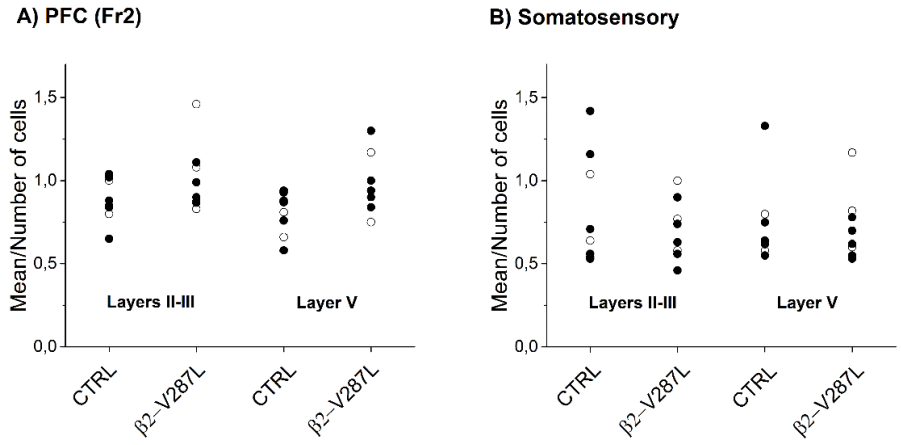

Fig. 9 Sex-dependent distribution of KCC2 expression, at P60. (A) Data points represent the densitometric results for KCC2 expression in PFC, obtained as explained in Fig. 8, for individual mice of the indicated sex. Overall, 8 mice were studied for CTRL (6 males and 2 females), and 8 for β2-V287L (5 males and 3 females). Black: males; white: females. Genotypes and layers are denoted as in Fig. 8. (B) Same as (A), for the somatosensory cortex.

In TH, our densitometric analysis was focused on RT and on the main somatosensory relay nucleus VB. Representative images at P60 are shown in **Fig. 10A-B**. In RT, no significant differences were observed between genotypes at early postnatal stages. However, at P60, the average KCC2 amount decreased by ~20% in β2-V287L mice, compared to CTRL (**Fig. 10C**).

To test whether the higher KCC2 amount observed in the PFC of adult β2-V287L mice could be partly ascribed to changes in the GABAergic neuronal populations, we analyzed the colocalization of KCC2 with GAD67. Qualitative analysis in PFC layer V at P60 revealed the typical KCC2+ outlines around the cell bodies of pyramidal neurons, but not GAD67+ neurons, in WT (**Fig. 6D**) and CTRL (**Fig. 11A-A'**), although they appeared in a few GAD67+ neurons of β2-V287L (**Fig. 11B-B'**). The contribution of these GABAergic interneurons to the total KCC2 increment was estimated by quantifying the overall colocalization of KCC2 and GAD67 (i.e. comprising neuronal cell bodies, processes and puncta). The degree of overlap was defined by M1 and M2 Manders' coefficients, and was not different between CTRL and β2-V287L mice. At P60, in PFC layer V, M1 (fraction of colocalization on the total KCC2+ signal) was 0.17139 ± 0.00565 in CTRL, and 0.17008 ± 0.00743 in β2-V287L ($p = 0.895$, with t-test; $n = 3$); M2 (fraction of colocalization on the total GAD67+ signal) was 0.36657 ± 0.00933 in CTRL, and 0.35333 ± 0.01154 in β2-V287L ($p = 0.423$, with t-test; $n = 3$). No such analysis was performed in RT, in which the KCC2+ signal was always confined to the GAD67+ dendritic neuropil (**Fig. 6E; 10A, B**).

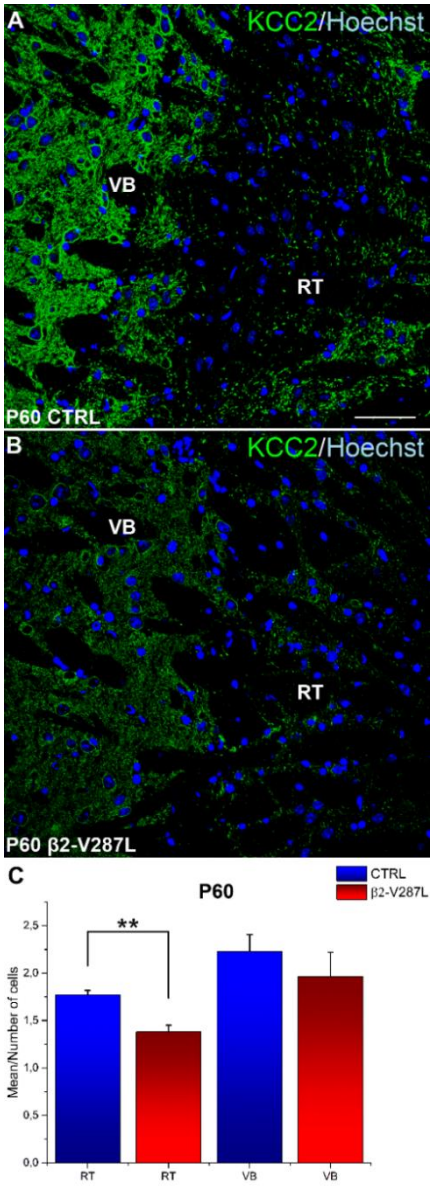

Fig. 10 Effect of β2-V287L on thalamic expression of KCC2 at P60. Representative immunofluorescence images for KCC2 (green) counterstained with Hoechst (blue), in TH nuclei of CTRL (A) and β2-V287L (B) mice. The corresponding densitometric analyses are shown in the bar graphs (C), for RT and VB nuclei, as indicated. Data are given as mean fluorescence intensity values divided by the number of neurons. Both RT and VB displayed a tendency to a decreased KCC2 expression in β2-V287L, which was statistically significant in RT (1.38 ± 0.07, vs. 1.77 ± 0.04 in CTRL; $p < 0.01$, with t-test; n = 3). Scale bar: 20 µm.

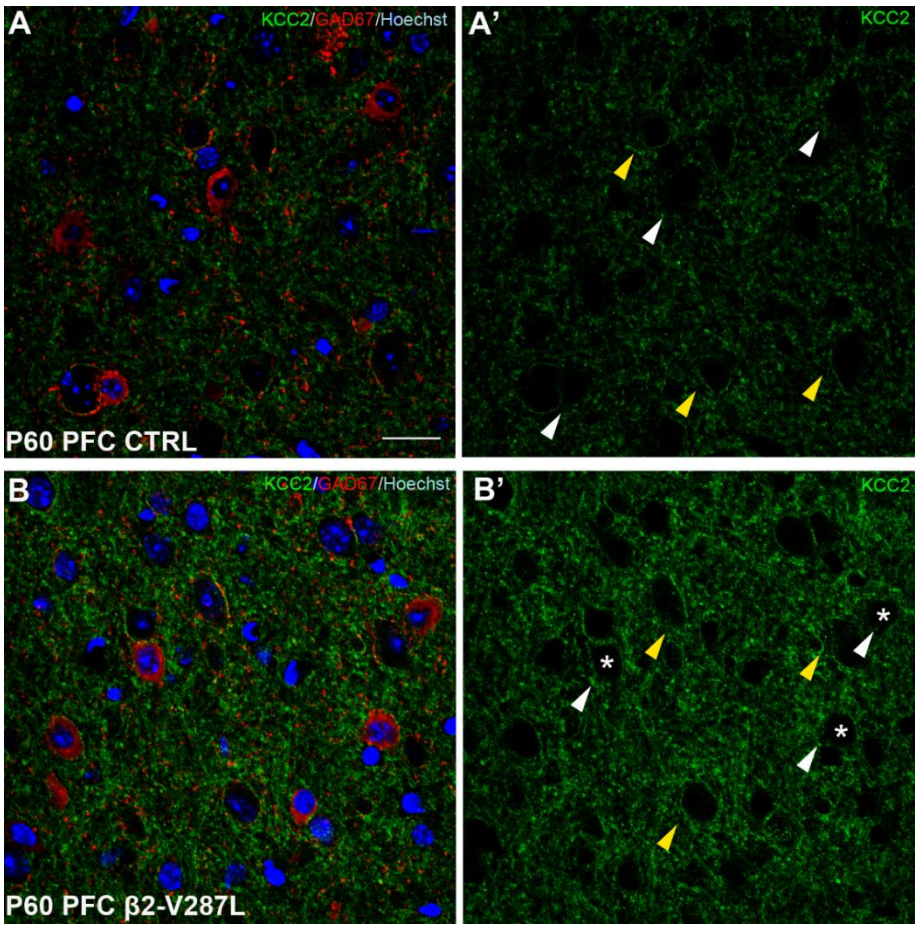

Fig. 11 Colocalization of KCC2 and GAD67 in PFC layer V of mice expressing or not β2-V287L. Double immunofluorescence images in PFC layer V at P60, combining KCC2 (green) and GAD67 (red) localizations with nuclear staining with Hoechst (blue), for CTRL (A) and β2-V287L (B). The corresponding single labeling for KCC2 is shown in (A') for CTRL and (B') for β2-V287L. Data represent the results obtained in 3 mice for each genotype. In CTRL, GAD67+ neurons showed a weak KCC2+ staining of somatic neuronal membranes (white arrowheads), but marked KCC2+ outlines of pyramidal neurons' somata (yellow arrowheads). In β2-V287L, the KCC2 immunoreactivity pointed out somatic outlines also on some GAD67+ neurons (asterisks in B'). Scale bar: 20 µm.

β2-V287L did not alter NKCC1 expression

Because $[Cl^-]_i$ is regulated by both KCC2 and NKCC1, we also performed a densitometric analysis of NKCC1 expression in PFC and TH, at P8 and P60 (**Fig. 12**), i.e. the regions and ages displaying altered KCC2 amounts in β2-V287L mice. Our analysis was based on the T4 antibody against NKCC1, which presents a very good specificity for the transporter (Chen et al., 2005), and was previously used in rodent neocortex, hippocampus and other regions (Ge et al., 2006; Liu et al., 2012; Marty et al., 2002; Yan et al., 2001). In PFC, NKCC1 expression presented no significant genotype-dependent alteration at P8 (**Fig. 12A**) and P60 (**Fig. 12C**). Similar results were obtained in TH (**Fig. 12B, D**).

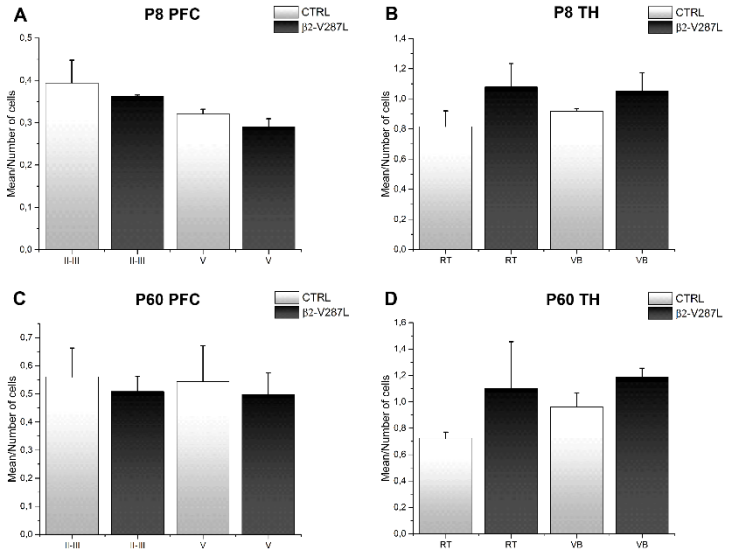

Fig. 12 Effect of β2-V287L on NKCC1 expression in developing PFC and TH. (A-D)**:** bars give the densitometric results of NKCC1 expression in PFC layers II-III and V, and in RT/VB, at P8 (A-B) and P60 (C-D). Data are expressed as mean fluorescence intensity divided by the number of neurons. At P8 (n = 3) and P60 (n = 3), no significant differences were observed in NKCC1 expression between CTRL and β2-V287L, in either PFC or TH.

β2-V287L delayed the GABAergic switch in PFC layer V

The retarded expression of KCC2 in β2-V287L mice could be associated with a delayed GABAergic switch. This was tested by measuring E_{GABA} in pyramidal cells of PFC layer V, in brain slices from P8-P9 and adult mice (older than P40). Layer V is prominent in the premotor Fr2 PFC, and presents large pyramidal neurons that are well recognizable since early postnatal stages. We have previously described in detail their morphological and electrophysiological properties (Aracri et al., 2010; 2013; 2015). In brief, these neurons display induced regular spiking with frequencies between 10 and 30 Hz, when depolarized by 150-300 pA current steps, and moderate adaptation. A comparison of the basic electrophysiological features of these cells is shown in **Table 2**, for a representative sample of P37-P50 mice bearing or not β2-V287L. No statistical difference was observed between CTRL and β2-V287L in V_{rest}, spike width, the ratio between the fourth and the first spike intervals, and after-hyperpolarization (with t-test). Similar values were measured in the second postnatal week (data not shown).

Table 2. Expression of β2-V287L did not alter V_{rest} and the firing properties of pyramidal cells in PFC layer V.

	V_{rest} (mV)	Spike width (ms)	4^{th}spike interval/ 1^{st}spike interval	AHP mV	*N*
CTRL	-69.4 ± 0.63	1.52 ± 0.08	1.8 ± 0.1	-9.3 ± 0.49	11
β2-V287L	-68.9 ± 0.52	1.51 ± 0.05	1.9 ± 0.09	-9.3 ± 0.59	9

Mice were aged P37-P50. The ratios between the fourth and the first spike interval were calculated in the presence of a 200 pA stimulation, and average firing frequency of ~15 Hz. No difference was observed between mice expressing or not β2-V287L (with unpaired t-test). AHP: after-hyperpolarization.

In such pyramidal cells, we measured E_{GABA} with the perforated patch method, to avoid perturbing $[Cl^-]_i$. Representative GABAergic current traces between -85 and -40 mV, or -80 and -20 mV (often applied at P8-P9) are displayed in **Fig. 13A**, for the indicated experimental group. During brain maturation, E_{GABA} progressively hyperpolarized, shifting from -48.6 ± 2.03 mV at P8-P9 (15 cells were sampled from 5 mice), to -58 ± 1.7 mV in adult mice (31 cells, from 10 mice; $p < 0.01$, compared with the younger mice). A similar pattern was observed in adult β2-V287L, where E_{GABA} was -56 ± 2.5 mV (13 cells, from 5 mice; not statistically different from CTRL). However, at P8-P9, in β2-V287L mice E_{GABA} was more depolarized than in the controls (-42 ± 1.65 mV; 11 cells from 4 mice; $p < 0.05$, compared with CTRL). These data are summarized **Fig. 13B**. They show that, in PFC layer V, the time course of E_{GABA} hyperpolarization was delayed in β2-V287L mice, in agreement with our immunofluorescence results (**Fig. 8**). The scatter plots in **Fig. 13C** show the sex distribution of these results. No significant differences were observed between sexes in the E_{GABA} time course.

Fig. 13 The effect of β2-V287L on the GABAergic switch. The time-course of E_{GABA} was followed by perforated-patch experiments. Layer V pyramidal neurons were studied at P8-P9 or adult stages. (A) Representative current traces (averages of 5 trials), elicited by voltage ramps (500 ms duration), in β2-V287L or CTRL mice, as indicated. The ramps between -85 and -40 mV are relative to adult mice. The ramp between -80 and -20 mV is relative to a P8 mouse. The background current was always subtracted to the current measured in the presence of GABA. (B) Average E_{GABA} values at the indicated stages, in CTRL and β2-V287L mice. (C) Sex-dependent distribution of the E_{GABA} values of CTRL and β2-V287L mice, at P8-P9 and adulthood, as indicated. White: females; black: males.

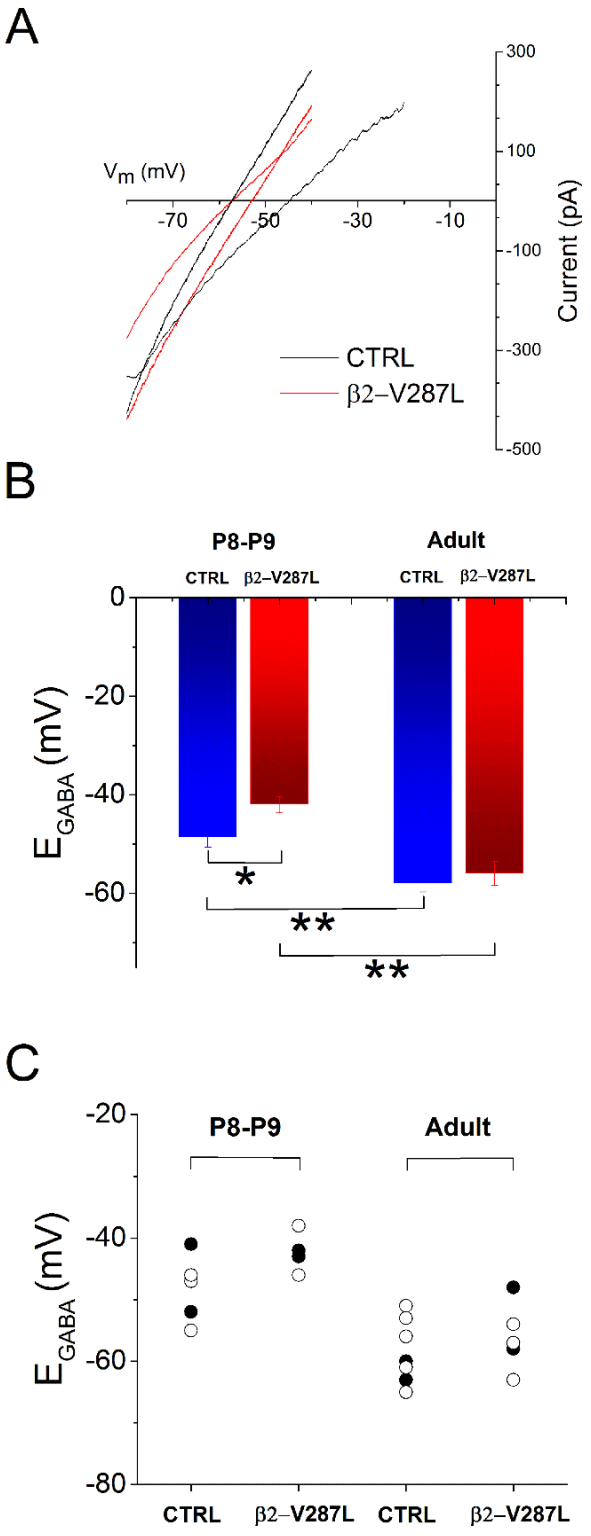
A
300
100
-100
-300
-500
Current (pA)
Vm (mV)
-70
-50
-30
-10
CTRL
β2–V287L
B
P8-P9
Adult
CTRL
β2–V287L
CTRL
β2–V287L
0
-20
-40
-60
EGABA (mV)
*
**
**
C
-20
-40
-60
-80
EGABA (mV)
P8-P9
Adult
CTRL
β2–V287L
CTRL
β2–V287L

DISCUSSION

The main finding of the present work was that the postnatal expression of KCC2 in PFC layer V was delayed in mice carrying the ADNFLE-linked subunit β2-V287L. This delay was accompanied by a retardation in the GABAergic switch. In the same region, the amount of KCC2 was larger in adult mice carrying the transgene. No such alteration was observed in SS, suggesting that the effect of β2-V287L was specifically related to the frontal hyperexcitability. By contrast, the RT nucleus displayed decreased amounts of KCC2 in adult mice bearing β2-V287L.

Topographical distribution of NKCC1 and KCC2 during development, in WT mice

Our Western blot data showed that the overall NKCC1 expression in FrCtx and ParCtx peaked at P14. Previous work in rodents revealed a complex timing and cellular distribution of NKCC1 expression**.** Nonetheless, our data agree with the frequent observation that the NKCC1 messenger and protein reach the highest amounts between P7 and P21. The results obtained in the adult are more variable, depending on central nervous system area, species and, above all, on the used antibodies and probes (Clayton et al., 1998; Dzhala et al., 2005; Hübner et al., 2001; Liu et al., 2012; Murguía-Castillo et al., 2013; Plotkin et al., 1997; Wang et al., 2002; Yan et al., 2001).

As to KCC2, at birth it was specifically localized in the marginal zone and infragranular layers. Next, its expression strongly increased during the first postnatal week, and reached the adult distribution by P14. This process paralleled the GABAergic switch, which in neocortex and hippocampus is delayed compared to the subcortical structures (Fiumelli and Woodin, 2007; Kovács et al., 2014). Our results are in good agreement with previous results in mouse showing that KCC2 increases in postnatal stages, although regional discrepancies are observed (Kovács et al., 2014; Markkanen et al., 2014; Wang et al., 2002). They also agree with several non-systematic determinations in rat (Lacoh et al., 2013), and human tissue (Hyde et al., 2011). Moreover, KCC2 expression was more precocious in SS. Together with other observations on more specific markers (Aracri et al., 2013; Hyde et al., 2011), these results support the notion that PFC matures more slowly than other brain regions, which could make it more liable to develop pathologies related to network maturation, such as epilepsy and schizophrenia (Hyde et al., 2011; Kovács et al., 2014; Lacoh et al., 2013; Kaila et al., 2014a).

A substantial difference in KCC2 amounts between neocortex and TH was observed as early as E14-E15, when the transporter was highly expressed in VLG and RT. Previous evidence, although fragmentary, is consistent with the view that these cotransporters, and especially KCC2, are found in TH at earlier stages (Horn et al., 2010; Hübner et al., 2001; Li et al., 2002; Markkanen et al., 2014; Stein et al., 2004; Wang et al., 2002). This may reflect the quicker time course of neuronal circuit wiring in TH, which is complete by P14-P15 (Amadeo et al., 2001). In fact, $[Cl^-]_i$ is essentially stable by the second postnatal week

in rat thalamic VB (Glykys et al., 2009). In our mice, KCC2 displayed precocious and conspicuous expression throughout TH (**Table 1**), which remained relatively stable thereafter, except in RT. In general, the so-called relay nuclei (comprising the anterior region), show a rapid maturation that reflects the early establishment of the connections implicated in the sensory map topography (Lopez-Bendito et al., 2003). By contrast, the adult RT is characterized by a weaker KCC2 immunolabeling compared with the more caudal adjacent relay nuclei (Barthò et al., 2004). Our results suggest that such difference is not precocious, but is caused by a specific postnatal decrease of KCC2 in RT. Although little is known about the development of synaptic connections in RT (Amadeo et al., 2001; Hou et al., 2016; Nagaeva et al., 2006), we hypothesize that proper synaptogenesis here requires KCC2 amounts similar to those present in other TH nuclei. Next, KCC2 would stabilize at lower levels in the adult RT, where E_{GABA} is more depolarized than in relay cells (Barthò et al., 2004; Sun et al., 2013; Ulrich and Huguenard, 1997), and the reciprocal GABAergic connections lead to excitatory effects (Sun et al., 2012).

Cellular distribution of NKCC1 and KCC2 in WT mice

In neocortex and TH, our ultrastructural analysis showed wide expression of NKCC1 in neurons, axons and astrocytes, in agreement with previous results (Hübner et al., 2001; Wang et al., 2002; Yan et al., 2001). NKCC1 was mainly found in the apical dendrites of cortical pyramidal neurons and in myelinated fiber bundles in TH, suggesting

that specific mechanisms of NKCC1 regulation operate in distinct neuronal compartments (Hübner et al., 2001; Yan et al., 2001). Moreover, electron and confocal microscopy also revealed NKCC1 in GABAergic (VGAT+) terminals in developing TH, and glutamatergic (VGLUT1+) terminals in PFC. Current evidence about the pre-synaptic function of NKCC1 concerns other regions of the central nervous system, where the transporter is implicated in GABA- and glycine-dependent pre-synaptic depolarization (Bos et al., 2011; Shen et al., 2013). Our results suggest that the same may apply to the developing TH.

At variance with NKCC1, the developmental distribution of KCC2 was considerably different in cortical and TH neurons. At birth, KCC2 displayed a punctate localization in the neocortex, and was prevalently found in cell bodies of pyramidal and GABAergic neurons. During the first postnatal week, KCC2 shifted to cell membranes and dendrites, even though a significant amount of the transporter was retained in the somatic membranes of pyramidal neurons. This presumably reflects the high density of GABAergic synapses around pyramidal cell bodies. The pattern we observed in mouse neocortex is broadly similar to the one observed in other species (Dzhala et al., 2005; Hyde et al., 2011; Kovács et al., 2014; Li et al., 2007; Stein et al., 2004). On the contrary, the KCC2 immunoreactivity of TH nuclei at birth was much closer to the adult's; this agrees with the aforementioned concept that, in rodents, KCC2 appears earlier in the TH *anlage* than in neocortex. The KCC2+ outlines observed around pyramidal cell bodies were absent or discontinuous in cortical and TH GABAergic cells, where KCC2 immunoreactivity was mainly confined to the dendrites. We attribute

such difference to the relatively low average density of reciprocal GABAergic terminals among inhibitory interneurons in neocortex and TH (Aracri et al., 2017; Hou et al., 2016; Pi et al., 2013).

The effect of β2-V287L on the GABAergic switch

In rodent neocortex, the nAChR subunit expression peaks in the second postnatal week, and recent lines of evidence indicate that synaptic maturation is regulated by both α7- and β2-containing nAChRs (Molas and Dierssen, 2014). Because the maximal nAChR expression is concomitant with the GABAergic switch, we studied if β2-V287L affected the expression of Cl^- cotransporters. In PFC layer V, the postnatal increase of KCC2 expression was delayed by β2-V287L, between the first and the second postnatal week. Because the effect was not accompanied by any alteration of NKCC1, we expected mice carrying β2-V287L to also display a more depolarized E_{GABA}, around P8. In fact, expression of the transgene retarded the GABAergic switch. These data suggest that KCC2 and nAChRs interact during synaptogenesis, particularly in layer V, where the action of ACh is dominated by β2-containing nAChRs (Aracri et al., 2013; Poorthuis et al., 2013). Because expression of β2-V287L does not change the total amount of heteromeric nAChRs on the plasma membrane (Manfredi et al., 2009), we attribute the action of the mutant subunit to the functional alterations it produces on nAChRs. Both β2-containing nAChRs (Lozada et al., 2012; Molas and Dierssen, 2014) and KCC2 (Fiumelli et al., 2013; Li et al., 2007) regulate the formation and maturation of

dendritic spines by mechanisms that are thought to involve the actin cytoskeleton. Because activating nAChRs leads to both membrane depolarization and Ca^{2+} influx, the hyperfunctional mutant receptors could alter KCC2 expression by interfering with the Ca^{2+}-dependent signaling. An alternative explanation is based on the observation that β2-V287L and other ADNFLE mutations favor the assembly of the high-affinity $(\alpha4)_2(\beta2)_3$ receptor's stoichiometry with respect to $(\alpha4)_3(\beta2)_2$ (Son et al., 2009). The altered abundance of stoichiometric forms could modify the nAChR binding to regulatory elements of the dendritic spine machinery, which in turn interact with KCC2.

Irrespective of the molecular mechanism, the effect we observed around P8 was transient. At P60, the amount of KCC2 in PFC layer V was higher in β2-V287L mice, even though E_{GABA} was similar in adult mice carrying or not the transgene. Because layer V is highly susceptible to develop seizures (Telfeian and Connors, 1998), we hypothesize that the steady-state increase of KCC2 levels in the mutants is a compensatory mechanism. A higher local Cl^- turnover would be necessary to sustain inhibition in an overactive network, and prevent a significant alteration of the steady state Cl^- levels. This explanation would be consistent with the observation that, in chronic epileptic conditions (Karlocai et al., 2016; Pathak et al., 2007), or peritumoral tissue (Conti et al., 2011), KCC2 levels usually increase, pointing to a long-term compensation of hyperexcitability. In fact, deleting KCC2 in mice facilitates epileptiform activity (Tornberg et al., 2005; Woo et al., 2002), and mutations impairing KCC2 are linked to human epilepsy (Kahle et al., 2014; Puskarjov et al., 2014). It must be however recalled that the physiological meaning of the changes of KCC2 expression observed in

epileptic networks is complex and still controversial, as the observed effects depend on the pathophysiological context and the studied region. For example, in temporal lobe, acutely induced epileptiform activity (Puskarjov et al., 2012; Rivera et al., 2002; Wake et al., 2007), and the induction of status epilepticus (Barmashenko et al., 2011; Li et al., 2008; Pathak et al., 2007) tend to produce a chronic decrease of KCC2 surface expression, which is attributed to the action of higher calpain levels (Kaila et al., 2014b). Finally, the relatively limited numerousness of our samples prevents definite conclusions about a possible sex dimorphism in the effects of β2-V287L. Nonetheless, our present results do not suggest any sex-dependent effect, in agreement with the fact that ADNFLE equally affects males and females (Tinuper et al., 2016).

As for the thalamic effects, mice bearing β2-V287L displayed a lower KCC2 level in the mature RT nucleus. Differently from GABAergic cells in adult PFC (Aracri et al., 2017), RT neurons in mice express a relatively high density of post-synaptic α4β2 nAChRs that can effectively trigger action potentials, when the cholinergic afferents are activated (Sun et al., 2013). Therefore, hyperfunctional mutant nAChRs could powerfully stimulate RT neurons and boost calcium signaling. As discussed earlier, this could favor a calpain-dependent KCC2 downregulation. Such a mechanism could also be facilitated by the typical propensity of RT cells to enter into burst-like firing states (Fogerson and Huguenard, 2016). Further functional studies will be necessary to clarify these issues, and to better define the possible role of the RT nucleus in sleep-related epilepsy.

REFERENCES

Amadeo, A., Ortino, B., Frassoni, C., 2001. Parvalbumin and GABA in the developing somatosensory thalamus of the rat: an immunocytochemical ultrastructural correlation. Anat. Embryol. 203, 109-119.

Aracri, P., Consonni, S., Morini, R., Perrella, M., Rodighiero, S., Amadeo, A., Becchetti, A., 2010. Tonic modulation of GABA release by nicotinic acetylcholine receptors in layer V of the murine prefrontal cortex. Cereb. Cortex 20, 1539-1555.

Aracri, P., Amadeo, A., Pasini, M.E., Fascio, U., Becchetti, A., 2013. Regulation of glutamate release by heteromeric nicotinic receptors in layer V of the secondary motor region (Fr2) in the dorsomedial shoulder of prefrontal cortex in mouse. Synapse 67, 338-357.

Aracri, P., Banfi, D., Pasini, M.E., Amadeo, A., Becchetti, A., 2015. Orexin (hypocretin) regulates glutamate input to fast-spiking interneurons in layer V of the Fr2 region of the murine prefrontal cortex. Cereb. Cortex 25, 1330-1347.

Aracri, P., Meneghini, S., Coatti, A., Amadeo, A., Becchetti, A., 2017. α4β2* nicotinic receptors stimulate GABA release onto fast-spiking cells in layer V of mouse prefrontal (Fr2) cortex. Neuroscience 340, 48-61.

Aronica, E., Boer, K., Redeker, S., Spliet, W.G., van Rijen, P.C., Troost, D., Gorter, J.A., 2007. Differential expression patterns of chloride transporters, Na^+-K^+-$2Cl^-$-cotransporters and K^+-Cl^--cotransporter, in epilepsy-associated malformations of cortical development. Neuroscience 145, 185-196.

Awad, P.N., Sanon, N.T., Chattopadhyaya, B., Carriço, J.N., Ouardouz, M., Gagné, J., Duss, S., Wolf, D., Desgent, S., Cancedda, L., Carmant, L., Di Cristo, G., 2016. Reducing premature KCC2 expression rescues

seizure susceptibility and spine morphology in atypical febrile seizures. Neurobiol. Dis. 91, 10-20.

Barmashenko, G., Hefft, S., Aertsen, A., Kirschstein, T., Köhling, R., 2011. Positive shifts of the $GABA_A$ receptor reversal potential due to altered chloride homeostasis is widespread after status epilepticus. Epilepsia 52, 1570-1578.

Barthó, P., Payne, J.A., Freund, T.F., Acsády, L., 2004. Differential distribution of the KCl cotransporter KCC2 in thalamic relay and reticular nuclei. Eur. J. Neurosci. 20, 965-975.

Becchetti, A., Aracri, P., Meneghini, S., Brusco, S., Amadeo, A., 2015. The role of neuronal nicotinic acetylcholine receptors in autosomal dominant nocturnal frontal lobe epilepsy. Front. Physiol. 6, 22.

Ben-Ari, Y., Gaiarsa, J.L., Tyzio, R., Khazipov, R., 2007. GABA: a pioneer transmitter that excites immature neurons and generates primitive oscillations. Physiol. Rev. 87, 1215-1284.

Bolte, S., Cordelières, F.P., 2006. A guided tour into subcellular colocalization analysis in light microscopy. J. Microsc. 224, 213-232.

Bos, R., Brocard, F., Vinay, L., 2011. Primary afferent terminals acting as excitatory interneurons contribute to spontaneous motor activities in the immature spinal cord. J. Neurosci. 31, 10184-10188.

Cancedda, L., Fiumelli, H., Chen, K., Poo, M.M. 2007. Excitatory GABA action is essential for morphological maturation of cortical neurons in vivo. J. Neurosci. 27, 5224-5235.

Chen, H., Luo, J., Kintner, D.B., Shull, G.E., Sun, D., 2005. Na(+)-dependent chloride transporter (NKCC1)-null mice exhibit less gray and white matter damage after focal cerebral ischemia. J. Cereb. Blood Flow Metab. 25, 54–66.

Clayton, G.H., Owens, G.C., Wolff, J.S., Smith, R.L., 1998. Ontogeny of cation-Cl^- cotransporter expression in rat neocortex. Brain Res. Dev. Brain Res. 109, 281-292.

Conti, L., Palma, E., Roseti, C., Lauro, C., Cipriani, R., de Groot, M., Aronica, E., Limatola, C., 2011. Anomalous levels of Cl^- transporters cause a decrease of GABAergic inhibition in human peritumoral epileptic cortex. Epilepsia 52, 1635-1644.

Damborsky, J.C., Winzer-Serhan, U.H., 2012. In rats, effects of sex and chronic neonatal nicotine treatment on $Na^+/K^+/Cl^-$ co-transporter 1, K^+/Cl^- co-transporter 2, brain-derived neurotrophic factor, NMDA receptor subunit 2A and NMDA receptor subunit 2B mRNA expression in the postnatal rat hippocampus. Neuroscience 225, 105-117.

De Fusco, M., Becchetti, A., Patrignani, A., Annesi, G., Gambardella, A., Quattrone, A., Ballabio, A., Wanke, E., Casari, G., 2000. The nicotinic receptor β2 subunit is mutant in nocturnal frontal lobe epilepsy. Nat. Genet. 26, 275-276.

Dzhala, V.I., Talos, D.M., Sdrulla, D.A., Brumback, A.C., Mathews, G.C., Benke, T.A., Delpire, E., Jensen, F.E., Staley, K.J., 2005. NKCC1 transporter facilitates seizures in the developing brain. Nat. Med. 11, 1205-1213.

Fiumelli, H., Woodin, M.A., 2007. Role of activity-dependent regulation of neuronal chloride homeostasis in development. Curr. Opin. Neurobiol. 17, 81-86.

Fiumelli, H., Briner, A., Puskarjov, M., Blaesse, P., Belem, B.J., Dayer, A.G., Kaila, K., Martin, J.L., Vutskits, L., 2013. An ion transport-independent role for the cation-chloride cotransporter KCC2 in dendritic spinogenesis in vivo. Cereb. Cortex 23, 378-388.

Fogerson, P.M., Huguenard, J.R., 2016. Tapping the brakes: cellular and synaptic mechanisms that regulate thalamic oscillations. Neuron 92, 687-704.

Franklin, K.B.J., Paxinos, G., 2008. The Mouse Brain in Stereotaxic Coordinates, third ed. Academic Press.

Galanopoulou, A.S., Kyrozis, A., Claudio, O.I., Stanton, P.K., Moshé, S.L., 2003. Sex-specific KCC2 expression and GABA(A) receptor function in rat substantia nigra. Exp. Neurol. 183, 628-637.

Galanopoulou, A.S., 2008. Dissociated gender-specific effects of recurrent seizures on GABA signaling in CA1 pyramidal neurons: role of GABA(A) receptors. J. Neurosci. 28, 1557-1567.

Ge, S., Goh, E.L., Sailor, K.A., Kitabatake, Y., Ming, G.L., Song, H., 2006. GABA regulates synaptic integration of newly generated neurons in the adult brain. Nature 439, 589-593.

Glykys, J., Dzhala, V.I., Kuchibhotla, K.V., Feng, G., Kuner, T., Augustine, G., Bacskai, B.J., Staley, K.J., 2009. Differences in cortical versus subcortical GABAergic signaling: a candidate mechanism of electroclinical uncoupling of neonatal seizures. Neuron 63, 657-672.

Horn, Z., Ringstedt, T., Blaesse, P., Kaila, K., Herlenius, E., 2010. Premature expression of KCC2 in embryonic mice perturbs neural development by an ion transport-independent mechanism. Eur. J. Neurosci. 31, 2142-2155.

Hou, G., Smith, A.G., Zhang, Z.W., 2016. Lack of intrinsic GABAergic connections in the thalamic reticular nucleus of the mouse. J. Neurosci. 36, 7246-7252.

Hübner, C.A., Lorke, D.E., Hermans-Borgmeyer, I., 2001. Expression of the Na-K-2Cl cotransporter NKCC1 during mouse development. Mech. Dev. 102, 267-269.

Hyde, T.M., Lipska, B.K., Ali, T., Mathew, S.V., Law, A.J., Metitiri, O.E., Straub, R.E., Ye, T., Colantuoni, C., Herman, M.M., Bigelow, L.B., Weinberger, D.R., Kleinman, J.E., 2011. Expression of GABA signaling molecules KCC2, NKCC1, and GAD1 in cortical development and schizophrenia. J. Neurosci. 31, 11088-11095.

Jensen, F.E., 2011. Epilepsy as a spectrum disorder: implications from novel clinical and basic neuroscience. Epilepsia 52(Suppl. 1), 1-6.

Kahle, K.T., Merner, N.D., Friedel, P., Silayeva, L., Liang, B., Khanna, A., Shang, Y., Lachance-Touchette, P., Bourassa, C., Levert, A., Dion, P.A., Walcott, B., Spiegelman, D., Dionne-Laporte, A., Hodgkinson, A., Awadalla, P., Nikbakht, H., Majewski, J., Cossette, P., Deeb, T.Z., Moss, S.J., Medina, I., Rouleau, G.A., 2014. Genetically encoded impairment of neuronal KCC2 cotransporter function in human idiopathic generalized epilepsy. EMBO Rep. 15, 766-774.

Kaila, K., Price, T.J., Payne, J.A., Puskarjov, M., Voipio, J., 2014a. Cation-chloride cotransporters in neuronal development, plasticity and disease. Nat. Rev. Neurosci. 15, 637-654.

Kaila, K., Ruusuvuori, E., Seja, P., Voipio, J., Puskarjov, M., 2014b. GABA actions and ionic plasticity in epilepsy. Curr. Opin. Neurobiol. 26, 34-41.

Karlócai, M.R., Wittner, L., Tóth, K., Maglóczky, Z., Katarova, Z., Rásonyi, G., Erőss, L., Czirják, S., Halász, P., Szabó, G., Payne, J.A., Kaila, K., Freund, T.F., 2016. Enhanced expression of potassium-chloride cotransporter KCC2 in human temporal lobe epilepsy. Brain Struct. Funct. 221, 3601-3615.

Khirug, S., Ahmad, F., Puskarjov, M., Afzalov, R., Kaila, K., Blaesse, P., 2010. A single seizure episode leads to rapid functional activation of KCC2 in the neonatal rat hippocampus. J. Neurosci. 30, 12028-12035.

Kovács, K., Basu, K., Rouiller, I., Sík, A., 2014. Regional differences in the expression of K(+)-Cl(-) 2 cotransporter in the developing rat cortex. Brain Struct. Funct. 219, 527-538.

Lacoh, C.M., Bodogan, T., Kaila, K., Fiumelli, H., Vutskits, L., 2013. General anaesthetics do not impair developmental expression of the KCC2 potassium-chloride cotransporter in neonatal rats during the brain growth spurt. Br. J. Anaesth. 110 (Suppl. 1), i10-i18.

Li, H., Tornberg, J., Kaila, K., Airaksinen, M.S., Rivera, C., 2002. Patterns of cation-chloride cotransporter expression during embryonic rodent CNS development. Eur. J. Neurosci. 16, 2358-2370.

Li, H., Khirug, S., Cai, C., Ludwig, A., Blaesse, P., Kolikova, J., Afzalov, R., Coleman, S.K., Lauri, S., Airaksinen, M.S., Keinänen, K., Khiroug, L., Saarma, M., Kaila, K., Rivera, C., 2007. KCC2 interacts with the dendritic cytoskeleton to promote spine development. Neuron 56, 1019-1033.

Li, X., Zhou, J., Chen, Z., Chen, S., Zhu, F., Zhou, L., 2008. Long-term expressional changes on Na^+-K^+-Cl^- co-transporter 1 (NKCC1) and K^+-Cl^- co-transporter 2 (KCC2) in CA1 region of hippocampus following lithium-pilocarpine induced status epilepticus (PISE). Brain Res. 1221, 141-146.

Liu, Q., Wong-Riley, M.T., 2012. Postnatal development of Na(+)-K(+)-2Cl(-) co-transporter 1 and K(+)-Cl(-) co-transporter 2 immunoreactivity in multiple brain stem respiratory nuclei of the rat. Neuroscience 210, 1-20.

Liu, Z., Neff, R.A., Berg, D.K., 2006. Sequential interplay of nicotinic and GABAergic signaling guides neuronal development. Science 314, 1610-1613.

Lopez-Bendito, G., Molnár, Z., 2003. Thalamocortical development: how are we going to get there? Nat. Rev. Neurosci. 4, 276-289.

Lozada, A.F., Wang, X., Gounko, N.V., Massey, K.A., Duan, J., Liu, Z., Berg, D.K., 2012. Induction of dendritic spines by β2-containing nicotinic receptors. J. Neurosci. 32, 8391-8400.

Manfredi, I., Zani, A.D., Rampoldi, L., Pegorini, S., Bernascone, I., Moretti, M., Gotti, C., Croci, L., Consalez, G.G., Ferini-Strambi, L., Sala, M., Pattini, L., Casari, G., 2009. Expression of mutant β2 nicotinic receptors during development is crucial for epileptogenesis. Hum. Mol. Genet. 18, 1075-1088.

Markkanen, M., Karhunen, T., Llano, O., Ludwig, A., Rivera, C., Uvarov, P., Airaksinen, M.S., 2014. Distribution of neuronal KCC2a and KCC2b isoforms in mouse CNS. J. Comp. Neurol. 522, 1897-1914.

Marty, S., Wehrlé, R., Alvarez-Leefmans, F.J., Gasnier, B., Sotelo, C., 2002. Postnatal maturation of Na^+, K^+, $2Cl^-$ cotransporter expression and inhibitory synaptogenesis in the rat hippocampus: an immunocytochemical analysis. Eur. J. Neurosci. 15, 233-245.

Molas, S., Dierssen, M., 2014. The role of nicotinic receptors in shaping and functioning of the glutamatergic system: a window into cognitive pathology. Neurosci. Biobehav. Rev. 46, 315-325.

Murguía-Castillo, J., Beas-Zárate, C., Rivera-Cervantes, M.C., Feria-Velasco, A.I., Ureña-Guerrero, M.E., 2013. NKCC1 and KCC2 protein expression is sexually dimorphic in the hippocampus and entorhinal cortex of neonatal rats. Neurosci. Lett. 552, 52-57.

Nagaeva, D.V., Akhamadeev, A.V., 2006. Structural organization, neurochemical characteristics, and connections of the reticular nucleus of the thalamus. Neurosci. Behav. Physiol. 36, 987-995.

Pathak, H.R., Weissinger, F., Terunuma, M., Carlson, G.C., Hsu, F.C., Moss, S.J., Coulter, D.A., 2007. Disrupted dentate granule cell chloride regulation enhances synaptic excitability during development of temporal lobe epilepsy. J. Neurosci. 27, 14012-14022.

Perrot-Sinal, T.S., Sinal, C.J., Reader, J.C., Speert, D.B., McCarthy, M.M., 2007. Sex-differences in the chloride transporters, NKCC1 and KCC2, in the developing hypothalamus. J. Neuroendocrinol. 19, 302-308.

Pi, H.J., Hangya, B., Kvitsiani, D., Sanders, J.I., Huang, Z.J., Kepecs, A., 2013. Cortical interneurons that specialize in disinhibitory control. Nature 503, 521–524.

Plotkin, M.D., Snyder, E.Y., Hebert, S.C., Delpire, E., 1997. Expression of the Na-K-2Cl cotransporter is developmentally regulated in postnatal rat brains: a possible mechanism underlying GABA's excitatory role in immature brain. J. Neurobiol. 33, 781-795.

Poorthuis, R.B., Bloem, B., Schak, B., Wester, J., de Kock, C.P., Mansvelder, H.D., 2013. Layer-specific modulation of the prefrontal cortex by nicotinic acetylcholine receptors. Cereb. Cortex 23, 148-161.

Puskarjov, M., Ahmad, F., Kaila, K., Blaesse, P., 2012. Activity-dependent cleavage of the K-Cl cotransporter KCC2 mediated by calcium-activated protease calpain. J. Neurosci. 32, 11356-11364.

Puskarjov, M., Seja, P., Heron, S.E., Williams, T.C., Ahmad, F., Iona, X., Oliver, K.L., Grinton, B.E., Vutskits, L., Scheffer, I.E., Petrou, S., Blaesse, P., Dibbens, L.M., Berkovic, S.F., Kaila, K., 2014. A variant of KCC2 from patients with febrile seizures impairs neuronal Cl^- extrusion and dendritic spine formation. EMBO Rep. 15, 723-729.

Rivera, C., Voipio, J., Payne, J.A., Ruusuvuori, E., Lahtinen, H., Lamsa, K., Pirvola, U., Saarma, M., Kaila, K., 1999. The K^+/Cl^- co-transporter KCC2 renders GABA hyperpolarizing during neuronal maturation. Nature 397, 251-255.

Rivera, C., Li, H., Thomas-Crusells, J., Lahtinen, H., Viitanen, T., Nanobashvili, A., Kokaia, Z., Airaksinen, M.S., Voipio, J., Kaila, K., Saarma, M., 2002. BDNF-induced TrkB activation down-regulates the K^+-Cl^- cotransporter KCC2 and impairs neuronal Cl^- extrusion. J. Cell Biol. 159, 747-752.

Sedmak, G., Jovanov-Milošević, N., Puskarjov, M., Ulamec, M., Krušlin, B., Kaila, K., Judaš, M., 2016. Developmental expression patterns of KCC2 and functionally associated molecules in the human brain. Cereb. Cortex 26, 4574-4589.

Shen, W., Purpura, L.A., Li, B., Nan, C., Chang, I.J., Ripps, H., 2013. Regulation of synaptic transmission at the photoreceptor terminal: a novel role for the cation–chloride co-transporter NKCC1. J. Physiol. 591, 133–147.

Shouse, M.N., Quigg, M.S., 2008. Chronobiology, in: Engel, J.J., Pedley, T.A. (Eds.), Epilepsy: A Comprehensive Textbook. Vol 2. Lippincott Williams and Wilkins, Philadelphia, pp. 1961-1974.

Son, C.D., Moss, F.J., Cohen, B.N., Lester, H.A. 2009. Nicotine normalizes intracellular subunit stoichiometry of nicotinic receptors carrying mutations linked to autosomal dominant nocturnal frontal lobe epilepsy. Mol. Pharmacol. 75, 1137-1148.

Stein, V., Hermans-Borgmeyer, I., Jentsch, T.J., Hübner, C.A., 2004. Expression of the KCl cotransporter KCC2 parallels neuronal maturation and the emergence of low intracellular chloride. J. Comp. Neurol. 468, 57-64.

Steinlein, O.K., Mulley, J.C., Propping, P., Wallace, R.H., Phillips, H.A., Sutherland, G.R., Scheffer, I.E., Berkovic, S.F., 1995. A missense mutation in the neuronal nicotinic acetylcholine receptor α4 subunit is associated with autosomal dominant nocturnal frontal lobe epilepsy. Nat. Genet. 11, 201-203.

Sun, Y.G., Wu, C.S., Renger, J.J., Uebele, V.N., Lu, H.C., Beierlein, M., 2012. GABAergic synaptic transmission triggers action potentials in thalamic reticular nucleus neurons. J. Neurosci. 32, 7782–7790.

Sun, Y.G., Pita-Almenar, J.D., Wu, C.S., Renger, J.J., Uebele, V.N., Lu, H.C., Beierlein, M., 2013. Biphasic cholinergic synaptic transmission controls action potential activity in thalamic reticular nucleus neurons. J. Neurosci. 33, 2048 –2059.

Takayama, C., Inoue, Y., 2010. Developmental localization of potassium chloride co-transporter 2 (KCC2), GABA and vesicular GABA transporter (VGAT) in the postnatal mouse somatosensory cortex. Neurosci. Res. 67, 137-148.

Talos, D.M., Sun, H., Kosaras, B., Joseph, A., Folkerth, R.D., Poduri, A., Madsen, J.R., Black, P.M., Jensen, F.E. 2012. Altered inhibition in tuberous sclerosis and type IIb cortical dysplasia. Ann. Neurol. 71, 539-551.

Telfeian, A.E., Connors, B.W. 1998. Layer-specific pathways for the horizontal propagation of epileptiform discharges in neocortex. Epilepsia 39, 700-708.

Tinuper, P., Bisulli, F., Cross, J.H., Hesdorffer, D., Kahane, P., Nobili, L., Provini, F., Scheffer, I.E., Tassi, L., Vignatelli, L., Bassetti, C., Cirignotta, F., Derry, C., Gambardella, A., Guerrini, R., Halasz, P., Licchetta, L., Mahowald, M., Manni, R., Marini, C., Mostacci, B., Naldi, I., Parrino, L., Picard, F., Pugliatti, M., Ryvlin, P., Vigevano, F., Zucconi, M., Berkovic, S., Ottman, R., 2016. Definition and diagnostic criteria of sleep-related hypermotor epilepsy. Neurology 86, 1834-1842.

Tornberg, J., Voikar, V., Savilahti, H., Rauvala, H., Airaksinen, M.S. 2005. Behavioural phenotypes of hypomorphic KCC2-deficient mice. Eur. J. Neurosci. 21, 1327-1337.

Ulrich, D., Huguenard, J.R., 1997. Nucleus-specific chloride homeostasis in rat thalamus. J. Neurosci. 17, 2348-2354.

Wake, H., Watanabe, M., Moorhouse, A.J., Kanematsu, T., Horibe, S., Matsukawa, N., Asai, K., Ojika, K., Hirata, M., Nabekura, J., 2007. Early changes in KCC2 phosphorylation in response to neuronal stress result in functional downregulation. J. Neurosci. 27, 1642-1650.

Wang, C., Shimizu-Okabe, C., Watanabe, K., Okabe, A., Matsuzaki, H., Ogawa, T., Mori, N., Fukuda, A., Sato, K., 2002. Developmental changes in KCC1, KCC2, and NKCC1 mRNA expressions in the rat brain. Brain Res. Dev. Brain Res. 139, 59-66.

Woo, N.S., Lu, J., England, R., McClellan, R., Dufour, S., Mount, D.B., Deutch, A.Y., Lovinger, D.M., Delpire, E., 2002. Hyperexcitability and epilepsy associated with disruption of the mouse neuronal-specific K-Cl cotransporter gene. Hippocampus 12, 258-268.

Yamada, J., Zhu, G., Okada, M., Hirose, S., Yoshida, S., Shiba, Y., Migita, K., Mori, F., Sugawara, T., Chen, L., Liu, F., Yoshida, S., Ueno, S., Kaneko, S., 2013. A novel prophylactic effect of furosemide treatment on autosomal dominant nocturnal frontal lobe epilepsy (ADNFLE). Epilepsy Res. 107, 127-137.

Yan, Y., Dempsey, R.J., Sun, D., 2001. Expression of Na(+)-K(+)-Cl(-) cotransporter in rat brain during development and its localization in mature astrocytes. Brain Res. 911, 43-55.

Zhu, L., Polley, N., Mathews, G.C., Delpire, E., 2008. NKCC1 and KCC2 prevent hyperexcitability in the mouse hippocampus. Epilepsy Res. 79, 201-212.

Chapter 3

NEUROMODULATION OF GLUTAMATE RELEASE ONTO PYRAMIDAL NEURONS IN LAYER V OF PREFRONTAL (FR2) CORTEX

Aurora Coatti, Andrea Becchetti

INTRODUCTION

As recalled in chapter 1, a complex neuromodulatory input regulates the PFC function (Dembrow and Johnston, 2014). The brainstem and basal forebrain nuclei reciprocally interact in a very complex way. Moreover, they exert more direct effects on the neocortex, by following two major pathways: 1) by projecting to the thalamus, where they stimulate non-specific thalamocortical glutamatergic neurons; 2) by directly innervating the neocortex, and particularly extensively the PFC (Jones, 2011). Disorders in the ascending regulatory systems may alter the PFC excitability and cause a variety of diseases, including several sleep-related pathologies. Especially relevant from the present standpoint is the balance of the cholinergic and noradrenergic systems (Jones, 2005).

The cholinergic system sustains cortical arousal, regardless of behavioural or motor activity. Cholinergic cells discharge during wakefulness and during REM sleep (Jones et al., 2008; Lee et al., 2005; Siegel, 2002), while they are silent during non-REM sleep. Within the

PFC, acetylcholine (ACh) excites layer V cells by modulating glutamate release from both thalamocortical fibres (Lambe et al., 2003) and intrinsic glutamatergic terminals, through heteromeric β2* nicotinic receptors (nAChRs; Aracri et al, 2010; Aracri et al., 2013). These latter are crucial for the control of neocortical tone, as they stimulate neurotransmitter release (Paterson and Nordberg, 2000). Consistently with this notion, mutations on α4β2* nAChRs are linked to sleep-related epilepsy, characterized by a hyperexcitable PFC network (Becchetti et al., 2015).

The noradrenergic LC maximally discharges during active wakefulness and is almost silent during both REM and non-REM sleep (Aston-Jones and Bloom, 1981). It exerts a widespread modulation on neuronal circuits and is crucial for alert waking and state-dependent cognitive processes (Berridge and Waterhouse, 2003). The simultaneous presence of ACh and norepinephrine (NE) is necessary to sustain the waking state with both cortical activation and muscle tone (Jones, 2005), but how these neurotransmitters interact in the local control of synaptic transmission in the neocortex is poorly understood.

A supplementary control of the cholinergic and noradrenergic systems is exerted by the recently discovered orexin A and B neuropeptides (OrxA and OrxB, Sakurai et al., 1998), which are mostly released during active wakefulness (Lee et al., 2005). Deficits in orexinergic system lead to narcolepsy with cataplexy in both humans and murine models (Chemelli et al., 1999; Peyron et al., 2000). Besides simulating all the subcortical arousal nuclei (Eggermann et al., 2001; Fadel et al., 2005; Fadel and Burk, 2010; Sutcliffe and de Lecea, 2002), orexins also profusely innervate the PFC (Aracri et al., 2015; Boutrel et al., 2010;

Peyron et al., 1998). Conspicuous labelling of OrxRs was observed in pyramidal neuron somata and in the intracortical glutamatergic terminals (but rarely in GABAergic structures), in layer V of murine PFC. Here, OrxA stimulates glutamate release onto FS interneurons (Aracri et al., 2015). Moreover, OrxRs are observed in layer I, where layer V pyramidal cells extend their apical dendrite tufts (Liu and Aghajanian, 2008). ACh and Orx cooperate to control cortical executive functions. In particular, nicotine and OrxB pre-synaptically modulate the same nonspecific thalamocortical projections to PFC (Bayer et al., 2002; Lambe et al., 2003; Lambe et al., 2005; Lambe and Aghajanian 2003) which target the apical dendrites of pyramidal neurons in PFC layer V (Lambe et al., 2007).

Overall, available evidence suggests that ACh and Orx cooperate to modulate glutamate release in PFC deep layers, but the interaction mechanism is poorly understood. A better comprehension of these mechanisms and the interplay between ACh and Orx is needed also to determine the cellular basis of the regulation of network oscillations, particularly theta rhythms (4-8 Hz), which are measurable in PFC during working memory tasks, behavioural monitoring, valuation of response outcomes and other cognitive functions (Luu et al., 2004; Mitchell et al., 2008). Global waves such as these are thought to depend on both extrinsic (i. e. dependent on subcortical input) and intracortical mechanism (Wang, 2000). In fact, theta waves can be generated in cortical slices even in the absence of subcortical input (Silva et al., 1991; Castro-Alamancos et al., 2007), as an emergent property of layer V pyramidal neurons, when synchronized by recurrent excitation (Silva et al., 1991). In Orx-deficient mice, the outbreak of aberrant theta wave

bursts is observed during cataplexy and REM sleep (Bastianini et al., 2012; Vassalli et al., 2013) and is also detected in narcoleptic children (Vassalli et al., 2013). It is thus possible that Orx, by regulating pyramidal neurons excitability, directly affects the cellular mechanisms underlying intracortical theta waves generation.

The previous studies that examined the medial PFC mainly focused on the prelimbic area (Jin, et al., 2016, Kang et al., 2015; Li et al., 2010; Udakis et al., 2016). We instead concentrated upon the dorsomedial shoulder of the murine PFC (Fig. 1A), which is considered homologous to the much larger human dorsolateral cortex (Uylings et al., 2003), and is involved in goal-oriented behaviour (Kargo et al., 2007) and the behavioural responses during attention-requiring situations (Hoover and Vertes, 2007). Therefore, this area, also known as frontal area 2 (Fr2), or as secondary motor (M2) cortex (Franklin et al., 2011), is a particularly relevant target of the arousal effects of the ascending regulatory systems (Heidbreder and Groenewegen, 2003). The neuromodulation of pyramidal neurons in Fr2 layer V is likely to have a major role in controlling the cortical circuit output, since layer V constitutes the main output channel to subcortical regions. Moreover, layer V is particularly prone to develop and spread hyperexcitability (Richardson et al., 2008).

Through electrophysiological experiments on murine brain slices, we explored some aspects of the complex interplay between the main neurotransmitters involved in cortical arousal, i. e. ACh, NE and OrxA, in order to better comprehend how dysregulations of these systems could alter cortical excitability and lead to some sleep-related disorders. In particular, we investigated the modulation of the glutamatergic input

onto pyramidal neurons in Fr2 layer V. Our results show that ACh, NE and OrxA are all implicated in regulating synaptic transmission, in this region. In particular, they enhanced glutamate release, without producing major alterations of the intrinsic electrophysiological features of pyramidal cells.

MATERIALS AND METHODS

Brain slices.

A total of 52 mature FVB wild type mice (Harlan, Italy) of either sex, ranging from P25 to P61, studied as follows: P25-33 (n = 15); P34-42 (n = 14); P43-51 (n = 15) and P52-61 (n = 8), were kept in pathogen-free conditions, with free access to food and water, and a 12h light-dark cycle. The described procedures followed the Italian law (2014/26, implementing the 2010/63/UE) and were approved by the local Ethical Committees and the Italian Ministry of Health.

After a deep anaesthesia with isoflurane, mice were decapitated and the brains were rapidly extracted and placed in ice-cold ACSF (artificial Cerebro-Spinal Fluid) solution containing (mM): 87 NaCl, 21 $NaHCO_3$, 1.25 NaH_2PO_4, 7 $MgCl_2$, 0.5 $CaCl_2$, 2.5 KCl, 25 D-glucose, 75 sucrose, 0.4 ascorbic acid, and bubbled with 95% O_2 and 5% CO_2 (pH 7.4). Fr2 coronal slices (300 um thick) were cut between + 2.68 mm and + 2.10 mm from bregma (Paxinos, 2013), with a VT1000S vibratome (Leica Microsystems) and then maintained at 30°C in the same ACSF solution for at least 1h before being transferred to the recording chamber.

Whole-cell recordings.

Cells were inspected through an Eclipse E600FN microscope, equipped with a water immersion differential interference contrast (DIC) objective (Nikon Instruments), and an infrared digital CCD (C8484-05G01) camera, operated by HCImage Live software (Hamamatsu). Voltage and current signals were recorded with a Multiclamp 700A (Molecular Devices), at 32-34°C. Micropipettes (2-4 MΩ) were pulled

from borosilicate capillaries (Science Products GmbH, GE) with a P-97 Flaming/Brown Micropipette Puller (Sutter Instruments Co., UK). The cell capacitance and series resistance were always compensated (up to 75%). Series resistance was generally below 10 MΩ. Neurons were both voltage- and current-clamped in whole-cell configuration and the input resistance was usually between 30 and 70 MΩ. Slices were perfused at 1.8-2 mL/min with an ACSF solution containing (mM): 129 NaCl, 21 $NaHCO_3$, 1.6 $CaCl_2$, 3 KCl, 1.25 NaH_2PO_4, 1.8 $MgSO_4$, 10 D-glucose, bubbled with 95% O_2 and 5% CO_2 (pH 7.4). Pipettes were filled with a solution containing (mM): 140 K-gluconate, 5 KCl, 1 $MgCl_2$, 0.5 BAPTA, 2 MgATP, 0.3 NaGTP, 10 HEPES (pH 7.25).
EPSCs were low-pass Bessel filtered at 2 kHz and digitized at 5 kHz, with pClamp9/Digidata 1322A (Molecular Devices). The resting membrane potential (V_{rest}) was measured in open circuit mode, soon after obtaining the whole-cell configuration. No correction was applied for liquid junction potentials. Drugs were perfused in the bath and their effects were calculated at the steady-state (usually reached within 2-3 min). Only one experiment was carried out in each slice, to avoid uncontrolled long-term effects of neuromodulators (e.g. on receptor desensitization).

Drugs and solutions.

We purchased acetylcholine chloride (ACh), nicotine, (-) norepinephrine (+)- bitartrate salt hydrate (NE) and dihydro-β-erythroidine hydrobromide (DHβE) from Sigma–Aldrich (Milan, Italy), SB-3348671 from Biotrend, while D-(-)-2-amino-5-phosphono-pentanoic acid (AP5), 6-cyano-7-nitroquinoxaline-2,3-dione (CNQX),

tetrodotoxin (TTX) and Orexin A (OrxA) from Tocris Bioscience, Bristol, UK. ACh, Nicotine, TTX, NE, DHβE, AP5 and OrxA were dissolved in distilled water, and stored at 20°C. Stock solutions of CNQX and SB-3348671 were prepared in dimethyl sulfoxide.

Analysis of patch-clamp data.

Resting potential (V_{rest}), action potentials (APs) and excitatory post-synaptic currents (EPSCs) were analysed off-line by using Clampfit 9.2 (Molecular Devices), and OriginPro 9.1 (OriginLab Corporation, Northampton, MA, USA). In **Table 1** and **Table 2**, all the AP features where analysed during 200 pA current injection. For each cell we averaged the parameters calculated on the third and the last AP of the induced train. Spike width was calculated at half-amplitude, spike amplitude was computed as the difference between the AP threshold and the peak. Adaptation was measured as the ratio between the fourth and the first spike interval. Spike intervals were measured between consecutive peaks. After hyperpolarization (AHP) was measured as the difference between the AP threshold and the most negative V_m reached on repolarization. Finally, the triggering depolarization slope was the difference between the most negative V_m reached on repolarization and the following AP threshold, divided by the relative time.

Individual EPSCs were inspected to reject spurious events. The baseline noise (peak-to-peak) was generally 5-6 pA and we set the detection threshold at 6 -8 pA. The effect of treatments (or recovery) was usually measured for 2 min after reaching the maximal effect. After washout, EPSC frequency was usually larger than 70% of the initial value. Cells in which this value was lesser than 50% were discarded.

Statistics.

The results from populations of experiments are given as mean values ± SEM. The number of experiments (N) refers to the number of tested neurons (in different brain slices). Unless otherwise indicated, statistical comparison between two groups were carried out with two-tailed paired Student's t-test, at the indicated level of significance (p), after testing for normality (with a Kolmogorov-Smirnov test) and variance homogeneity (with F test). The statistical comparison of cumulative distributions of EPSC amplitudes was conducted with the Kolmogorov-Smirnov (KS) test, on at least 2 min continuous recording (never containing less than about 250 events).

RESULTS

All the patch-clamp recordings were performed on pyramidal cells in Fr2 layer V **(Fig 1A)**, which are readily recognizable by their typical triangular shape and large size (somatic diameter around 20 μm). These neurons display subthreshold quasi-linear response when depolarized by 0.5 s current steps. Above threshold, they exhibit low-frequency (8-15 Hz) regular spiking with weak adaptation **(Fig 1B** shows an example of the response to 200 pA of injected current).

In the prominent layer V of Fr2 there are also several interneuron classes, which are distinguishable from pyramidal neurons by their round shape and small size (somatic diameter around 10-12 μm). Moreover, each interneuron type is characterized by a typical firing pattern in response to depolarizing current steps. The vast majority of GABAergic interneuron in layer V is constituted by fast spiking (FS) and regular spiking non pyramidal (RSNP) neurons (Tremblay et al., 2016). FS interneurons express parvalbumin and mainly target the pyramidal neurons somata and the axon hillock. Their firing pattern shows a high frequency of spikes (80- 100 Hz, with 200 pA current stimulus), and negligible adaptation **(Fig 1C)**. RSNP neurons express somatostatin and are thought to mainly target the apical dendrites of pyramidal cells. They show an intermediate frequency and little adaptation when stimulated by 200 pA of current (30-40 Hz) **(Fig 1D)**. During the experiments, the pyramidal neurons' membrane potential was set at -68 mV, near V_{rest} and close to the GABA reversal potential, to record excitatory post-synaptic currents (EPSCs) as large inward currents and minimize the amplitude of the inhibitory post synaptic

currents. In this way, we could avoid applying channel blockers, thus maintaining as far as possible the physiological conditions in the local network. EPSCs constitute a measurable index of glutamate release onto the cell under examination. We mostly considered mice during their second month of life. This guarantees a good compromise between feasibility of patch-clamp experiments, which decreases with mice age, and a good degree of maturity of the cortical circuit. In fact, the ionotropic receptors' expression reaches a steady state starting from the third week of life. Furthermore, we can assume a complete maturation of the local cortical circuits and regulatory systems (Molas and Dierssen, 2014; La Magueresse and Monyer, 2013).

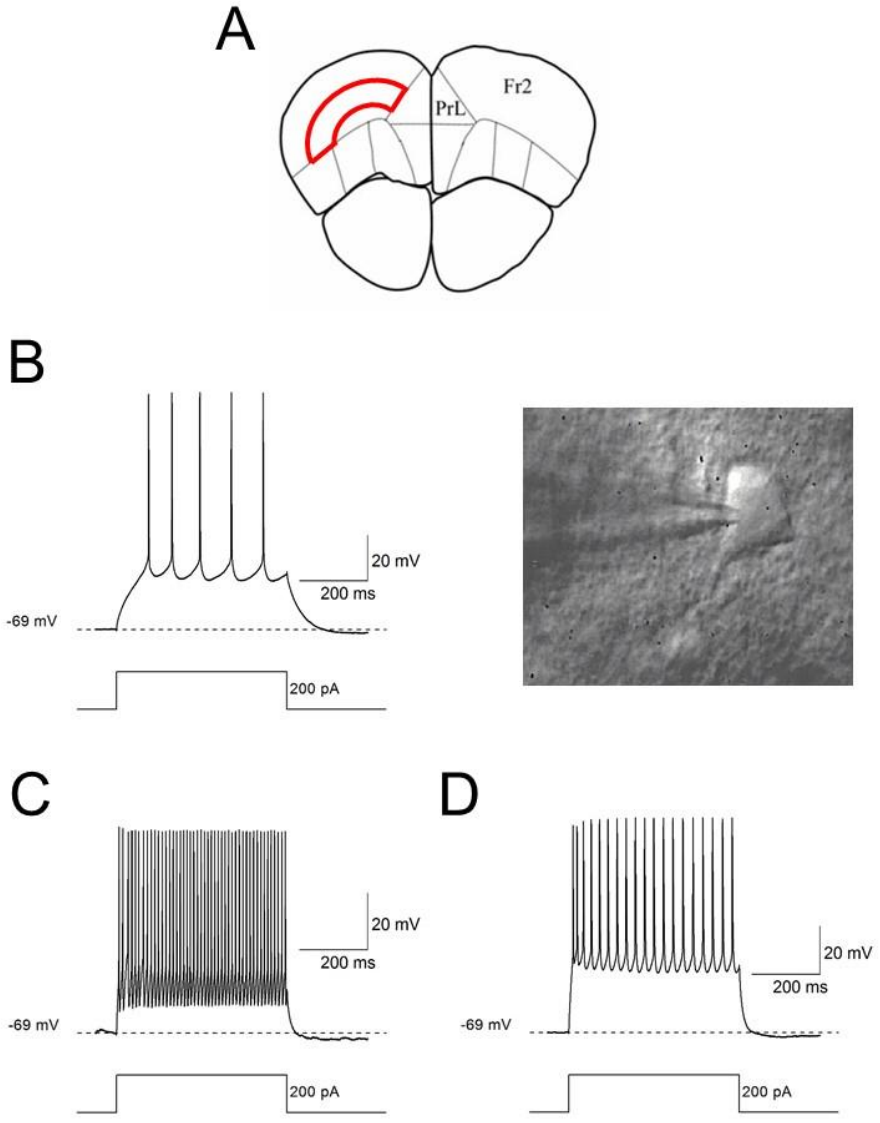

Fig 1 Pyramidal neurons in Fr2 layer V. **(A)** Schematic representation of a coronal murine brain section (modified, from Paxinos, 2013), cut between +2.68 and +2.10 mm from bregma. PrL: prelimbic area; Fr2: frontal region 2. Layer V is highlighted by the red shape. **(B)** Typical low-frequency and regular firing response to a 200 pA depolarizing current step, applied for 500 ms, on a pyramidal neuron. **Right panel**: a typically triangular-shaped pyramidal neuron under patch-clamp recording. **(C)** High frequency and non-adapting firing response to a 200 pA depolarizing injected current of a FS interneuron. **(D)** Firing response to 200 pA depolarizing current (500 ms) of a RSNP cell.

ACh increased the spontaneous EPSC frequency in pyramidal neurons.

We first studied whether ACh affected glutamate release onto pyramidal neurons, by measuring the spontaneous EPSCs. After obtaining the whole-cell configuration and assessing the firing properties of the neuron, we recorded the EPSCs for 5 min in control condition. Next, we applied in the bath 10 µM ACh and recorded the EPSCs for further 5 min. **Fig 2A** illustrates typical current traces in the indicated conditions. The time-course of a representative experiment is shown in **Fig 2B**, in which bars represent the number of EPSCs in 10 s intervals covering the entire experiment. At this concentration of ACh, the steady-state open probability of nicotinic receptors is close to its maximal value (Giniatullin et al., 2005). The average EPSC frequencies were calculated for 2 min at the steady state for each condition. ACh produced a ~ 50% increase in EPSC frequency, (**Fig 2D**), in a reversible way. On the other hand, ACh did not affect EPSC amplitudes (KS test). **Fig 2C** shows the cumulative distribution of the EPSC amplitudes for a typical experiment. Detailed statistics are given in the figure legend. This result suggests that ACh stimulated glutamate release onto pyramidal cells in layer V.

Fig 2 ACh increased the EPSC frequency on pyramidal neurons in layer V Fr2. **(A)** Representative EPSC traces, recorded from a pyramidal neuron at -68 mV, in the indicated conditions. ACh increased the EPSC frequency, in a reversible way. **(B)** Typical time-course of the EPSC frequency throughout an experiment. Bars give the number of synaptic events measured within consecutive 10 s intervals, in the same experiment shown in (A). **(C)** Cumulative distribution of the EPSC amplitudes recorded in a typical experiment for 2 min at the steady state, with or without ACh. The neurotransmitter did not affect the cumulative distribution of event amplitudes

(NS with KS test). **(D)** Bars give the average EPSC frequency, calculated from 2 min continuous recording in the indicated conditions, at the steady state. On average, ACh produced a ~ 51% increase in EPSC frequency, bringing it from 11.63 ± 1.63 Hz to 17.53 ± 2.38 Hz (N = 13, p = 0.0017 with paired *t*-test). **(E)** Representative action potentials induced by 200 pA depolarizing current during control condition and ACh administration. ACh reduced the spike duration.

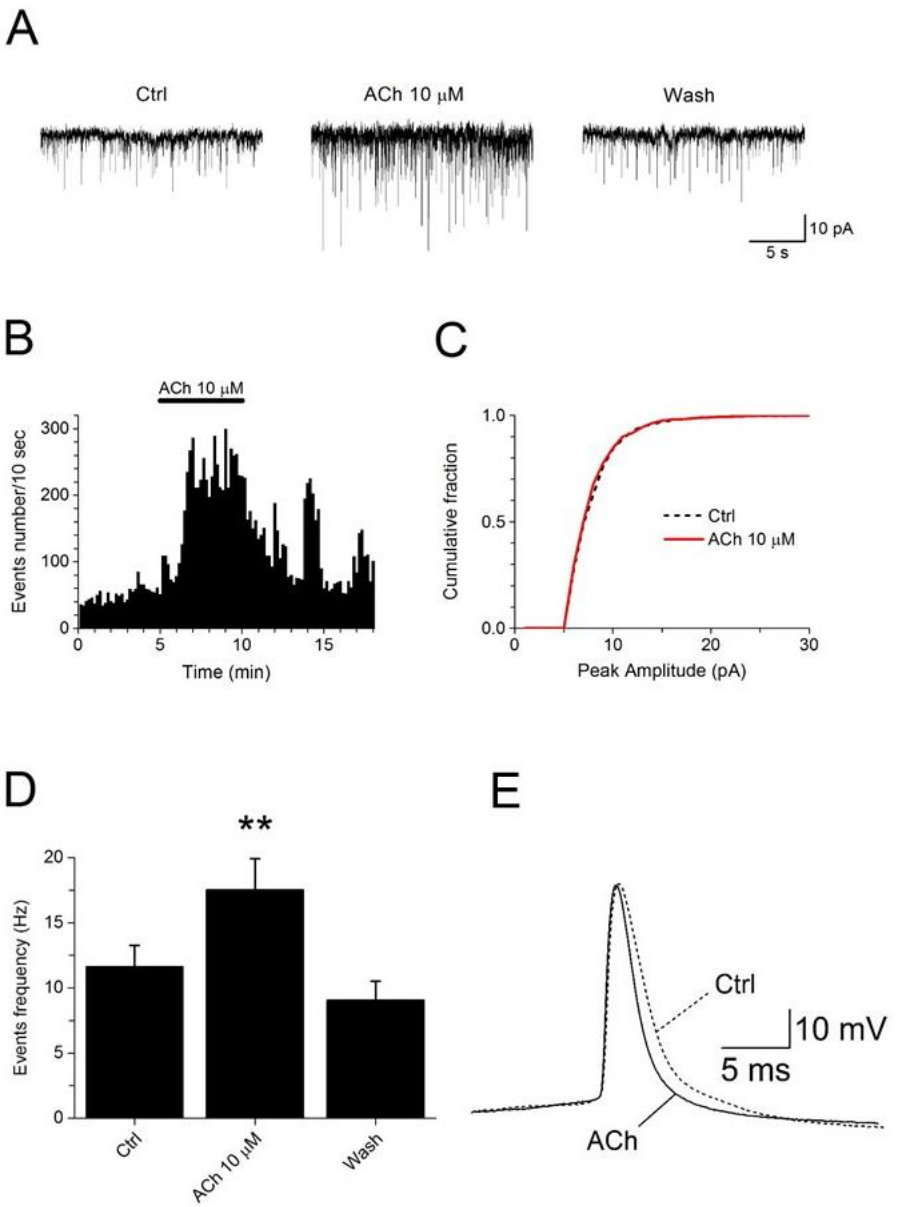

ACh reduced action potential width in pyramidal neurons

We next analysed the direct effect of ACh on pyramidal neurons activity, i. e. on the action potential shape or V_{rest}. To this purpose, we applied series of 1 s depolarizing current steps in order to analyse the pyramidal neurons firing patterns in control conditions. Thereafter, we administered ACh 10 µM and repeated the firing test. We next analysed different electrophysiological properties. During ACh administration no difference was observed in most of the analysed features, compared to control conditions (V_{rest}, spike threshold, frequency, AHP and degree of adaptation, **Table 1**). Nevertheless, ACh reduced the spike width measured at half amplitude, bringing it from 1.81 ± 0.10 ms in control condition to 1.68 ± 0.07 ms during ACh application ($p < 0.05$, *t*-test, N = 8). This effect is likely to be mediated by the muscarinic receptor-dependent intracellular cascades that stimulate voltage-gated potassium channels (probably M_4 receptor in the neocortex; Iversen et al., 2008). **Fig 2E** shows two representative action potentials induced by 200 pA injected current in the specified conditions.

Table 1. Electrophysiological features of pyramidal neurons action potential in control conditions and during ACh 10 µM exposure. Firing parameters in the indicated conditions. All differences between treatments were NS, except for spike width (p = 0.04917, with paired *t*-test, N = 8).

Condition (200 pA)	V_{rest}	Spike width	Spike threshold	Frequency	AHP	4th spike interval /1st
	mV	ms	mV	Hz	mV	
Ctrl	-68.29 ± 0.82	1.81 ± 0.10	-35.93 ± 0.81	12.88 ± 2,05	-9.35 ± 0.53	2.74 ± 0.27
ACh 10 µM	-68.79 ± 1.69	1.68* ± 0.07	-36.52 ± 0.83	13.50 ± 1.75	-9.23 ± 0.72	2.34 ± 0.27

The increase of EPSC frequency exerted by ACh was prevented by DHβE

The ACh effect on EPSC frequency is comparable to the one exerted by nicotine 5 µM (Aracri et al., 2013), which is largely mediated by activation of α4β2* nAChRs. To better assess the nature of the effect produced by the physiological agonist ACh, we administered DHβE 1 µM, a blocker of α4-containing nAChRs, dissolved in ACSF (Harvey et al., 1996). **Fig 3A** illustrates the current traces from a representative experiment. We recorded spontaneous EPSCs in control condition, then we pre-treated the slice with the antagonist for 5 min. DHβE did not produce any effect on EPSCs: it did not alter either the events frequency or their amplitude. When ACh 10 µM was applied in the presence of DHβE, it did not produce the usual increase of EPSC frequency. An example of the time-course of an entire experiment is shown in **Fig 3B**, in which bars represent the number of synaptic input calculated in 10 s

intervals. The average EPSC frequency, depicted in **Fig 3C**, was measured for 2 min at the steady state and was unaltered during ACh administration. In particular, the synaptic events frequency was 15.73 ± 1.80 Hz before ACh application and was 13.41 ± 1.88 in the presence of DHβE plus ACh (NS, paired *t*-test, N = 11). Further statistics are given in the figure legend. The inhibition caused by DHβE on the effect of ACh on EPSCs confirmed that steady concentrations of ACh can regulate glutamate release in layer V mostly by activating nicotinic α4-receptors. Therefore, the contribution of muscarinic receptors is less relevant on this parameter.

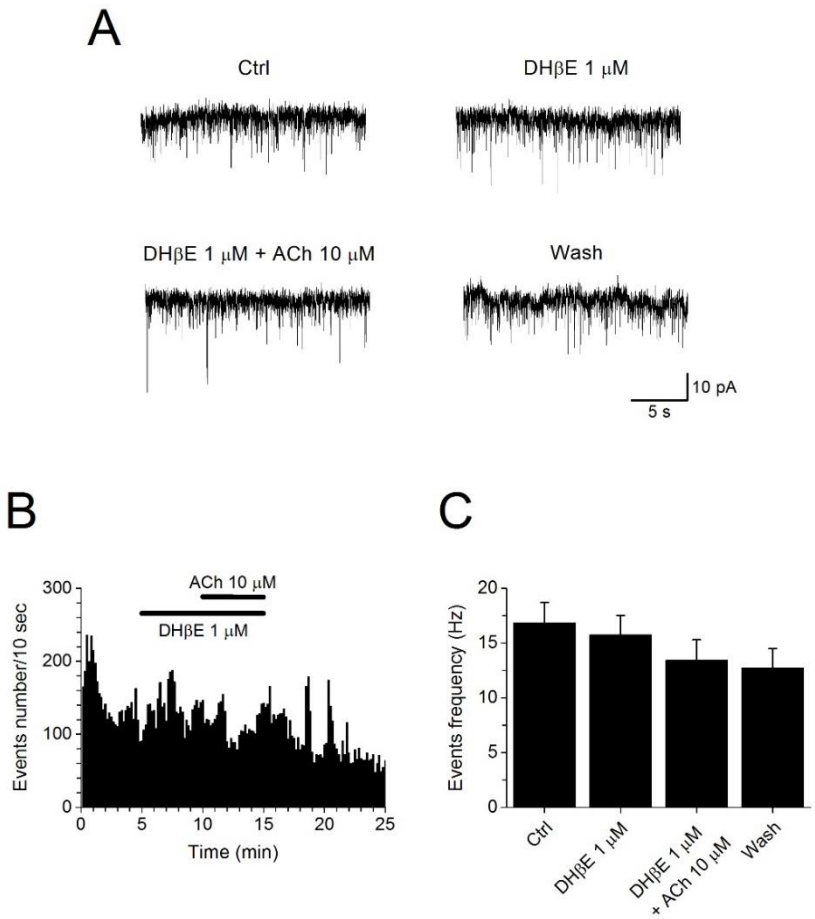

Fig 3 ACh effect on EPSCs is mediated by α_4-containing nAChRs. (A) Representative EPSC traces, recorded from a pyramidal neuron at -68 mV, in the indicated conditions. DHβE 1 μM prevented ACh effect on EPSC frequency. **(B)** Time course of a characteristic experiment. Bars give the number of synaptic events measured within consecutive 10 s intervals, in the same experiment shown in (A). **(C)** DHβE blocked the ACh-dependent increase of EPSC frequency, calculated from 2 min continuous recordings at the steady state. On average, EPSC frequency was 16.83 ± 1.89 Hz (Ctrl), 15.73 ±1.80 Hz (DHβE), 13.41 ± 1.88 (DHβE + ACh; NS compared to DHβE; N = 11) and 12.71 ± 1.80 after wash out.

OrxA stimulated glutamate release onto pyramidal neurons

We next investigated whether OrxA modulates the same excitatory input on layer V pyramidal neurons that is regulated by ACh. Once again, the spontaneous EPSCs were measured at -68 mV. Representative traces are shown in **Fig 4A**. As shown in a typical experiment (**Fig 4B)**, after a 5 min control recording, we added OrxA 500 nM for 5 min. This concentration is known to stimulate both OrxRs 1 and 2 (Ohno and Sakurai, 2008). OrxA administration increased the EPSC frequency from 14.04 ± 5.51 Hz to 19.24 ± 6.10 Hz ($p < 0.05$, paired *t*-test, N = 7; **Fig 4D**). This result suggests that orexin promotes glutamate release from excitatory terminals. The effect was generally reversible after orexin removal, although recovering was usually slower then in the case of ACh, probably due to the long term effect of activated intracellular signalling cascades. **Fig 4C** shows an illustrative cumulative distribution of EPSCs amplitudes recorded for 2 min at the steady state in the presence or in the absence of OrxA. In 6 out of 7 experiments, OrxA produced no significant effect on the amplitude of the synaptic events (KS test).

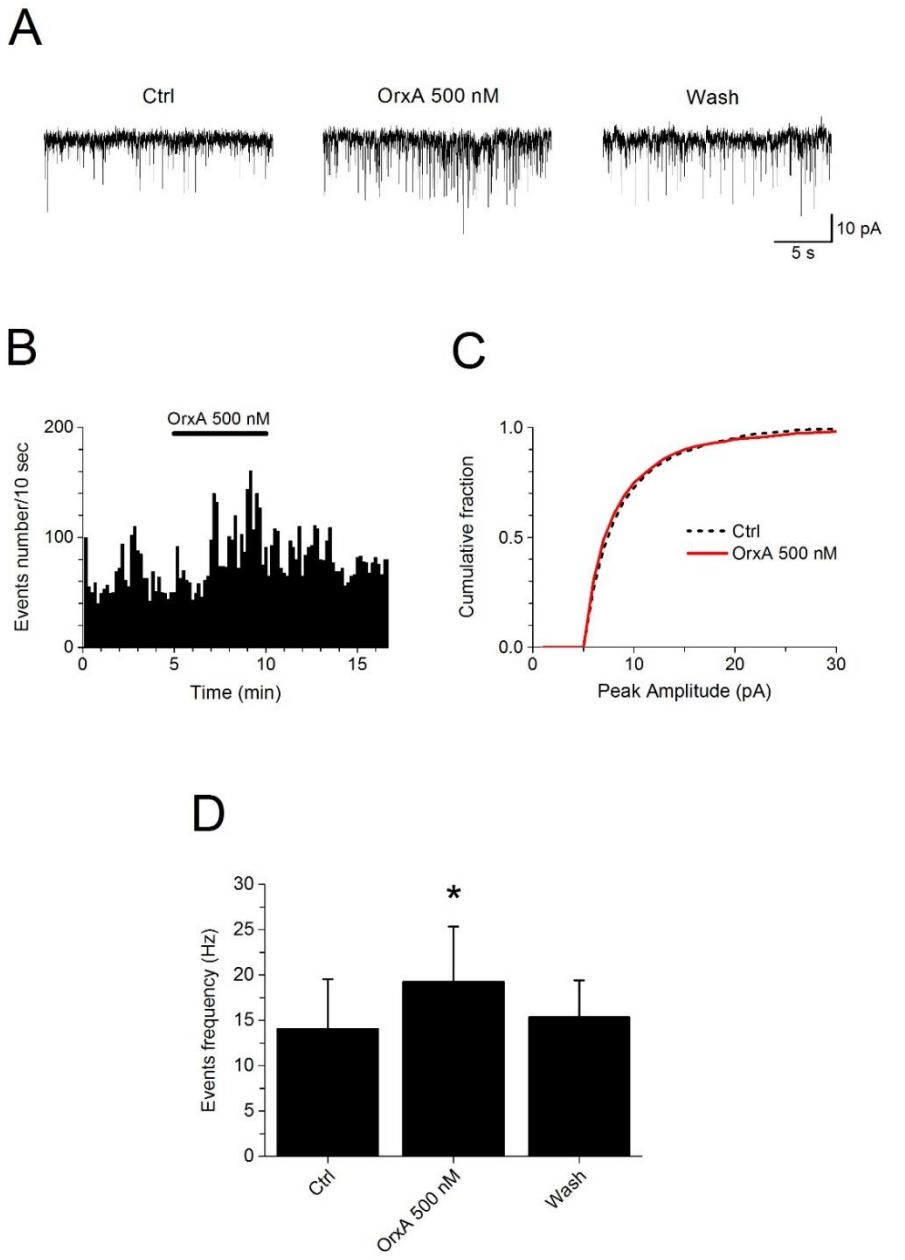

Fig 4 OrxA increases EPSC frequency onto pyramidal neurons in layer V Fr2. **(A)** Representative EPSC traces, recorded from a pyramidal neuron at -68 mV, in the indicated conditions. OrxA (500 nM) increased the EPSC frequency, in a not completely reversible way. **(B)** Typical time course of the EPSC frequency, modulated by OrxA 500 nM. Bars give the number of synaptic events measured

within consecutive 10 s intervals, in the same experiment shown in (A). **(C)** Cumulative distribution of the EPSC amplitudes recorded in an illustrative neuron for 2 min (steady-state) in the presence or absence of OrxA. In 6 out of 7 experiments, OrxA produced no significant effect on the amplitude of the synaptic events (KS test). **(D)** OrxA produced a significant stimulatory effect. Bars give the average EPSC frequency, calculated from 2 min continuous recording in the indicated conditions, at the steady state. On average, OrxA produced a ~ 37% increase in EPSC frequency, bringing it from 14.04 ± 5.51 Hz to 19.24 ± 6.10 Hz ($p = 0.02275$, with paired *t*-test, $N = 7$). The effect was not completely reversible after wash out.

OrxA effect on miniature EPSCs and firing properties

Aracri et al. (2015) examined OrxRs distribution in glutamatergic structures and noticed a widespread expression of OrxR1 in intracortical glutamatergic synaptic terminals. Therefore, we hypothesize that OrxA could exert some of its effects pre-synaptically, by increasing the vesicular release probability. One way to better distinguish if the effects of a neurotransmitter are exerted on pre-synaptic terminals is to study miniature EPSCs (mEPSCs). We administered 1 µM TTX (e.g. Lambe and Aghajanian, 2003; Aracri et al., 2015) to block voltage-gated sodium channels and thus inhibit the action potential generation. In this way we were able to avoid the massive action potential-dependent vesicular release which can induce ample EPSCs. The remaining synaptic events are mEPSCs, induced by exiguous and spontaneous vesicular release, which exclusively depends on the synaptic bouton conditions.

Hence, we compared the mEPSC frequency in the absence and in the presence of OrxA 500 nM. A typical experiment is illustrated in **Fig 5A**. As usual, bars represent the number of synaptic input calculated in

10 s intervals. After 3 min in control condition, we perfused TTX 1 μM for 10 min. Afterwards, we administered OrxA 500 nM in the presence of TTX. Finally, we removed OrxA and recorded mEPSCs in TTX for further 10 min. TTX produced the expected decrease of EPSC frequency and amplitude (**Fig 5B**), but unfortunately, the effect did not reach the steady state, not even after 20 min. For this reason, to detect the OrxA-dependent increase in the mEPSC frequency was rather arduous. **Fig 5C** shows the average EPSC frequencies, measured for 2 min. In particular, the synaptic events frequency was 17.76 ± 2.57 Hz in ACSF and decreased to 4.03 ± 0.54 Hz in the presence of TTX ($p < 0.01$, with paired *t*-test, N = 5). Further statistics are given in the figure legend. EPSC frequency during OrxA application was 2.80 ± 0.60 Hz (NS with paired t-test compared to TTX) and decreased more during the washing out in TTX (1.83 ± 0.55 Hz, significantly minor compared to the previous TTX effect, $p < 0.05$, with paired *t*-test, N = 5). So far, it is not possible to confirm that OrxA stimulates glutamate release by operating at the pre-synaptic level.

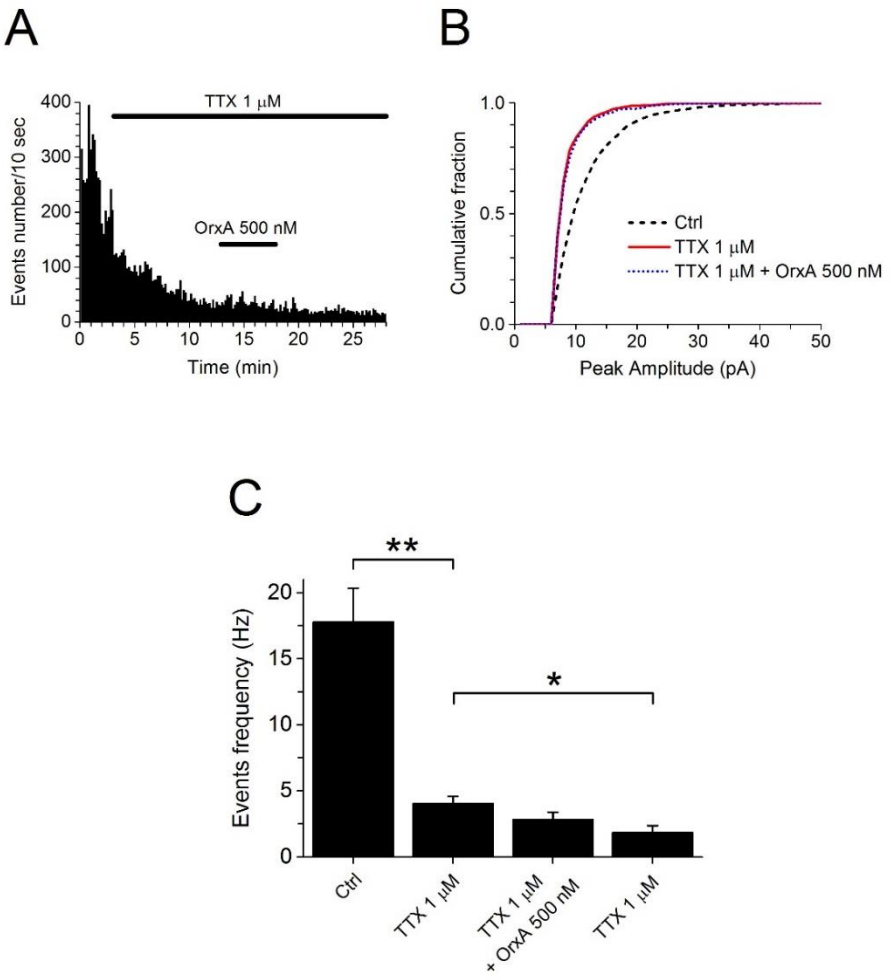

Fig 5 OrxA effect on miniature EPSCs. (A) Typical time course of the mEPSC frequency, isolated by the administration of TTX 1 μM. Bars give the number of synaptic events measured within consecutive 10 s intervals. After 10 min, TTX did not reach the steady state and the OrxA 500 nM effect was not significant. **(B)** Cumulative distribution of the EPSC amplitudes recorded in an illustrative neuron for 2 min (steady-state) in the presence or absence of TTX 1 μM and OrxA. TTX produced a significant decrease of synaptic events amplitudes (KS test), whereas OrxA addition did not further alter the cumulative distribution of the amplitudes. **(C)** TTX induced a significant decrease in EPSC frequency, which however continued till the end of the experiment, without reaching a steady state. The superimposed effect of OrxA was not strong enough to emerge. Bars give the average EPSC frequency, calculated from 2 min continuous recording in the indicated conditions, at the steady state. On average, the synaptic events frequency was 17.76 ± 2.57 Hz in ACSF and decreased to 4.03 ± 0.54 Hz in the presence of TTX ($p = 0.00411$, with paired *t*-test,

N = 5). OrxA brought the mEPSC frequency to 2.80 ± 0.60 Hz (NS with paired t-test compared to TTX). mEPSC frequency decreased more during the washing out in TTX (1.83 ± 0.55 Hz, significantly minor compared to the previous TTX effect, p = 0.02206, with paired *t*-test, N = 5).

In addition, we investigated if OrxA had any direct effect on pyramidal neurons' activity, considering that OrxR1 immunoreactivity is widely observed in layer V neuronal cell bodies (Aracri et al., 2015). OrxA produced no significant effect on the cell's V_{rest}. Moreover, we analysed the firing pattern by applying consecutive current steps in the absence or presence of OrxA 500 nM. During OrxA administration no difference was observed in any analysed feature, such as spike width, spike threshold, frequency, AHP, degree of adaptation and triggering depolarization slope (**Table 2**).

Table 2. Electrophysiological features of pyramidal neurons action potential in the absence or presence of OrxA 500 nM. Firing parameters in the indicated conditions. All differences between treatments were NS with paired *t*-test (N = 11).

Condition (200 pA)	V_{rest}	**Spike width**	**Spike threshold**	**Frequency**	**AHP**	**4th spike interval/1st**	**Triggering depolarization slope**
	mV	ms	mV	Hz	mV		mV/ms
CTRL	-67,13 ± 1,15	2,07 ± 0,13	-35,67 ± 1,08	10 ± 0,86	-8,3 ± 0,55	1,82 ± 0,10	0,113 ± 0,0067
OrxA 500 nM	-66,54 ± 1,14	2,16 ± 0,19	-34,78 ± 1,39	9,55 ± 0,91	-8,34 ± 0,62	1,81 ± 0,09	0,108 ± 0,0056

Co-application of nicotine and OrxA increased the spontaneous EPSC frequency in pyramidal neurons

Because previous work suggested that ACh (through nAChRs) and OrxA targets may overlap, we investigated how their contemporary administration affects glutamate release onto pyramidal neurons. After assessing the pyramidal nature of the neuron, we recorded the EPSCs in control condition for 5 min. Next, we perfused OrxA 100 nM for 2 min, which corresponds to the concentration used by Aracri and colleagues (2015) to measure EPSCs on FS and IPSCs on pyramidal neurons. Then we added, in the presence of OrxA, nicotine 10 µM for 5 min, which produces a close to maximal steady state activation of α4β2 nAChRs. At this concentration the activation of α7 receptors (the other major nAChR type in the PFC) is negligible (e. g. Brusco et al., 2015; Giniatullin et al., 2005). After nicotine was washed out, OrxA was left for further 5 min. Typical spontaneous EPSCs are shown in **Fig 6A**. The time-course of an entire experiment is illustrated in **Fig 6B.** The average EPSC frequencies were calculated for 2 min at the steady state for each condition. OrxA 100 nM was sufficient to increase the EPSC frequency and brought it from 11.55 ± 3.49 Hz to 14.26 ± 3.63 Hz ($p < 0.05$, paired *t*-test, N = 6). Moreover, the administration of nicotine 10 µM further enhanced the EPSC frequency to 24.12 ± 5.88 Hz ($p < 0.05$ compared to OrxA alone, paired *t*-test, N = 6, **Fig 6D**). The co-application of OrxA and nicotine more than doubled (~110% increased) the EPSC frequency compared to control condition, in a reversible way. Nicotine stimulated EPSCs in the presence of OrxA. On the other hand, in most experiments co-administration of nicotine and

OrxA did not affect the EPSC amplitudes (NS with KS test). **Fig 6C** shows the cumulative distribution of the EPSC amplitudes for a typical experiment. Detailed statistics are given in the figure legend.

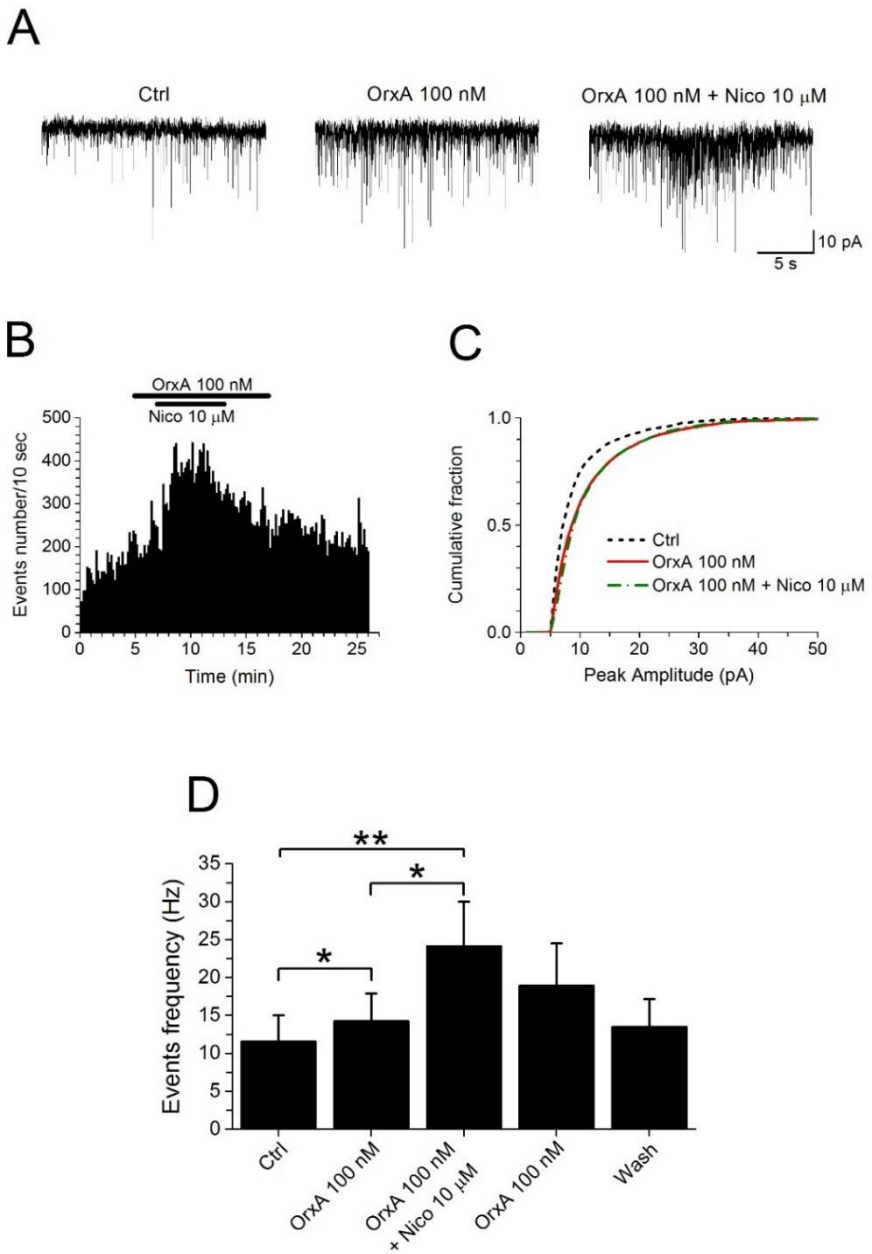

Fig 6 OrxA and Nicotine cooperate to increase the spontaneous EPSC frequency in pyramidal neurons. (A) Exemplifying EPSC traces, recorded from a pyramidal neuron at -68 mV, in the indicated conditions. Both OrxA 100 nM administration and nicotine 10 μM supplementation increased synaptic events frequency. **(B)** Time-course of a typical experiment. Bars indicate the number of EPSCs measured within consecutive 10 s intervals, in the same experiment shown in (A). **(C)** Cumulative distribution of the EPSC amplitudes recorded in an illustrative neuron for 2 min (steady-state) in the indicated conditions. In most tested neurons, OrxA and nicotine co-administration did not affect the distribution of the EPSC amplitudes (NS with KS test). **(D)** Bars give the average EPSC frequency, calculated from 2 min continuous recording in the indicated conditions, at the steady state. OrxA 100 nM produced a significant stimulatory effect. On average, OrxA produced a ~ 23% increase in EPSC frequency, bringing it from 11.55 ± 3.49 Hz to 14.26 ± 3.63 Hz ($p = 0.03638$, with paired *t*-test, N = 6). The administration of nicotine 10 μM further enhanced the EPSC frequency to 24.12 ± 5.88 Hz ($p = 0.01214$ compared to OrxA alone, paired *t*-test, N = 6). The effect was completely reversible after wash out. The overall effect exerted by OrxA and nicotine together was a 109 % increase in EPSC frequency ($p = 0.00608$, with *t*-test, N = 6)

ACh increased the spontaneous EPSC frequency in pyramidal neurons, in the presence of OrxA

To compare the specific nAChR involvement with the broader cholinergic action, we repeated the same experiment, replacing nicotine with ACh. **Fig 7A** illustrates typical EPSC traces in the indicated conditions. The time-course of a representative experiment is shown in **Fig 7B**. After 5 min in control conditions, we perfused OrxA 100 nM for 2 min. Afterwards, we added 10 μM ACh for 5 min in the presence of OrxA. The average EPSC frequency was calculated for 2 min at the steady state for each condition. OrxA 100 nM was confirmed to increase the EPSC frequency and brought it from 10.56 ± 1.57 Hz to 13.55 ± 1.82 Hz ($p < 0.05$, paired *t*-test, N = 11). Moreover, the administration of ACh 10 μM further enhanced the EPSC frequency to

18.59 ± 2.67 Hz ($p < 0.05$ compared to OrxA alone, paired *t*-test, N = 11, **Fig 7D**). The co-application of ACh and OrxA produced a ~ 76 % increase in EPSC frequency compared to control condition and this effect was reversible. In most experiments ACh and OrxA co-administration did not significanlty affect EPSC amplitudes (KS test). **Fig 7C** shows the cumulative distribution of the EPSC amplitudes for a typical experiment. Detailed statistics are given in the figure legend.

In conclusion, the steady state effect of OrxA plus ACh was similar to the one produced by OrxA plus nicotine. However, the effect of OrxA slowed down the ACh's, whose peak shifted, on average, from the second to the fourth minute. This is possibly due to the interaction between intracellular cascades induced by OrxRs and mAChRs.

Fig 7 ACh and OrxA cooperate to increase the spontaneous EPSC frequency in pyramidal neurons. (A) Representative EPSC traces, recorded from a pyramidal neuron at -68 mV, in the indicated conditions. Both OrxA 100 nM and ACh 10 μM plus OrxA increased synaptic events frequency. **(B)** Time course of a characteristic experiment. Bars give the number of synaptic events measured within consecutive 10 s intervals, in the same experiment shown in (A). **(C)** Cumulative distribution of the EPSC amplitudes recorded in an illustrative neuron for 2 min (steady-state) in the indicated conditions. In most tested neurons, ACh and OrxA co-administration did not affect the distribution of the EPSC amplitudes (KS test). **(D)** Bars give the average EPSC frequency, calculated from 2 min continuous recording in the indicated conditions, at the steady state. OrxA 100 nM produced a significant stimulatory effect. On average, OrxA produced a ~ 28% increase in EPSC frequency, bringing it from 10.56 ± 1.57 Hz to 13.55 ± 1.82 Hz ($p = 0.03831$, with paired *t*-test, N = 11). The administration of ACh 10 μM further enhanced the EPSC frequency to 18.59 ± 2.67 Hz ($p = 0.01208$ compared to OrxA alone, paired *t*-test, N = 11). The effect was completely reversible after wash out. The overall effect exerted by OrxA and ACh together was a 76 % increase in EPSC frequency ($p = 0.00365$, with *t*-test, n = 11).

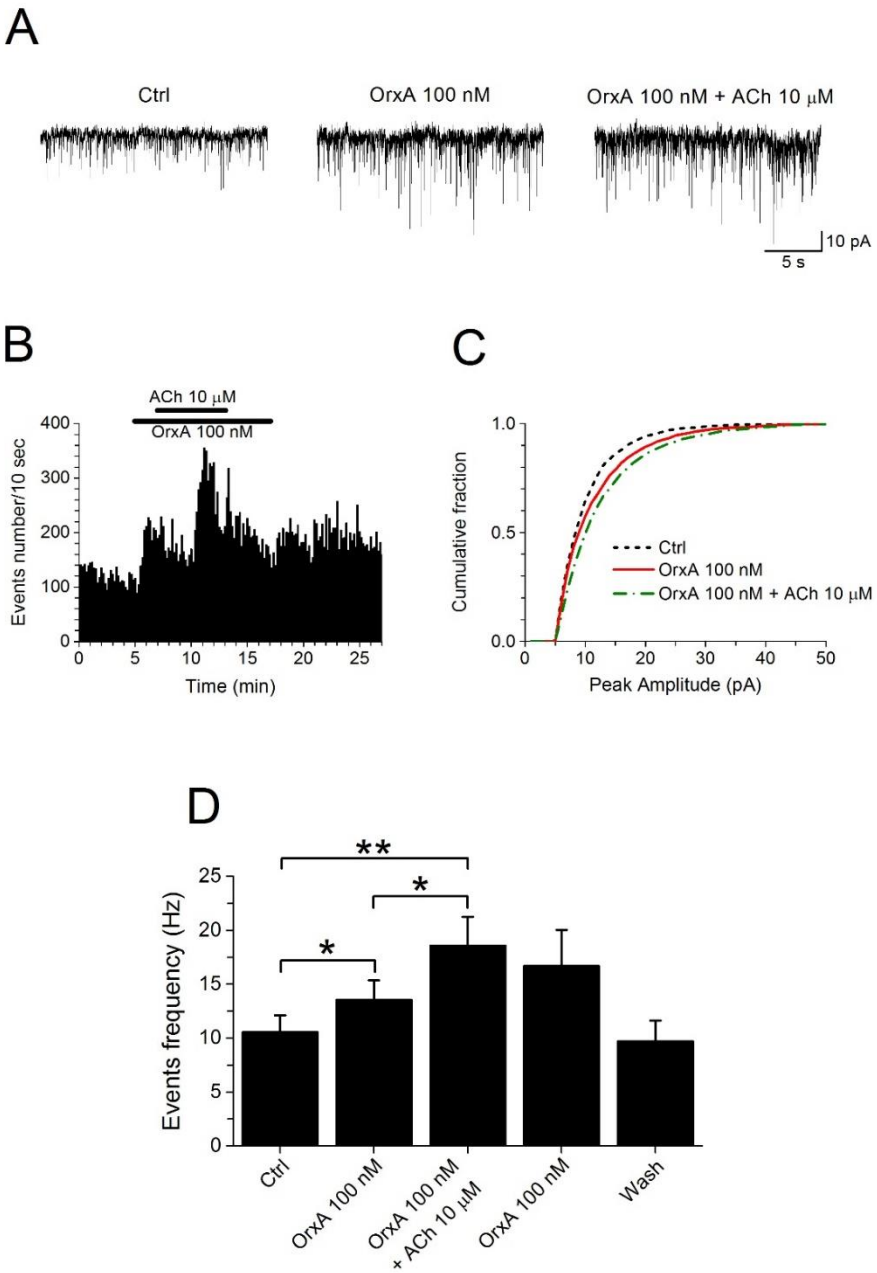
A
Ctrl
OrxA 100 nM
OrxA 100 nM + ACh 10 μM
10 pA
5 s
B
ACh 10 μM
OrxA 100 nM
Events number/10 sec
Time (min)
C
Cumulative fraction
Peak Amplitude (pA)
Ctrl
OrxA 100 nM
OrxA 100 nM + ACh 10 μM
D
Events frequency (Hz)
Ctrl
OrxA 100 nM
OrxA 100 nM + ACh 10 μM
OrxA 100 nM
Wash

The increase of EPSC frequency exerted by OrxA was prevented by SB-334867

We next examined whether the EPSCs stimulation exerted by OrxA was mediated by OrxR1. For this purpose, we pre-treated the slice with SB-334867 1 µM, a specific inhibitor of OrxR1 (Smart et al., 2001). **Fig 8A** illustrates typical current traces in the indicated conditions, from a representative experiment. We recorded spontaneous EPSCs in control condition, then we administered the antagonist for 3 min. SB-334867 did not alter either the events frequency or their amplitude. Subsequent administration of OrxA 100 nM in the presence of SB-334867 had no effect on the EPSC frequency. The time-course of a representative experiment is shown in **Fig 8B**. On average, the EPSC frequency, measured for 2 min at the steady state, was unaltered after OrxA administration. As shown in **Fig 8C,** the EPSC frequency was 13.64 ± 2.51 Hz in control condition, 12.12 ± 2.35 Hz during application of OrxR1 antagonist (NS with paired t-test, N = 5). In the presence of SB-334867 plus OrxA it was 11.37 ± 2.39 Hz (NS, paired *t*-test, N = 5). We conclude that the orexinergic stimulation of EPSCs was impeded by SB-334867, confirming that OrxA modulates excitatory input in layer V through specific peptide interaction with OrxR1.

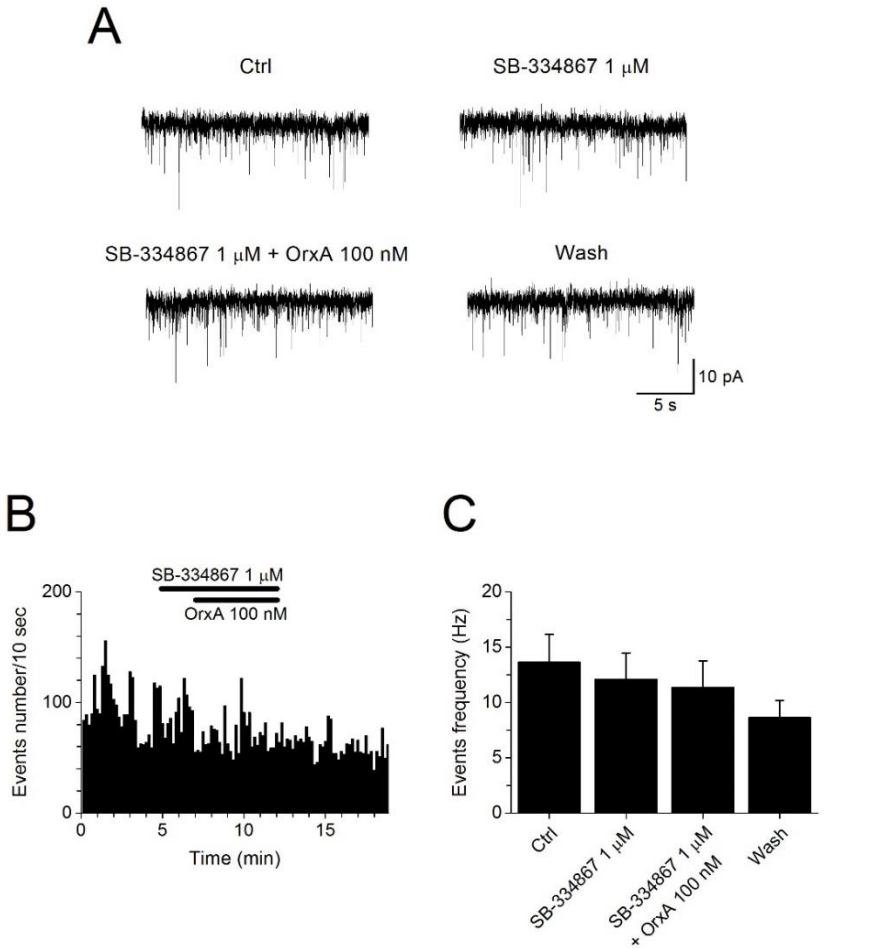

Fig 8 OrxA stimulates EPSCs through OrxR1. (A) Representative EPSC traces, recorded from a pyramidal neuron at -68 mV, in the indicated conditions. SB-334867 1 µM prevented OrxA effect on EPSC frequency. **(B)** Time course of a characteristic experiment. Bars give the number of synaptic events measured within consecutive 10 s intervals, in the same experiment shown in (A). **(C)** SB-334867 1 µM blocked the OrxA-dependent increase of EPSC frequency, calculated from 2 min continuous recordings at the steady state. On average, EPSC frequency was 13.64 ± 2.51 Hz (Ctrl), 12.12 ± 2.35 Hz (SB-334867), 11.37 ± 2.39 (SB-334867 + OrxA; NS compared to SB-334867; N = 5) and 8.64 ± 1.56 after wash out.

NE stimulated EPSCs in pyramidal cells

To better describe the overall modulation of Fr2 layer V excitability, we also investigated the effect of NE on the spontaneous excitatory input measured in pyramidal neurons. Once again, we recorded the spontaneous EPSCs, as illustrated in representative traces in **Fig 9A**. After 5 min control recording, we administered NE 10 nM, a concentration that mimics the tonic and basal concentration of NE, detected in the neocortex through microdyalisis (e. g. Bymaster et al., 2002). NE produced a small (~ 10 %) but significant increase in EPSC frequency, bringing it from 15.71 ± 2.34 Hz to 17.25 ± 2.33 Hz ($p < 0.05$, paired *t*-test, N = 17; **Fig 9C**). The results suggest that NE, even at low tonic concentrations, can contribute to regulate glutamate release in PFC layer V. The effect was fully reversible after NE removal. **Fig 9B** shows a representative cumulative distribution of EPSCs amplitudes recorded for 2 min at the steady state in the presence or in the absence of NE. The effect of NE on EPSC amplitudes was modest, as only in 3 out of 17 experiments we observed a significant increase of cumulative distribution (KS test).

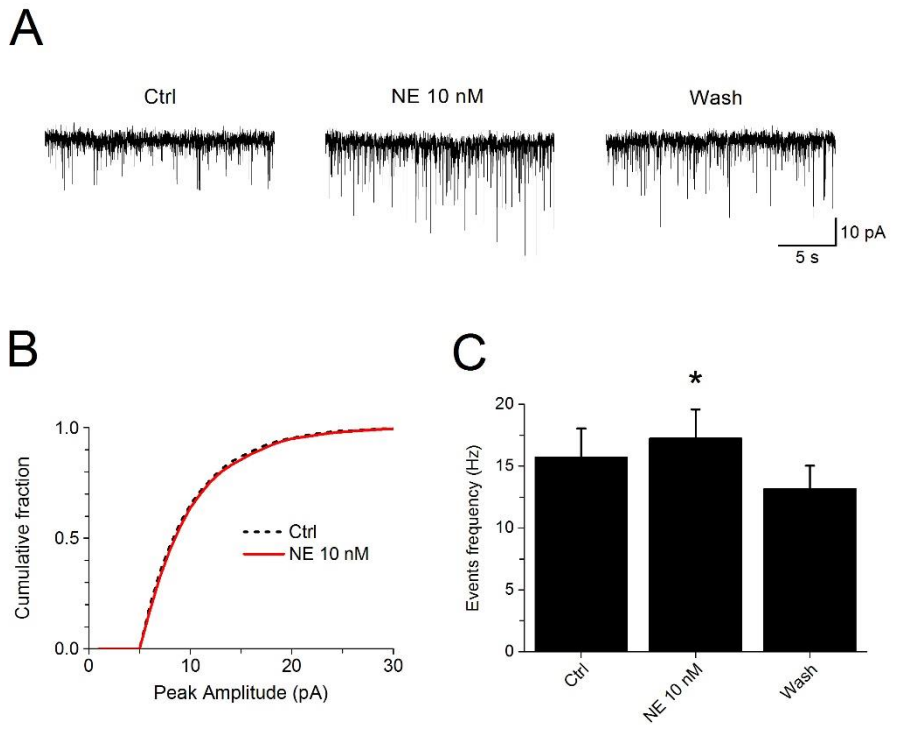

Fig 9 NE increased glutamate release onto pyramidal neurons in layer V of Fr2. **(A)** Illustrative EPSC traces, recorded from a pyramidal neuron at -68 mV, in the indicated conditions. NE (10 nM) increased the EPSC frequency, in a reversible way. **(B)** Cumulative distribution of the EPSC amplitudes recorded in a representative neuron for 2 min (steady-state) in presence or in absence of NE. In most experiments, NE produced no significant effect on the amplitude of the synaptic events (NS with KS test), only in 3 cases it increased the cumulative distribution (significant with KS test). **(C)** NE significantly increased the EPSC frequency onto pyramidal neurons. Bars specify the average EPSC frequency, calculated from 2 min continuous recordings in the indicated conditions, at the steady state. On average, NE produced a ~ 10% increase in EPSC frequency, bringing it from 15.71 ± 2.34 Hz to 17.25 ± 2.33 Hz ($p = 0.01636$, with paired *t*-test, $N = 17$). The effect was reversible after wash out.

Co-application of ACh and NE increased the spontaneous EPSC frequency in pyramidal neurons

ACh and NE release is high in PFC during awake state. We studied their cooperation in regulating the excitability of layer V. We recorded the spontaneous EPSCs and tested the response to ACh 10 µM and NE 10 nM contemporary exposure. **Fig 10A** displays 3 typical EPSC traces before, during and after neurotransmitters administration. The entire experiment is described by **Fig 10B**, in which the bars correspond to 10 s intervals. We measured the average spontaneous EPSCs at the steady state. The frequency analysis showed a transient stimulation of excitatory input, reverted after compounds removal. The co-presence of ACh and NE significantly increased the events frequency and brought it from 9.34 71 ± 1.17 Hz to 15.11 ± 1.41 Hz ($p < 0.001$, paired *t*-test, N =14) as shown in **Fig 10D**. The effect on events amplitudes cumulative distribution was negligible (NS with KS). **Fig 10C** shows representative cumulative distributions in control condition and during ACh and NE application.

Fig 10 ACh and NE co-application increased EPSC frequency. (A) Sample EPSC traces, recorded at -68 mV from a pyramidal neuron, in the indicated conditions. Simultaneous application of ACh 10 µM and NE 10 nM produced the expected increase of the EPSC frequency, in a reversible way. **(B)** Time course of the EPSC frequency during the entire experiment. Bars show the number of synaptic events measured within consecutive 10 s intervals, in the same experiment shown in (A). **(C)** Corresponding cumulative distribution of the EPSC amplitudes recorded in a same representative neuron for 2 min (steady-state) in the presence or absence of the two neurotransmitters. The effect on events amplitudes cumulative distribution was negligible (NS with KS). **(D)** The coexistence of ACh and NE significantly increased the EPSC frequency onto pyramidal neurons. Bars give the average EPSC frequency, calculated from 2 min continuous recordings in the indicated conditions, at the steady

state. On average, ACh and NE together produced a ~ 62% increase in EPSC frequency, bringing it from 9.34 ± 1.17 Hz to 15.11 ± 1.41 Hz (p = 1.034E-5, with paired *t*-test, N = 14). The effect was reversible after wash out.

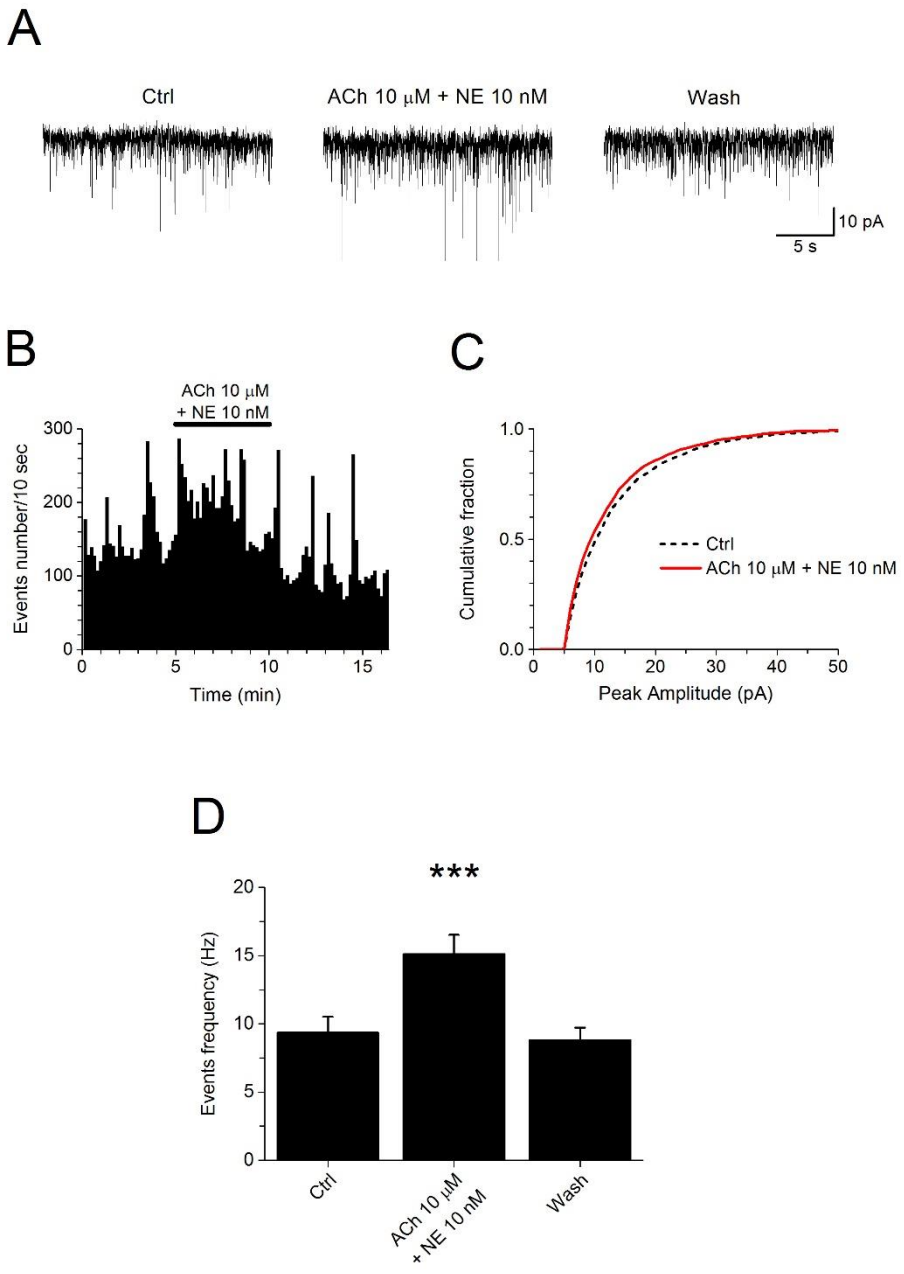

NE did not affect the EPSC stimulation exerted by ACh alone

To isolate the effect of both ACh and NE, we repeated the latter experiment separating their administrations. We recorded EPSC in control conditions for 5 min, then we applied ACh 10 μM alone and measured the synaptic currents for 2 min, before NE 10 nM addition. After 5 min, during which ACh and NE were simultaneously present, NE was withdrawn. The time-course is depicted in **Fig 11B**. Emblematic current traces in each experimental condition are shown in **Fig 11A**. In control conditions the average EPSC frequency, calculated from 2 min continuous recording, was 12.63 ± 2.58 Hz. ACh exposure produced the expected increase of EPSC frequency, bringing it to 20.21 ± 3.92 Hz ($p < 0.01$, paired *t*-test, N = 12). Instead, NE addition did not lead to any further stimulation: the average EPSC frequency during ACh and NE co-existence was 19.88 ± 3.40 Hz (NS compared to ACh, N = 12), as illustrated in **Fig 11C**. These results suggest that, at low tonic concentrations of NE, the regulatory effect on EPSCs is dominated by the cholinergic stimulus.

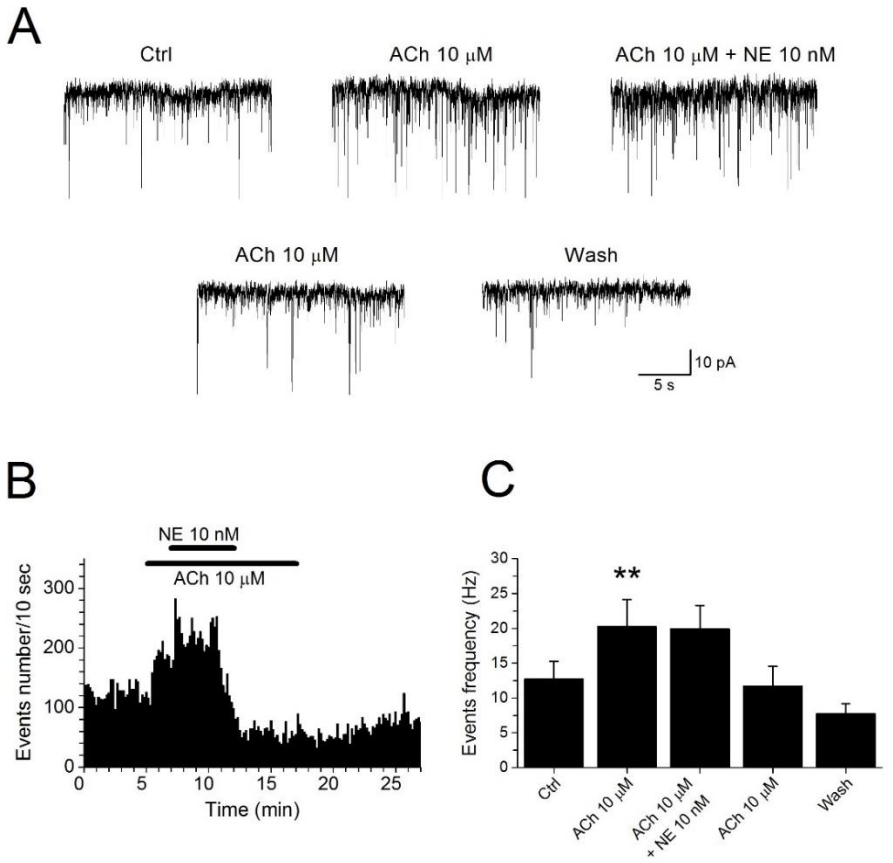

Fig 11 The interaction between ACh and NE does not produce a synergistic effect. (A) Illustrative EPSC traces, recorded at -68 mV from a pyramidal neuron, in the indicated conditions. Consecutive application of ACh (10 μM) and NE (10 nM) produced an increase of the EPSC frequency, in a reversible way. **(B)** Representative time course of the EPSC frequency during the entire experiment. Bars give the number of synaptic events measured within consecutive 10 s intervals, in the same experiment shown in (A). **(C)** NE-dependent increase of EPSC frequency onto pyramidal neurons was secondary compared to ACh-mediated. Their interaction did not produce a synergistic effect. Bars indicate the average EPSC frequency, calculated from 2 min continuous recordings in the indicated conditions, at the steady state. On average, ACh alone produced a ~ 60% increase in EPSC frequency, bringing it from 12.63 ± 2.58 Hz to 20.21 ± 3.92 Hz ($p = 0.00112$, with paired *t*-test, N = 12), while NE addition did not produce any further increase (19.88 ± 3.40; NS compared to ACh; DF = 11). The effect was reversible after wash out.

SUMMARY, CONCLUSIONS AND FUTURE PERSPECTIVES

ACh modulates developing cortical circuits

In chapter 2, we considered mice in which expressing β2-V287L subunit during circuit maturation (until P15) is sufficient to develop a sleep-related epileptic phenotype (Manfredi et al., 2009). Hyperfunctional nAChRs clearly exert their epileptogenic action during sensitive phase of network development: they generate a synaptic unbalance which causes a permanently aberrant network, thus facilitating the triggering of epileptiform activity in mature circuits (Meneghini et al., 2017).

The nAChR roles during neural circuit wiring are largely unknown. We analysed one of the mechanisms through which mutant nAChRs could lead to long-term structural alterations. Physiologically, the excitatory to inhibitory GABAergic switch overlaps with maximal nAChR expression. We showed that, in mice expressing β2-V287L, postnatal KCC2 expression was delayed in PFC layer V during development. Such delay was accompanied by a delayed GABAergic switch, and points to an interaction between KCC2 and nAChRs during synaptogenesis, hypothetically through calcium-depending signalling. On the other hand, E_{GABA} was similar in control and transgenic adult mice, suggesting that the overexpression of KCC2 in the adult circuit is a compensatory effect, necessary to sustain inhibition in a hyperexcitated network, by maintaining the physiological $[Cl^-]_i$.

Finally, the postnatal KCC2 expression resulted to be lower in RT nucleus, in mice expressing β2-V287L. This observation indicates that

the thalamic circuit could be also affected in our mice. The cellular bases of this effect and the possible implications for ADNFLE will be the object of further studies.

ACh modulates glutamatergic transmission in mature Fr2 layer V

In chapter 3, we studied neuromodulation on synaptic transmission in PFC slices, in which all the subcortical afferents were cut off and exogenous neurotransmitters washed out. Nevertheless, our tissue was not silent, in fact we were able to measure spontaneous glutamate release. This residual activity is stable and balanced and is likely maintained by pacemaker or reverberating neurons (Le Bon-Jego and Yuste, 2007; Wenger-Combremont et al., 2016). We could thus administer several neuromodulatory drugs to investigate their ability to affect the spontaneous network activity, seeking to mimic different arousal conditions. In general, none of the tested compounds significantly affected the amplitude of post-synaptic currents, so I mainly focused on their effect on frequencies.

Previous works in prelimbic PFC (Lambe et al., 2003) and Fr2 (Aracri et al., 2013) showed that nicotine stimulated EPSCs in layer V, by activating heteromeric nAChRs. Here, we investigated the effect of the physiological agonist ACh, and showed that moderate ACh concentrations stimulate Fr2 excitability, by enhancing glutamate release onto layer V pyramidal neurons, by ~ 50 %. By using DHβE, we found the effect was exerted through α4-containing nAChRs, which are largely constituted by the α4β2 subtype, and are highly expressed

throughout Fr2, in both intracortical and thalamocortical glutamatergic terminals (respectively recognized by labelling VGLUT1 and VGLUT2; Aracri et al., 2013). There are two possible mechanisms through which pre-synaptic nAChRs can regulate neurotransmitter release (Marchi and Grilli, 2010): 1) their permeability to Ca^{2+} directly stimulates vesicular fusion; 2) their permeability to monovalent cations induces a membrane depolarization, which consequently opens voltage-gated calcium channels. The ACh concentration we tested is comparable to the one tonically released by paracrine and volume transmission in the cerebral cortex (Sarter et al., 2009). This concentration is not sufficient to produce significant activation of α7* nAChRs, whose EC_{50} for ACh is 100 – 200 μM (Dani and Bertrand, 2007). α4β2 nAChRs mediate the tonic neocortical activation produced by the ascending cholinergic signalling typically occurring during wakefulness and REM sleep. This is consistent with the involvement of heteromeric nAChRs in sleep-related epilepsy.

The second way through which ACh could influence glutamate release is by regulating cell firing. We did not observe whole-cell somatic currents at V_{rest}, in agreement with similar studies carried out with nicotine in PFC (Aracri et al., 2013; Couey et al., 2007). However, we noticed a reduction of pyramidal neuron spike width, which may facilitate high frequency firing. This effect is likely to be mediated by muscarinic receptors and would be further investigated.

In conclusion, ACh enhanced Fr2 layer V pyramidal cell activity by stimulating glutamate release, without accompanying this effect with a significant somatic depolarization. Moreover, ACh also produced spike shape regulation.

A recent study conducted in our laboratory (Aracri et al., 2017) shows that heteromeric nAChRs can also stimulate reciprocal inhibition between interneurons. This latter effect could overlap with the increase of glutamate release to stimulate network excitability during cognitive tasks.

Implications for epilepsy

A proper balance between excitatory and inhibitory input is needed for PFC to perform its function and defects in the ability to sustain it can lead to neurological diseases. The link between ADNFLE and gain of function mutations in nAChRs is well established (De Fusco et al., 2000; Phillips et al., 2001; Aridon et al., 2006; Hoda et al., 2008). Considering the physiological role of nAChR in both developing and mature PFC networks, our results indicate that: 1) the structure of synaptic connections between neurons is stably altered in ADNFLE subjects, because of a delay in the GABAergic switch during synaptogenesis; 2) in the mature circuit, during non-REM sleep, when the cholinergic tone is low, small changes in ACh levels may shift the balance of the local network towards hyperexcitability, because of the expression of hyperfunctional heteromeric nAChRs, which could produce excessive stimulation of glutamatergic transmission.

Noneheless, both theoretical and experimental works suggest that hyperexcitability is difficult to be generated without some degree of network disinhibition (Becchetti et al., 2015). Therefore, our future work on the cholinergic modulation of layer V synaptic transmission

will focus on two interneuron classes. In fact, pyramidal neuron activity is thightly controlled by FS interneurons, which are involved in feed-back and feed-forward inhibition. However, other interneuron populations are involved in controlling layer V output. The main is constituted by regular spiking non pyramidal (RSNP) neurons, largely expressing somatostatin (Tremblay et al., 2016). They are highly responsive to ACh and may be involved in hyperexciting layer V network when the cholinergic tone is low (i. e. during non-REM sleep). Moreover, subpopulations of these interneurons express neuronal nitric oxide synthase (nNOS) and the receptor for substance P (NK1R), which are activated during non-REM sleep. Cholinergic neurons of basal forebrain modulate these cells, thus contributing to the regulation of cortical activity across arousal states (Williams et al., 2017).

OrxA modulates synaptic transmission in Fr2 layer V

Here we show the stimulatory effect of OrxA on glutamate release onto pyramidal neurons. OrxA 500 nM produced a ~ 37% increase in EPSC frequency, while OrxA 100 nM induced a 23 – 28 % stimulation (In agreement with biochemical studies by Putula and Kukkonen, 2012; Sakurai et al., 1998). The increase of EPSC frequency was mediated by OrxR1, as it was abolished after SB-334867 pre-treatment (Smart et al., 2001). This result is in agreement with the OrxR1 distribution in layer V in VGLUT1 terminals and the efficacy of OrxA in increasing glutamate release onto FS cells (Aracri et al., 2015). In this case, OrxA was found to stimulate glutamate release from pre-synaptic terminals,

thus regulating the excitatory drive onto FS interneurons and, presumably, pyramidal neurons.

In the present work, unfortunately, we could not prove that the stimulation of EPSC onto pyramidal neurons exerted by OrxA had a pre-synaptic component, because the experimental procedure to isolate mEPSCs with TTX concealed the orexinergic effect. To better isolate the miniature events, we will carry out further experiments with TTX plus Cd^{2+} to also block pre-synaptic voltage-gated Ca^{2+} channels.

To continue the analysis of the OrxA effect on layer V pyramidal cells, we investigated direct cellular alterations: OrxA acts through two G protein coupled receptors (OrxR1 and R2), leading to a variety of intracellular events, such as protein kinase C activation (Kukkonen and Leonard, 2014), which can inhibit K+ (Xia et al., 2005) and hyperpolarization-activated HCN channels (Li et al., 2010). We hypothesized OrxA could directly stimulate pyramidal cell excitability by reshaping the action potential or altering V_{rest}, but, we did not observe OrxA-dependent changes in V_{rest}, spike threshold, frequency, afterhyperpolarization, repolarization slope or adaptation. We can hypothesize that the OrxR1 immunoreactivity observed in pyramidal cell somata of Fr2 layer V (Aracri et al., 2015) is confined to intracellular vesicles, and not exposed on the cellular membrane. Nevertheless, in other central nervous system regions, orexins have been reported to be able to stimulate pyramidal cell depolarization and spiking (Leonard and Kukkonen, 2014; Yang and Ferguson, 2002; Murai and Akaike, 2005; Xia et al., 2005).

Orexinergic system may be implicated in theta rhythms regulation

The neocortical function depends on the orchestration of highly organized and interconnected neurons, which generate synchronous rhythms, measurable as electroencephalogram (EEG) signals. In particular, theta rhythms (4-8 Hz) are found in PFC during working memory tasks, particularly in the frontal midline and are implicated in behavioural monitoring, evaluation of response outcomes and other cognitive functions (Luu et al., 2004; Mitchell et al., 2008; Vassalli et al., 2013). These waves can be generated by intracortical mechanisms, as they can be reproduced in neocortex slices (Silva et al., 1991; Castro-Alamancos et al., 2007). Gamma rhythms (>30 Hz) often accompany theta rhythm in PFC during attentive behavioural states, and can also be experimentally reproduced in cortical slices (McNally et al., 2011). Each neuron displays an intrinsic preferred frequency which induces a maximal response (Lampl and Yarom, 1997). Such resonance frequency resides in the theta range for layer V pyramidal neurons (Silva et al., 1991) and in gamma range for fast-spiking interneurons (Cardin et al., 2009; McNally et al., 2001), suggesting differential roles of specific cell types in layer V network oscillations.

Our present and previous results suggest that OrxA may affect the cellular mechanisms underlying theta and gamma rhythms as it regulates in Fr2 layer V both pyramidal cells and interneurons. Theta rhythms are a typical feature of narcolepsy with cataplexy, a sleep-related pathology linked to orexin deficit. Orx-KO mice display inability to maintain an active waking state characterized by high theta and fast-gamma EEG power during exploratory behaviour, known as

theta-dominated wakefulness (TDW; Vassalli and Franken, 2017). TDW stability thus depends on the Orx-dependent neuromodulation of the circuits generating theta/gamma. Our data indicate that an intracortical component of this effect may depend on Orx increasing the probability of pyramidal neurons to shift to regular spiking (Silva et al., 1991). In contrast, Orx-KO mice display paroxysmal theta bursts at the beginning of cataplexy attacks, which typically interrupt intense goal-oriented activity and during REM sleep (Bastianini et al., 2012; Vassalli et al., 2013). Transient increase in ACh (but not NE) release may be involved in these paroxysmal theta bursts, as it may activate reciprocal inhibition between interneurons, disinhibiting the local circuit. Orx may prevent overexcitation, by regulating the whole microcircuit activity (composed of both pyramidal neurons and GABAergic feedback). It would be interesting to assess whether the Orx-dependent regulation of theta and gamma waves can be reproduced *in vitro*.

NE modulates glutamatergic transmission in Fr2 layer V

To complete a preliminary overview on the neuromodulation of layer V excitability, we also considered NE, which is released in PFC during active wakefulness and prevents sleep (Berridge and Abercrombie, 1999). If ACh alone (in REM sleep) sustains cortical arousal, during wakefulness, NE helps ACh in sustaining also behavioural arousal. We used lower NE concentrations compared to other similar studies (5 - 30 µM) to better mimic physiological conditions: we based on extracellular levels measured by microdialysis in PFC (Bymaster et al.,

2002; Berridge and Abercrombie, 1999; Florin-Lechner et al., 1996). Tonic NE 10 nM administration was able to produce a small (~ 10 %) increase of glutamatergic release onto Fr2 layer V pyramidal neurons. This is a preliminary result, which is inserted in a very complex context: NE modulates synaptic transmission through highly variable mechanisms which depend on receptors distribution and second messenger coupling to α1, α2 and β1 adrenoceptors (Iversen et al., 2008). In other studies, conducted in layer V of rat mPFC, high concentrations of NE depressed glutamate release onto FS, but not onto pyramidal cells, while the effects on GABAergic transmission are conflicting (Roychowdhury et al., 2014; Wang et al., 2013; Kawaguchi and Shindou, 1998, Salgado et al., 2010). Nevertheless, data doubtless indicate the existence of noradrenergic-controlled network in the PFC, where layer V constitutes a "bottleneck for behavioural inhibition" (Roychowdhury et al., 2014).

ACh, NE and OrxA interact in modulating synaptic transmission in Fr2 layer V

After assessing the contribution of each arousal-linked neurotransmitters, we explored some aspects of their complex interplay (**Fig 12**).

ACh 10 µM and OrxA 100 nM together produced a ~ 76% increase of the spontaneous EPSC onto pyramidal neurons and this result is confirmed also substituting ACh with nicotine 10 µM, indicating a major contribution of nAChRs. The cooperative effect on glutamate

release is in agreement with previous studies showing that nicotine and Orx pre-synaptically modulate the same thalamocortical terminals in PFC (Lambe and Aghajanian 2003; Lambe et al., 2003; Lambe et al., 2005). These terminals constitute a small percentage of the total synaptic terminals in the PFC. However, both nAChRs and OrxRs are also widely expressed in intracortical glutamatergic fibres in Fr2 (Aracri et al., 2013). Therefore, we conclude that ACh and Orx cooperate in modulating the overall excitation in Fr2 deep layers.

The additive effects of ACh and OrxA may explain why in Orx-KO mice the TDW state is more difficult to maintain (Vassalli and Franken, 2017), as ACh and Orx are both implicated in regulating pyramidal neurons. On the other hand, paroxysmal theta bursts observed in cataplexy attacks and REM sleep (Bastianini et al., 2012; Vassalli et al., 2013), both characterized by a high cholinergic tone, could depend on an impaired GABAergic feedback in the presence of powerful cholinergic bouts.

By contrast, the effects of ACh was similar in the presence or absence of 10 nM NE. This suggests that, in PFC, in condition of tonic stimulation at low NE concentrations, the effect of cholinergic receptors tends to prevail.

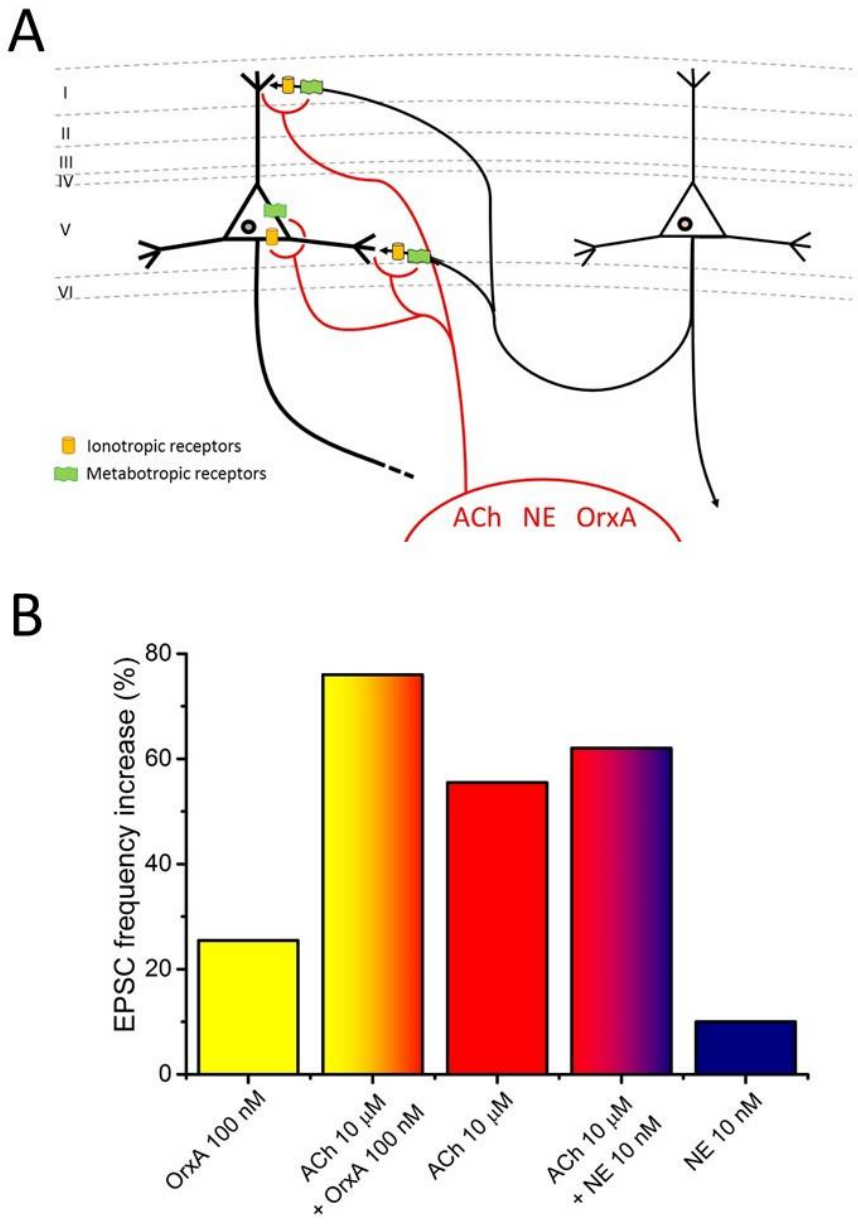

Fig 12 Global overview on the neuromodulation of Fr2 layer V excitability. (A) Schematic Fr2 network, in which reciprocal excitatory connections among pyramidal neurons are regulated by the actions of ACh, OrxA and NA exerted on pre-synaptic terminals. **(B)** EPSC frequency percent increase produced by indicated conditions. OrxA, ACh and NE cooperate in controlling the overall glutamate release in Fr2 layer V. Association of two neurotransmitters perfectly sums up the effect of each neuromodulator alone.

Possible contribution of other neurotransmitters

Dopamine, serotonin and histamine may be matter of interest to obtain a global overview on the arousal modulation of Fr2 layer V excitability. For example, dopaminergic input in PFC is associated to positive emotions. It may be involved in triggering cataplexy attacks in narcoleptic subjects, thus suggesting an interaction with orexinergic system. Zhang et al. (2010) observed the dopaminergic system (as the cholinergic one) to converge on mPFC layer V pyramidal cells. They indicated that the modulation of mPFC exerted by dopaminergic fibres would be mostly inhibitory and localized at the output level. Moreover, cholinergic system would modulate both the local circuit and dopaminergic fibres.

Histamine, finally, may be also involved, in these mechanisms. Orx neurons increase histamine release (Huang et al., 2001). In addition, in Orx and histamine double KO, Anaclet and colleagues (2010) noticed aberrant hypersynchronization during both wakefulness and cataplexy episodes. Moreover, Bastianini and colleagues (2016) observed that histamine deficiency is sufficient to generate high-amplitude theta bursts during REM sleep, even though histamine is not physiologically present in this phase. This behaviour is very similar to the one induced by orexinergic system defects, and merits further investigation.

REFERENCES

Aracri, P., Amadeo, A., Pasini, M. E., Fascio, U., & Becchetti, A. (2013). Regulation of glutamate release by heteromeric nicotinic receptors in layer V of the secondary motor region (Fr2) in the dorsomedial shoulder of prefrontal cortex in mouse. *Synapse*, *67*(6), 338-357.

Aracri, P., Banfi, D., Pasini, M. E., Amadeo, A., & Becchetti, A. (2015). Hypocretin (orexin) regulates glutamate input to fast-spiking interneurons in layer V of the Fr2 region of the murine prefrontal cortex. *Cerebral Cortex*, *25*(5), 1330-1347.

Aracri, P., Consonni, S., Morini, R., Perrella, M., Rodighiero, S., Amadeo, A., & Becchetti, A. (2010). Tonic modulation of GABA release by nicotinic acetylcholine receptors in layer V of the murine prefrontal cortex. *Cerebral Cortex*, *20*(7), 1539-1555.

Aracri, P., Meneghini, S., Coatti, A., Amadeo, A., & Becchetti, A. (2017). α4β2∗ nicotinic receptors stimulate GABA release onto fast-spiking cells in layer V of mouse prefrontal (Fr2) cortex. *Neuroscience*, *340*, 48-61.

Aridon, P., Marini, C., Di Resta, C., Brilli, E., De Fusco, M., Politi, F., ... & Curia, G. (2006). Increased sensitivity of the neuronal nicotinic receptor α2 subunit causes familial epilepsy with nocturnal wandering and ictal fear. *American Journal of Human Genetics*, *79*(2), 342-350.

Aston-Jones, G., & Bloom, F. E. (1981). Activity of norepinephrine-containing locus coeruleus neurons in behaving rats anticipates fluctuations in the sleep-waking cycle. *Journal of Neuroscience*, *1*(8), 876-886.

Bastianini, S., Lo Martire, V., Berteotti, C., Silvani, A., Ohtsu, H., Lin, J. S., & Zoccoli, G. (2016). High-amplitude theta wave bursts characterizing narcoleptic mice and patients are also produced by histamine deficiency in mice. *Journal of Sleep Research*, *25*(5), 591-595.

Bastianini, S., Silvani, A., Berteotti, C., Lo Martire, V., & Zoccoli, G. (2012). High-amplitude theta wave bursts during REM sleep and cataplexy in hypocretin-deficient narcoleptic mice. *Journal of Sleep Research*, *21*(2), 185-188.

Bayer, L., Eggermann, E., Saint-Mleux, B., Machard, D., Jones, B. E., Mühlethaler, M., & Serafin, M. (2002). Selective action of orexin (hypocretin) on nonspecific thalamocortical projection neurons. *Journal of Neuroscience*, *22*(18), 7835-7839.

Becchetti, A., Aracri, P., Meneghini, S., Brusco, S., & Amadeo, A. (2015). The role of nicotinic acetylcholine receptors in autosomal dominant nocturnal frontal lobe epilepsy. *Frontiers in Physiology*, *6*.

Berridge, C. W., & Abercrombie, E. D. (1999). Relationship between locus coeruleus discharge rates and rates of norepinephrine release within neocortex as assessed by in vivo microdialysis. *Neuroscience*, *93*(4), 1263-1270.

Berridge, C. W., & Waterhouse, B. D. (2003). The locus coeruleus–noradrenergic system: modulation of behavioral state and state-dependent cognitive processes. *Brain Research Reviews*, *42*(1), 33-84

Boutrel, B., Cannella, N., & de Lecea, L. (2010). The role of hypocretin in driving arousal and goal-oriented behaviors. *Brain Research*, *1314*, 103-111.

Brusco, S., Ambrosi, P., Meneghini, S., & Becchetti, A. (2015). Agonist and antagonist effects of tobacco-related nitrosamines on human α4β2 nicotinic acetylcholine receptors. *Frontiers in Pharmacology*, *6*.

Bymaster, F. P., Katner, J. S., Nelson, D. L., Hemrick-Luecke, S. K., Threlkeld, P. G., Heiligenstein, J. H., ... & Perry, K. W. (2002). Atomoxetine increases extracellular levels of norepinephrine and dopamine in prefrontal cortex of rat: a potential mechanism for efficacy in attention deficit/hyperactivity disorder. *Neuropsychopharmacology*, *27*(5), 699-711.

Cardin, J. A., Carlén, M., Meletis, K., Knoblich, U., Zhang, F., Deisseroth, K., ... & Moore, C. I. (2009). Driving fast-spiking cells induces gamma rhythm and controls sensory responses. *Nature*, *459*(7247), 663-667.

Castro-Alamancos, M. A., Rigas, P., & Tawara-Hirata, Y. (2007). Resonance (~ 10 Hz) of excitatory networks in motor cortex: effects of voltage-dependent ion channel blockers. *Journal of Physiology*, *578*(1), 173-191.

Chemelli, R. M., Willie, J. T., Sinton, C. M., Elmquist, J. K., Scammell, T., Lee, C., ... & Fitch, T. E. (1999). Narcolepsy in orexin knockout mice: molecular genetics of sleep regulation. *Cell*, *98*(4), 437-451.

Couey, J. J., Meredith, R. M., Spijker, S., Poorthuis, R. B., Smit, A. B., Brussaard, A. B., & Mansvelder, H. D. (2007). Distributed network actions by nicotine increase the threshold for spike-timing-dependent plasticity in prefrontal cortex. *Neuron*, *54*(1), 73-87.

Dani, J. A., & Bertrand, D. (2007). Nicotinic acetylcholine receptors and nicotinic cholinergic mechanisms of the central nervous system. *Annual Review of Pharmacology and Toxicology.*, *47*, 699-729.

De Fusco, M., Becchetti, A., Patrignani, A., Annesi, G., Gambardella, A., Quattrone, A., ... & Casari, G. (2000). The nicotinic receptor [beta] 2 subunit is mutant in nocturnal frontal lobe epilepsy. *Nature Genetics*, *26*(3), 275-277.

Dembrow, N., & Johnston, D. (2014). Subcircuit-specific neuromodulation in the prefrontal cortex. *Frontiers in Neural Circuits*, *8*.

Eggermann, E., Serafin, M., Bayer, L., Machard, D., Saint-Mleux, B., Jones, B. E., & Mühlethaler, M. (2001). Orexins/hypocretins excite basal forebrain cholinergic neurones. *Neuroscience*, *108*(2), 177-181.

Fadel, J., & Burk, J. A. (2010). Orexin/hypocretin modulation of the basal forebrain cholinergic system: role in attention. *Brain Research*, *1314*, 112-12

Fadel, J., Pasumarthi, R., & Reznikov, L. R. (2005). Stimulation of cortical acetylcholine release by orexin A. *Neuroscience*, *130*(2), 541-547.

Florin-Lechner, S. M., Druhan, J. P., Aston-Jones, G., & Valentino, R. J. (1996). Enhanced norepinephrine release in prefrontal cortex with burst stimulation of the locus coeruleus. *Brain Research*, *742*(1), 89-97.

Franklin, K. J. B., Chudasama, Y., Watson, C., Paxinos, G., & Puelles, L. (2011). The prefrontal cortex. In: *The Mouse Nervous System*, 727-735.

Giniatullin, R., Nistri, A., & Yakel, J. L. (2005). Desensitization of nicotinic ACh receptors: shaping cholinergic signaling. *Trends in Neurosciences*, *28*(7), 371-378.

Harvey, S. C., Maddox, F. N., & Luetje, C. W. (1996). Multiple Determinants of Dihydro-β-Erythroidine Sensitivity on Rat Neuronal Nicotinic Receptor α Subunits. *Journal of Neurochemistry*, *67*(5), 1953-1959.

Heidbreder, C. A., & Groenewegen, H. J. (2003). The medial prefrontal cortex in the rat: evidence for a dorso-ventral distinction based upon functional and anatomical characteristics. *Neuroscience & Biobehavioral Reviews*, *27*(6), 555-579.

Hoda, J. C., Gu, W., Friedli, M., Phillips, H. A., Bertrand, S., Antonarakis, S. E., ... & Patel, J. (2008). Human nocturnal frontal lobe epilepsy: pharmocogenomic profiles of pathogenic nicotinic acetylcholine receptor β-subunit mutations outside the ion channel pore. *Molecular Pharmacology*, *74*(2), 379-391.

Hoover, W. B., & Vertes, R. P. (2007). Anatomical analysis of afferent projections to the medial prefrontal cortex in the rat. *Brain Structure and Function*, *212*(2), 149-179.

Huang, Z. L., Qu, W. M., Li, W. D., Mochizuki, T., Eguchi, N., Watanabe, T., ... & Hayaishi, O. (2001). Arousal effect of orexin A depends on activation of the histaminergic system. *Proceedings of the National Academy of Sciences*, *98*(17), 9965-9970.

Iversen, L., Iversen, S., Bloom, F. E., & Roth, R. H. (2008). *Introduction to Neuropsychopharmacology*. Oxford University Press.

Jin, J., Chen, Q., Qiao, Q., Yang, L., Xiong, J., Xia, J., ... & Chen, F. (2016). Orexin neurons in the lateral hypothalamus project to the medial prefrontal cortex with a rostro-caudal gradient. *Neuroscience Letters*, *621*, 9-14.

Jones, B. E. (2005). From waking to sleeping: neuronal and chemical substrates. *Trends in Pharmacological Sciences*, *26*(11), 578-586.

Jones, B. E. (2008). Modulation of cortical activation and behavioral arousal by cholinergic and orexinergic systems. *Annals of the New York Academy of Sciences*, *1129*(1), 26-34.

Jones, B. E. (2011). Neurobiology of waking and sleeping. In: *Handbook of Clinical Neurology* (Vol. 98, pp. 131-149). Elsevier.

Kang, L., Tian, M. K., Bailey, C. D., & Lambe, E. K. (2015). Dendritic spine density of prefrontal layer 6 pyramidal neurons in relation to apical dendrite sculpting by nicotinic acetylcholine receptors. *Frontiers in Cellular Neuroscience*, *9*.

Kargo, W. J., Szatmary, B., & Nitz, D. A. (2007). Adaptation of prefrontal cortical firing patterns and their fidelity to changes in action–reward contingencies. *Journal of Neuroscience*, *27*(13), 3548-3559.

Kawaguchi, Y., & Shindou, T. (1998). Noradrenergic excitation and inhibition of GABAergic cell types in rat frontal cortex. *Journal of Neuroscience*, *18*(17), 6963-6976.

Kukkonen, J. P., & Leonard, C. S. (2014). Orexin/hypocretin receptor signalling cascades. *British Journal of Pharmacology*, *171*(2), 314-331.

Lambe, E. K., & Aghajanian, G. K. (2003). Hypocretin (orexin) induces calcium transients in single spines postsynaptic to identified thalamocortical boutons in prefrontal slice. *Neuron*, *40*(1), 139-150.

Lambe, E. K., Liu, R. J., & Aghajanian, G. K. (2007). Schizophrenia, hypocretin (orexin), and the thalamocortical activating system. *Schizophrenia Bulletin*, *33*(6), 1284-1290.

Lambe, E. K., Olausson, P., Horst, N. K., Taylor, J. R., & Aghajanian, G. K. (2005). Hypocretin and nicotine excite the same thalamocortical synapses in prefrontal cortex: correlation with improved attention in rat. *Journal of Neuroscience*, *25*(21), 5225-5229.

Lambe, E. K., Picciotto, M. R., & Aghajanian, G. K. (2003). Nicotine induces glutamate release from thalamocortical terminals in prefrontal cortex. *Neuropsychopharmacology*, *28*(2), 216-225.

Lampl, I., & Yarom, Y. (1997). Subthreshold oscillations and resonant behavior: two manifestations of the same mechanism. *Neuroscience*, *78*(2), 325-341.

Le Bon-Jego, M., & Yuste, R. (2007). Persistently active, pacemaker-like neurons in neocortex. *Frontiers in Neuroscience*, *1*(1), 123.

Le Magueresse, C., & Monyer, H. (2013). GABAergic interneurons shape the functional maturation of the cortex. *Neuron*, *77*(3), 388-405.

Lee, M. G., Hassani, O. K., & Jones, B. E. (2005). Discharge of identified orexin/hypocretin neurons across the sleep-waking cycle. *Journal of Neuroscience*, *25*(28), 6716-6720.

Leonard, C. S., & Kukkonen, J. P. (2014). Orexin/hypocretin receptor signalling: a functional perspective. *British Journal of Pharmacology*, *171*(2), 294-313.

Li, B., Chen, F., Ye, J., Chen, X., Yan, J., Li, Y., ... & Hu, Z. (2010). The modulation of orexin A on HCN currents of pyramidal neurons in mouse prelimbic cortex. *Cerebral Cortex*, *20*(7), 1756-1767.

Liu, R. J., & Aghajanian, G. K. (2008). Stress blunts serotonin-and hypocretin-evoked EPSCs in prefrontal cortex: role of corticosterone-mediated apical dendritic atrophy. *Proceedings of the National Academy of Sciences*, *105*(1), 359-364.

Luu, P., Tucker, D. M., & Makeig, S. (2004). Frontal midline theta and the error-related negativity: neurophysiological mechanisms of action regulation. *Clinical Neurophysiology*, *115*(8), 1821-1835.

Manfredi, I., Zani, A. D., Rampoldi, L., Pegorini, S., Bernascone, I., Moretti, M., ... & Sala, M. (2009). Expression of mutant β2 nicotinic receptors during development is crucial for epileptogenesis. *Human Molecular Genetics*, *18*(6), 1075-1088.

Marchi, M., & Grilli, M. (2010). Presynaptic nicotinic receptors modulating neurotransmitter release in the central nervous system: functional interactions with other coexisting receptors. *Progress in Neurobiology*, *92*(2), 105-111.

McNally, J. M., McCarley, R. W., McKenna, J. T., Yanagawa, Y., & Brown, R. E. (2011). Complex receptor mediation of acute ketamine application on in vitro gamma oscillations in mouse prefrontal cortex: modeling gamma band oscillation abnormalities in schizophrenia. *Neuroscience*, *199*, 51-63.

Meneghini, S., Brusco, S., Coatti, A., Aracri. P., Modena. D., Carraresi. L., Arcangeli. A., Amadeo. A., & Becchetti, A. (2017). The role of neuronal nicotinic receptors in the pathogenesis of autosomal dominant nocturnal frontal lobe epilepsy: a study on wild-type and conditional transgenic mice expressing the β2-V287L subunit. *Fondazione Telethon XIX Scientific Convention.*

Mitchell, D. J., McNaughton, N., Flanagan, D., & Kirk, I. J. (2008). Frontal-midline theta from the perspective of hippocampal "theta". *Progress in Neurobiology*, *86*(3), 156-185.

Molas, S., & Dierssen, M. (2014). The role of nicotinic receptors in shaping and functioning of the glutamatergic system: A window into

cognitive pathology. *Neuroscience & Biobehavioral Reviews*, *46*, 315-325.

Murai, Y., & Akaike, T. (2005). Orexins cause depolarization via nonselective cationic and K+ channels in isolated locus coeruleus neurons. *Neuroscience research*, *51*(1), 55-65.

Ohno, K., & Sakurai, T. (2008). Orexin neuronal circuitry: role in the regulation of sleep and wakefulness. *Frontiers in Neuroendocrinology*, *29*(1), 70-87.

Paterson, D., & Nordberg, A. (2000). Neuronal nicotinic receptors in the human brain. *Progress in Neurobiology*, *61*(1), 75-111.

Paxinos, G. (2013). *Paxinos and Franklin's the mouse brain in stereotaxic coordinates*. Academic Press.

Peyron, C., Faraco, J., Rogers, W., Ripley, B., Overeem, S., Charnay, Y., ... & Li, R. (2000). A mutation in a case of early onset narcolepsy and a generalized absence of hypocretin peptides in human narcoleptic brains. *Nature Medicine*, *6*(9), 991-997.

Peyron, C., Tighe, D. K., Van Den Pol, A. N., De Lecea, L., Heller, H. C., Sutcliffe, J. G., & Kilduff, T. S. (1998). Neurons containing hypocretin (orexin) project to multiple neuronal systems. *Journal of Neuroscience*, *18*(23), 9996-10015.

Phillips, H. A., Favre, I., Kirkpatrick, M., Zuberi, S. M., Goudie, D., Heron, S. E., ... & Mulley, J. C. (2001). CHRNB2 is the second acetylcholine receptor subunit associated with autosomal dominant nocturnal frontal lobe epilepsy. *American Journal of Human Genetics*, *68*(1), 225-231.

Putula, J., & Kukkonen, J. P. (2012). Mapping of the binding sites for the OX 1 orexin receptor antagonist, SB-334867, using orexin/hypocretin receptor chimaeras. *Neuroscience Letters*, *506*(1), 111-115.

Richardson, K. A., Fanselow, E. E., & Connors, B. W. (2008). Neocortical anatomy and physiology. *Epilepsy. A Comprehensive Textbook*, 323-335.

Roychowdhury, S., Zwierzchowski, A. N., Garcia-Oscos, F., Olguin, R. C., Delgado, R. S., & Atzori, M. (2014). Layer-and area-specificity of the adrenergic modulation of synaptic transmission in the rat neocortex. *Neurochemical Research*, *39*(12), 2377-2384.

Sakurai, T., Amemiya, A., Ishii, M., Matsuzaki, I., Chemelli, R. M., Tanaka, H., ... & Arch, J. R. (1998). Orexins and orexin receptors: a family of hypothalamic neuropeptides and G protein-coupled receptors that regulate feeding behavior. *Cell*, *92*(4), 573-585.

Salgado, H., Garcia-Oscos, F., Patel, A., Martinolich, L., Nichols, J. A., Dinh, L., ... & Atzori, M. (2010). Layer-specific noradrenergic modulation of inhibition in cortical layer II/III. *Cerebral Cortex*, *21*(1), 212-221.

Sarter, M., Parikh, V., & Howe, W. M. (2009). Phasic acetylcholine release and the volume transmission hypothesis: time to move on. *Nature Reviews Neuroscience*, *10*(5), 383-390.

Siegel, J. (2002). The neural pathways that produce arousal. *The Neural Control of Sleep and Waking*, 47-52.

Silva, L. R., Amitai, Y., & Connors, B. W. (1991). Intrinsic oscillations of neocortex generated by layer 5 pyramidal neurons. *Science*, *251*(4992), 432.

Smart, D., Sabido-David, C., Brough, S. J., Jewitt, F., Johns, A., Porter, R. A., & Jerman, J. C. (2001). SB-334867-A: the first selective orexin-1 receptor antagonist. *British Journal of Pharmacology*, *132*(6), 1179-1182.

Sutcliffe, J. G., & de Lecea, L. (2002). The hypocretins: setting the arousal threshold. *Nature Reviews Neuroscience*, *3*(5), 339-349.

Tremblay, R., Lee, S., & Rudy, B. (2016). GABAergic interneurons in the neocortex: from cellular properties to circuits. *Neuron*, *91*(2), 260-292.

Udakis, M., Wright, V. L., Wonnacott, S., & Bailey, C. P. (2016). Integration of inhibitory and excitatory effects of α7 nicotinic acetylcholine receptor activation in the prelimbic cortex regulates network activity and plasticity. *Neuropharmacology*, *105*, 618-629.

Uylings, H. B., Groenewegen, H. J., & Kolb, B. (2003). Do rats have a prefrontal cortex?. *Behavioural Brain Research*, *146*(1), 3-17.

Vassalli, A., & Franken, P. (2017). Hypocretin (orexin) is critical in sustaining theta/gamma-rich waking behaviors that drive sleep need. *Proceedings of the National Academy of Sciences*, *114*(27), E5464-E5473.

Vassalli, A., Dellepiane, J. M., Emmenegger, Y., Jimenez, S., Vandi, S., Plazzi, G., ... & Tafti, M. (2013). Electroencephalogram paroxysmal theta characterizes cataplexy in mice and children. *Brain*, *136*(5), 1592-1608.

Wang, S., Kurada, L., Cilz, N. I., Chen, X., Xiao, Z., Dong, H., & Lei, S. (2013). Adenosinergic depression of glutamatergic transmission in the entorhinal cortex of juvenile rats via reduction of glutamate release probability and the number of releasable vesicles. *PloS One*, *8*(4), e62185.

Wang, X. J. (2010). Neurophysiological and computational principles of cortical rhythms in cognition. *Physiological Reviews*, *90*(3), 1195-1268.

Wenger Combremont, A. L., Bayer, L., Dupré, A., Mühlethaler, M., & Serafin, M. (2016). Effects of Hypocretin/Orexin and Major Transmitters of Arousal on Fast Spiking Neurons in Mouse Cortical Layer 6B. *Cerebral Cortex*, *26*(8), 3553-3562.

Williams, R. H., Vazquez-DeRose, J., Thomas, A. M., Piquet, J., Cauli, B., & Kilduff, T. S. (2017). Cortical nNOS/NK1 Receptor Neurons are

Regulated by Cholinergic Projections From the Basal Forebrain. *Cerebral Cortex*, 1-21.

Xia, J., Chen, X., Song, C., Ye, J., Yu, Z., & Hu, Z. (2005). Postsynaptic excitation of prefrontal cortical pyramidal neurons by hypocretin-1/orexin a through the inhibition of potassium currents. *Journal of Neuroscience Research*, *82*(5), 729-736.

Yang, B., & Ferguson, A. V. (2002). Orexin-A depolarizes dissociated rat area postrema neurons through activation of a nonselective cationic conductance. *Journal of Neuroscience*, *22*(15), 6303-6308.

Zhang, Z. W., Burke, M. W., Calakos, N., Beaulieu, J. M., & Vaucher, E. (2010). Confocal analysis of cholinergic and dopaminergic inputs onto pyramidal cells in the prefrontal cortex of rodents. *Frontiers in Neuroanatomy*, *4*.